A Comparative Investigation of Transgene Expression and Gene Silencing of Non-functionalized Layered Double Hydroxides versus Amino-acid Functionalized Hydrotalcites

by

NIRASHA NUNDKUMAR

Submitted in fulfilment of the academic requirements for the degree of

DOCTOR OF PHILOSOPHY

In the School of Life Sciences, University of KwaZulu-Natal, Durban

December 2017

As the candidate's supervisor I have approved this thesis/dissertation for submission.

Supervisor: Prof. M. Singh **Signed: …… Date: ……**

Co-Supervisor: Dr S. Singh

ABSTRACT

The highly tunable properties of anionic clays make them potential candidates as gene delivery vehicles. The initial momentum created by LDH-mediated gene delivery has subsided somewhat due to recent reports indicating lower LDH-mediated transfection efficiency as a result of degradation of the genetic material within the endosome. Functionalization of the vector to bring about quicker endosomal escape appears to be a suitable strategy to overcome this hurdle. In this study, the hydrotalcites (HTs) were functionalized with positively charged amino acids in an attempt to achieve higher transfection efficiency by exploitation of the proton-sponge effect.

Hydrotalcites (HTs), amino acid functionalized hydrotalcites (aa-HTs) and layered double hydroxides (LDHs) were synthesized using the co-precipitation method. These compounds were characterized using X-Ray diffraction (XRD), inductively coupled plasma-optical emission spectroscopy (ICP-OES), Fourier Transform Infrared Spectroscopy (FTIR), transmission electron microscopy (TEM), scanning electron microscopy (SEM) and nanoparticle tracking analysis (NTA). The characterization assays confirmed that the compounds prepared were LDH in nature, and of the desired M^{2+}:M^{3+} ratio. TEM and NTA was successfully utilized to assess morphology, size and zeta potential of the nanomaterials and their nucleic acid:LDH nanocomplexes. The optimal nucleic acid binding capacity was determined using gel retardation assays.

The nucleic acid:LDH complexes were found to be relatively non-cytotoxic to four mammalian cell lines (HEK293, Caco-2, HepG2 and HeLa *tat luc*) using the MTT assay. The ability of the prepared LDHs to effectively transfect pCMV-*luc* DNA into mammalian cell lines was investigated by the luciferase reporter gene assay. It was found that the degree of transfection was largely cell line dependent, with the HEK293 cells exhibiting the greatest degree of transfection, followed by the Caco-2 cell line. The transfection efficiency in these two cell lines were approximately 800 fold greater than that in the HepG2 cells. Overall, the HTs prepared in the M^{2+}:M^{3+} ratio of 2:1 displayed significantly higher transfection than those prepared in the 3:1 ratio. The histidine functionalized HTs complexes appeared to be better transfection agents than their arginine functionalized counterparts. These aa-HTs also showed significantly better transfection than MgAl 0.25. However, the non-functionalized HT, MgAl 0.33 showed the greatest degree of

transfection in all cell lines. MgFe 0.33, and the ZnAl LDHs showed promising results with MgFe 0.33 showing up to 50 fold greater transfection than several of the other compounds. Gene silencing studies conducted in the Hela *tat luc* cell line, showed that the aa-HTs elicited significantly higher levels of gene knockdown than the non-functionalized HTs, with MgAl 0.25 performing better than MgAl 0.33. The gene knockdown efficiency of the MgFe LDHs were comparable to that observed for the non-functionalized HTs, whilst the ZnAl LDHs showed a marginal but measurable degree of gene silencing. Overall, these LDHs have shown the potential to bind, protect and efficiently deliver both pDNA and siRNA, *in vitro,* necessitating further studies in an *in vivo* system.

Keywords: Hydrotalcite, Layered double hydroxide, gene transfection, gene silencing

PREFACE

The experimental work described in this thesis was carried out in the School of Life Sciences, University of KwaZulu-Natal, Durban, from July 2012 to December 2017, under the supervision of Professor Moganavelli Singh and co-supervision of Dr Sooboo Singh.

These studies represent original work by the author and have not otherwise been submitted in any form for any degree or diploma to any tertiary institution. Where use has been made of the work of others it is duly acknowledged in the text.

DECLARATION – PLAGIARISM

I, Nirasha Nundkumar declare that

1. The research reported in this thesis, except where otherwise indicated, is my original research.

2. This thesis has not been submitted for any degree or examination at any other university.

3. This thesis does not contain other persons' data, pictures, graphs or other information, unless specifically acknowledged as being sourced from other persons.

4. This thesis does not contain other persons' writing unless specifically acknowledged as being sourced from other researchers. Where other written sources have been quoted, then:

    - Their words have been re-written but the general information attributed to them has been referenced.
    - Where their exact words have been used, then their writing has been placed in italics and inside quotation marks, and referenced.

5. This thesis does not contain text, graphics or tables copied and pasted from the internet, unless specifically acknowledged, and the source being detailed in the thesis and in the Reference section.

Signed: 

TABLE OF CONTENTS

CHAPTER ONE

CHAPTER TWO

CHAPTER THREE

CHAPTER FOUR

CHAPTER FIVE

LIST OF FIGURES

LIST OF TABLES

ABBREVIATIONS

aa	:	amino acid
AONS	:	Antisense oligonucleotides
ATP	:	Adenosine triphosphate
BCA	:	Bicinchoninic acid
Caco-2	:	Colorectal adenocarcinoma cells
DMSO	:	Dimethyl sulphoxide
DNA	:	Deoxyribonucleic acid
EDTA	:	Ethylenediaminetetraacetic acid
EMEM	:	Eagle's Minimum Essential Medium
EMSA	:	Electrophoretic mobility shift assay
FBS	:	Foetal bovine serum
FTIR	:	Fourier transform infrared spectroscopy
HBS	:	HEPES-buffered saline
HEK293	:	Human embryonic kidney cells
Hela *tat-luc*	:	cervical carcinoma cells transfected with tat protein and stably expressing the luciferase gene
HEPES	:	2-[-(2-hydroxyethyl)-piperazinyl]-ethanesulphonic acid
HepG2	:	Liver hepatocellular carcinoma cells
HT	:	Hydrotalcite
HT-like	:	Hydrotalcite-like
ICP-OES	:	Inductively coupled plasma-optical emission spectroscopy
LDH	:	Layered double hydroxide
miRNA	:	Micro ribonucleic acid

MTT	:	3-(4,5-dimethylthiazol-2-yl)-2,5-diphenyltetrazolium
nm	:	Nanometres
NTA	:	Nanoparticle tracking analysis
PBS	:	Phosphate-buffered saline
pCMV	:	Plasmid containing cytomegalovirus promoter
pDNA	:	Plasmid DNA
RISC	:	RNA-induced-silencing-complex
RLU	:	Relative light units
RNAi	:	RNA interference
SEM	:	Scanning electron microscopy
shRNA	:	Short hairpin ribonucleic acid
siRNA	:	Small interfering ribonucleic acid
TEM	:	Transmission electron microscopy
Tris	:	Tris(hydroxymethyl)aminomethane
v/v	:	volume to volume ratio
w/w	:	weight to weight ratio
XRD	:	X-Ray diffraction
µg	:	micrograms
µL	:	microlitres

ACKNOWLEDGEMENTS

I would like to express my sincere gratitude to:

- Prof. M. Singh for her invaluable supervision and guidance. The unselfish sharing of her immense knowledge, words of encouragement, constructive criticism and insightful comments will always be greatly appreciated.
- Dr. S. Singh for his expert guidance in the chemistry aspects of this study.
- Drushan Padayachee for assistance with the chemical analyses.
- My colleagues in the non-viral gene delivery for always being supportive and helpful.
- My mum and dad Nirmala and Devjith Bhagwandin, my sister Nerushka, brothers Navesh and Nikesh as well as my mother-in-law Shanthi Nundkumar for their constant love and blessings.
- My husband Prashant Nundkumar and my son Ashmil, for always believing in me. I am most grateful for your love, support and encouragement.

DEDICATION

This thesis is dedicated to

Miler and Ashmil

CHAPTER ONE

1. INTRODUCTION

1.1 BACKGROUND OF STUDY

Gene therapy encompasses a range of methods aimed at regulating gene expression by insertion of exogenous nucleic acids, such as deoxyribonucleic acid (DNA), small interfering ribonucleic acid (siRNA), micro RNA (miRNA), short hairpin RNA (shRNA) and antisense oligonucleotides (AONS), to either replace or repair a defective gene. Unlike conventional therapeutic approaches which tend to treat the symptoms of a disease, gene therapy offers a strategy to treat the underlying cause of a disorder or disease.

Naked nucleic acids cannot easily traverse the cell membrane, partly due to their negative charge, and even when they do enter the cell, they are prone to degradation by nucleases. A suitable "carrier" or "vector" is therefore required to efficiently transport the nucleic acids into the cell. Thus far, the most successful vectors employed have been of viral origin, but they suffer from a number of major drawbacks such as immunogenic responses, low DNA carrying capacity, insertional mutagenesis, lack of specific cell targeting and high cost [Ragusa *et al.,* 2007]. Over the years a number of non-viral vectors have been explored; such as liposomes [Templeton, 2002; Daniels *et al.,* 2013; Habib *et al.,* 2013; Naicker *et al*., 2014; Lee *et al*., 2017], gold nanoparticles [Riley and Vermerris, 2017], dendrimers [Pan *et al.,* 2007; Pan *et al.,* 2009], quantum dots [Kralj and Pavelic, 2003], carbon nanotubes [Singh *et al.,* 2005; Gao *et al.,* 2006; Lacerda *et al.,* 2007; Ahmed *et al.,* 2009; Ahmed[1] *et al.,* 2009] magnetic nanoparticles [Mulens *et al.,* 2013; Riley and Vermerris, 2017] and functionalized polymers [Perez *et al.,* 2001; Nimesh *et al.,* 2006]. These non-viral carriers also suffer from a number of disadvantages, the most common being cytotoxicity and immunogenic responses. Thus, there remains a need for the development of safe and effective gene delivery vehicles.

Anionic clays such as layered double hydroxides (LDH) or hydrotalcite-like (HT-like) materials, have recently attracted much attention as carriers of bioactive molecules and genes [Ladewig[1] *et*

al., 2010; Choy *et al.,* 2000; Nalawade *et al.,* 2009; Balcomb *et al*., 2015]. Hydrotalcites (HTs) refer specifically to magnesium aluminium LDHs. LDHs can complex with various types of molecules such as drugs [Choy *et al.,* 2004; Costantino *et al.,* 2008], sugar phosphates [Jellicoe and Fogg, 2012], fullerenes [Fortner *et al.,* 2012], and biomolecules such as oligomers, DNA and nucleotides [Kwak *et al.,* 2002; Choy *et al.,* 2007].

Unlike most inorganic nanoparticles that require chemical and/or biological pre-modification to obtain the desirable properties for cellular delivery, anionic clays allow for direct loading of anionic drugs or biomolecules due to their anion-exchange properties [Ladewig *et al.,* 2009; Xu *et al.,* 2006]. Mg-Al LDH's are less toxic than most inorganic nanoparticles [Kriven *et al.,* 2004; Choi *et al.,* 2008]. LDH nanoparticles upon disintegration in the cytoplasm results in cyto-friendly ions such as Mg^{2+}, Al^{3+} and NO_3^- [Xu *et al.,* 2006; Kura *et al.,* 2014]. Research into the use of LDHs as gene delivery vehicles has thus far, shown promising results.

Reports indicate that functionalization of other non-viral gene delivery vectors has resulted in enhanced gene delivery, with up to a 1000 fold increase in transfection [Smith *et al.,* 1997]. It has been suggested that better transfection occurs upon functionalization as a result of enhanced uptake through receptors on the cell surface, which may retain complexes at the cell surface rather than merely relying on non-specific electrostatic attraction between the nanoparticles and the cell surface [Wu and Wu, 1987; Choy *et al.,* 2000]. The possibility thus exists that functionalization of the LDHs could result in greater, more effective transfection. Del Hoyo and co-workers (2007), observed that LDHs displayed lower transfection efficiency due to pH related degradation of DNA in the endosome, a hurdle that could possibly be overcome by functionalization of the LDH. Functionalization of the LDHs with amino acids containing cationic side-chains could result in enhancement of the 'proton-sponge' effect, leading to quicker and more efficient endosomal escape and improved transfection, when compared to non-functionalized LDHs.

1.2 AIMS AND OBJECTIVES OF STUDY

The aim of the study was to prepare LDHs (both non-functionalized and amino acid functionalized) and compare their efficiencies as vectors for transfection, to achieve gene expression and gene silencing.

In order to accomplish this aim, the objectives of the study were to:

1. Prepare amino acid functionalized and non-functionalized LDHs using the co-precipitation method.
2. Characterize the prepared LDHs.
3. Evaluate the DNA and siRNA binding capacity of the prepared LDHs.
4. Investigate the cytotoxicity of the prepared LDHs.
5. Investigate and compare the transfection and gene silencing efficiency of the amino acid functionalized versus the non-functionalized LDHs.

1.3 SIGNIFICANCE OF THE STUDY

Amino acid functionalized LDHs offers a novel and promising concept for enhanced gene delivery *in vitro*. The potential benefits of this study may include the following:

- Although there have been many reports of the use of LDHs (both functionalized and non-functionalized) as gene delivery vehicles in literature, there has as yet not been any study involving amino acid functionalized LDHs as carriers of genes. Hence, we undertook to prepare amino acid functionalized LDHs, which will exhibit enhanced cellular uptake and rapid endosomal escape, leading to a greater degree of gene expression or knockdown.
- It is anticipated that this project could possibly lead to the development of a potential gene delivery vector to aid in realizing the dream of using gene therapy to overcome human genetic diseases.

1.4 NOVELTY OF THE STUDY

There have been several published reports on the use of LDHs as DNA delivery vehicles *in vitro* [Choy *et al.,* 2000; Choy *et al.,* 2004; Del Hoyo, 2007; Xu *et al.,* 2007; Ladewig[1] *et al.,* 2010] and in the delivery of siRNA [Ladewig[2] *et al.,* 2010; Chen *et al.,* 2013; Li *et al.,* 2014]. It has been further shown that arginine functionalization of hydroxyapatites [Wang et al., 2015], and amino acid modification of chitosan [Zheng *et al.,* 2015], improved transfection efficiency. The intercalation of amino acids into layered double hydroxides [Aisawa *et al.,* 2000; Aisawa *et al.,* 2001; Nakayama *et al.,* 2004; Aisawa *et al.,* 2006], have been attempted but was not exploited as gene delivery vehicles. This study reports for the first time on DNA transfection and gene silencing using amino acid functionalized LDHs. The transfection efficiency of amino acid functionalized versus non-functionalized LDHs is also investigated.

1.5 OVERVIEW OF THE DISSERTATION

Chapter 1 briefly introduces and summarizes the background to the study. It outlines the challenges encountered with current gene therapy vectors and explores the rationale for and novelty of the study. The aim and objectives of the study are also described.

Chapter 2 is a detailed literature review covering the historical background of LDHs, the chemical compositions of various LDHs, the applications of LDHs and their use in gene therapy.

Chapter 3 describes the preparation and characterization of LDHs. Methods of preparation of LDHs are briefly discussed and the characterization of the prepared LDHs using X-ray diffraction (XRD), Inductively coupled plasma-optical emission spectroscopy (ICP-OES), Fourier transform infrared spectroscopy (FTIR), Transmission electron microscopy (TEM), scanning electron microscopy (SEM), and nanoparticle tracking analysis (NTA) are described and discussed.

Chapter 4 includes the nucleic acid binding studies using gel retardation assays. The nucleic acid:LDH complexes are characterized using TEM, XRD and NTA. The susceptibility of the nucleic acid:LDH complex to serum nucleases is also investigated.

Chapter 5 describes the *in vitro* cell culture assays such as the cytotoxicity studies, gene transfection and gene knockdown studies. Cytotoxicity was evaluated in the HepG2, HEK293, Caco-2 and Hela *tat luc* cells, while pCMV-*luc* DNA transfection was assessed in the HepG2, HEK293 and Caco-2 only. The knockdown of the luciferase gene (stably expressed in Hela *tat luc* cells) by anti-*luc*-siRNA, employing the synthesized LDHs as carriers is also investigated.

Chapter 6 provides the conclusions derived from this study and includes recommendations for future studies.

CHAPTER TWO

2. LITERATURE REVIEW

2.1 HISTORICAL BACKGROUND OF LAYERED DOUBLE HYDROXIDES

There are two main classes of clays, viz. cationic clays which are made up of negatively charged aluminosilicate or magnesiosilicate layers with positive ions in the interlayer region [Rajamathi *et al*., 2001] and anionic clays which consist of lamellar metal hydroxides composed of two (or more) kinds of metals in the main layers and anions in the interlayer region [He *et al*., 2005; de Roy *et al*., 2006; Boulet *et al*., 2006]. Anionic clays are generally referred to as layered double hydroxides (LDHs).

Hydrotalcite (HT) is an anionic clay mineral that was first reported by Hochstetter in Sweden in 1842 [Bravo-Suarez, 2004]. The formula for HT was proposed by an Italian professor of mineralogy, Professor E. Manasse, in Florence Italy in 1915 and confirmed by Foshag in 1920 [Mills *et al*., 2012]. Investigations by Aminoff and Broome in 1930 revealed the existence of two polytypes, viz. hydrotalcite and manasseite, the latter named in honour of Manasse [Cavani *et al*., 1991]. The two polytypes differ in their symmetry with the HT being rhombohedral and the manasseite, hexagonal [Belloto *et al*., 1996]. Since HT is one of the most representative minerals of the anionic clays, other layered double hydroxides are often referred to as hydrotalcite-like compounds (HT-like). The general LDH formula, based on a combination of divalent and trivalent metal cations can be written as:

$$[M^{II}_{1-x}M^{III}_{x}(OH)_2]A^{q-}_{x/q}.nH_2O$$

Where $\mathbf{M^{II}}$ and $\mathbf{M^{III}}$ represent the divalent and trivalent cations respectively, $\mathbf{A^{q-}}$ represents an exchangeable anion, **x** is the $M^{III}/M^{II} + M^{III}$ molar ratio and **n** is the number of moles of water [Posati *et al*., 2012; Ladewig *et al*., 2009; Luan *et al*., 2009].

The divalent and trivalent cations, the interlayer anions as well as the value of the stoichiometric co-efficient (***x***) may be widely varied, giving rise to a large class of isostructural materials [Kuang

et al., 2010; Seftel *et al*., 2008]. The value of ***x*** typically falls between 0.17 and 0.33 [Kloprogge *et al*., 2002; Kovanda *et al*., 2009]. The general formula of LDH is in no way limited by the above, as LDHs with more than two types of cations have also been reported [Qian *et al*., 2015]. Mills and co-workers (2012) have extensively reviewed the HT super-group, comprising all HT and HT-like compounds (Table 2.1).

LDHs are formed naturally from the weathering of basalts, or as deposits from ground water, and are generally not found in large quantities in nature [Frost *et al*., 2003]. Fortunately, they can be easily prepared in the laboratory, and specifically tailored by varying the constituent cations and anions, as well as altering the synthetic parameters to obtain the desired structural properties. The first reported synthesis of HT was by Feitknect in 1942 [cited by Bravo-Suarez, 2004; Cavani *et al*., 1991] who prepared magnesium/aluminium LDHs by co-precipitation using aluminium and magnesium chlorides, and caustic soda [Gastuche *et al*., 1967]. The name layered double hydroxide was derived from Feitknect, who named his synthesized HT compounds "Doppelschichtstrukturen" which means double sheet structures [Cavani *et al*., 1991].

Initial proposed structures showed the principal $Mg(OH)_2$ layers with a brucite structure interleaved with disordered or amorphous $Al(OH)_3$ layers, with the 3.06 Å thick interlayer containing the trivalent cations, oxygens and hydroxyls [Brown and Gastuche, 1967]. This structure was later disproved, and it was proposed that the brucite-like layers of the HT-like compounds sjögrenite was composed of both magnesium and iron, with the interlayer region comprising of water molecules and carbonate ions [Ingram and Taylor, 1967]. Similar results for sjögrenite were previously presented by Allmann and Lohse in 1966 [Ingram and Taylor, 1967; Taylor 1969]. The name sjögrenite is now discredited as sjögrenite has been proven to be just the 2H polytype of pyroaurite [Mills *et al*., 2012].

Table 2.1 Hydrotalcite super-groups [adapted from Mills *et al.*, 2012].

	Name	Cell Parameters (Å)		Polytype	Formula
		a	c		
1	Hydrotalcite	3.065	23.07	3R	$Mg_6Al_2(OH)_{16}[CO_3].4H_2O$
2	Manasseite	3.06	15.34	2H	$Mg_6Al_2(OH)_{16}[CO_3].4H_2O$
3	Pyroaurite	3.089	23.23	3R	$Mg_6Fe_2^{3+}(OH)_{16}[CO_3].4H_2O$
4	Sjögrenite	3.097	15.56	2H	$Mg_6Fe_2^{3+}(OH)_{16}[CO_3].4H_2O$
5	Stichtite	3.09	23.19	3R	$Mg_6Cr_2(OH)_{16}[CO_3].4H_2O$
6	Barbertonite	3.085	15.52	2H	$Mg_6Cr_2^{3+}(OH)_{16}[CO_3].4H_2O$
7	Meixnerite	3.046	22.93	3R	$Mg_6Al_2(OH)_{18}.4H2O$
8	Iowaite	3.1183	24.113	3R	$Mg_6Fe_2^{3+}(OH)_{16}Cl_2.4H_2O$
9	Droninoite	6.206	46.184	6R	$Ni_6Fe_2^{3+}(OH)_{16}Cl_2.4H_2O$
10	Woodallite	3.102	24.111	3R	$Mg_6Cr_2(OH)_{16}Cl_2.4H_2O$
11	Desautelsite	3.114	24.39	3R	$Mg_6Mn_2^{3+}(OH)_{16}[CO_3].4H_2O$
12	Takovite	3.0250	22.595	3R	$Ni_6Al_2(OH)_{16}[CO_3].4H_2O$
13	Reevesite	3.082	22.770	$3R_1$	$Ni_6Fe_2^{3+}(OH)_{16}[CO_3].4\ H_2O$
14	Jamborite	3.07	23.3	3R	$Ni_6^{2+}Ni_2^{3+}(OH)]_{16}S.4H_2O$
15	Quintinite	10.751	22.71/15.171	3T/2H	$Mg_4Al_2(OH)_{12}[CO_3].3H_2O$
16	Charmarite	10.985	15.10/22.63	2H/3T	$Mn_4Al_2(OH)_{12}[CO_3].3H_2O$
17	Caresite	10.805	22.48	3T	$Fe_4^{2+}Al_2(OH)_{12}[CO_3].3H_2O$
18	Zaccagnaite	3.0662	22.6164	3R	$Zn_4Al_2(OH)_{12}[CO_3].3H_2O$
19	Chlormagaluminite	5.29	15.46	2H	$Mg_4Al_2(OH)_{12}Cl_2.\ 3H_2O$
20	Comblainite	3.038	22.79	3R	$Ni_4Co_2^{3+}(OH)_{12}(CO_3)\cdot 3H_2O$
21	Fougerite	3.17-3.18	22.7-22.9	3R	$Fe_4^{2+}Fe_2^{3+}(OH)_{12}[CO_3].3H_2O$
22	Mossbauerite	3.079	22.253	3R	$Fe_6^{3+}O_4(OH)_8[CO_3].3H_2O$
23	Woodwardite	3.00	27.3	3R	$Cu_{1-x}Al_x(OH)_2[SO_4]_{x/2}.6H_2O$
24	Zincowoodwardite	3.063	8.91/25.42	1T/3R	$Zn_{1-x}Al_x(OH)_2[SO_4]_{x/2}.nH_2O$
25	Honessite	3.083	25.8	3R	$(Ni_{1-x}Fe^{3+}{}_x)(OH)_2[SO_4]_{x/2}.nH_2O$ $n < 3x/2$

HYDROTALCITE SUPERGROUP

QUINTINITE SUPERGROUP

FOUGÈRITE SUPERGROUP

WOODWARDITE SUPERGROUP

Table 2.1 (continued)…

	Name	Cell Parameters (Å)		Polytype	Formula	
		a	c			
26	Glaucocerinite	3.057-3.070	32.52-32.65	$3R_1$	$(Zn_{1-x}Al_x)(OH)_2[SO_4]_{x/2}.nH_2O$	GLAUCOCERINITE SUPERGROUP
27	Hydrowoodwardite	3.066	32.80	3R	$Cu_{1-x}Al_x(OH)_2[SO_4]_{x/2}.nH_2O$	
28	Carrboydite	3.022	32.45	$3R_1$	$(Ni_{1-x}Al_x)(OH)_2[SO_4]_{x/2}.nH_2O$	
29	Hydrohonessite	3.09	33.4	$3R_2$	$(Ni_{1-x}Fe^{3+}{}_x)(OH)_2[SO_4]_{x/2}.nH_2O$ $n > 3x/2$	
30	Mountkeithite	10.698	22.545	2H	$(Mg_{1-x}Fe^{3+}{}_x)(OH)_2[SO_4]_{x/2}.nH_2O$	
31	Zincaluminite	No structural data available			$(Zn_{1-x}Al_x)(OH)_2[SO_4]_{x/2}.nH_2O$	
32	Wermlandite	9.303	22.57	1T	$Mg_7Al_2(OH)_{18}[Ca(H_2O)_6]\ [SO_4]_2.6H_2O$	WERMLANDITE SUPERGROUP
33	Shigaite	9.512	33.074	3R	$Mn_6Al_3(OH)_{18}[Na(H_2O)_6]\ [SO_4]_2.6H_2O$	
34	Nikischerite	9.347	33.000	3R	$Fe_6^{2+}Al_3(OH)_{18}[Na(H_2O)_6]\ [SO_4]_2.6H_2O$	
35	Motukoreaite	9.172	33.51	3R	$Mg_6Al_3(OH)_{18}[Na(H_2O)_6]\ [SO_4]_2.6H_2O$	
36	Natroglaucocerinite	No structural data available			$Zn_6Al_3(OH)_{18}[Na(H_2O)_6]\ [SO_4]_2.6H_2O$	
37	Karchevskyite	16.0556	25.66	1T	$Mg_{18}Al_9(OH)_{54}Sr_2(CO_3)_9(H_2O)_6(H_3O)_5$	
38	Cualstibite	9.15	9.745	1T	$Cu_2Al(OH)_6[Sb(OH)_6]$	CAULSTIBITE SUPERGROUP
39	Cyanophyllite	9.941	5.498	1M	$Cu_2Al(OH)_6[Sb(OH)_6]$	
40	Zincalstibite	5.327	9.792	1T	$Zn_2Al(OH)_6[Sb(OH)_6]$	
41	Omsite	5.351	19.5802	2T	$Ni_2Fe^{3+}(OH)_6[Sb(OH)_6]$	
42	Hydrocalumite	5.765	46.978	3R	$Ca_4Al_2(OH)_{12}Cl_2.4H_2O$	HYDROCALUMITE SUPERGROUP
43	Kuzelite	5.76	53.66	3R	$Ca_4Al_2(OH)_{12}[SO_4].6H_2O$	
44	Coalingite	3.12	37.4	3R	$Mg_{10}Fe_2^{3+}(OH)_{24}\ [CO_3].2H_2O$	UNCLASSIFIED
45	Brugnatellite	5.47	15.97	1T	$Mg_6Fe^{3+}\ CO_3(OH)_{13}.4H_2O$	
46	Muskoxite	3.07	4.6	Further investigation required	$Mg_{7(}Fe^{3+})\ (OH)_{26}.H_2O$	

2.2 LAYERED DOUBLE HYDROXIDE STRUCTURE AND COMPOSITION

The LDH structure is based on the naturally occurring mineral brucite, the major difference being a partial replacement of divalent cations by trivalent cations resulting in a net positive charge on the lattice sheets [Bellotto *et al*., 1996]. This positive charge is neutralized by the presence of anions contained in the interlayer region [Cavanni *et al*., 1991]. As in brucite, each metal cation in LDH is directly bonded to six hydroxide groups and each hydroxide group is directly bonded to 3 metal cations (Figure 2.1). The trivalent cations are positioned such that they are spread out within the lattice sheets and are not next to each other resulting in "charge homogeneity" throughout the LDH lattice sheet [Evans and Slade, 2006]. Vucelic and co-workers (1997) have demonstrated that although there is no long range trivalent cation ordering in LDHs, there is a high degree of local ordering, such that the trivalent cations are never neighboring each other. The positively charged lattice sheets are stacked on top of each other in either 2 or 3 layer sequences e.g. 2H (2-layer hexagonal) or 3R (3-layer rhombohedral), with the 3-layer sequence being preferred in HTs [Bellotto *et al*., 1996].

Water molecules are also contained within the interlayer region, the actual amount of water present being dependent on factors such as the nature of the anions, the water vapour pressure and temperature [Hou *et al*., 2003]. The amount of water present in the interlayer may be calculated either by thermogravimetric analysis of weight loss, or by calculating the difference between the total number of sites occupied by oxygen less the sites occupied by the anions (Vacarri, 1998). Water found within the interlayer region has been referred to as 'intrinsic' or 'interparticle pore' water, whereas water molecules attached to the outer layers/external surfaces of the LDHs have been called 'adsorbed surface' or 'extrinsic' water [Evans and Slade, 2006]. Similarly, the anions found between the LDH layers are referred to as being intercalated and the anions attached to the edges or the outer surfaces of the LDH layers are said to be adsorbed.

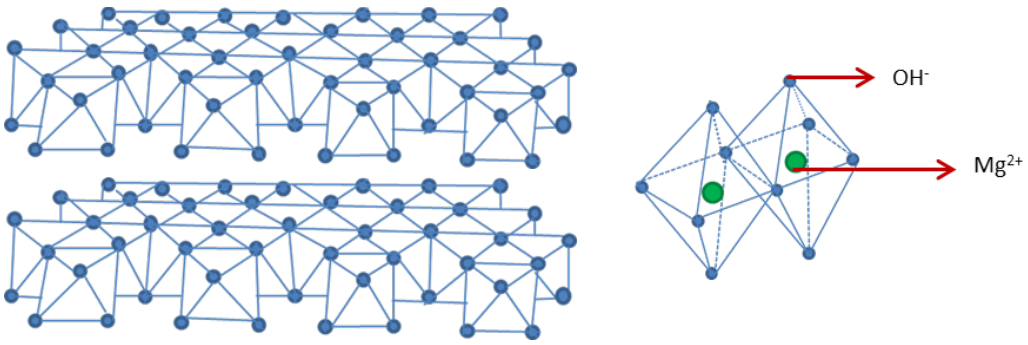

(a)

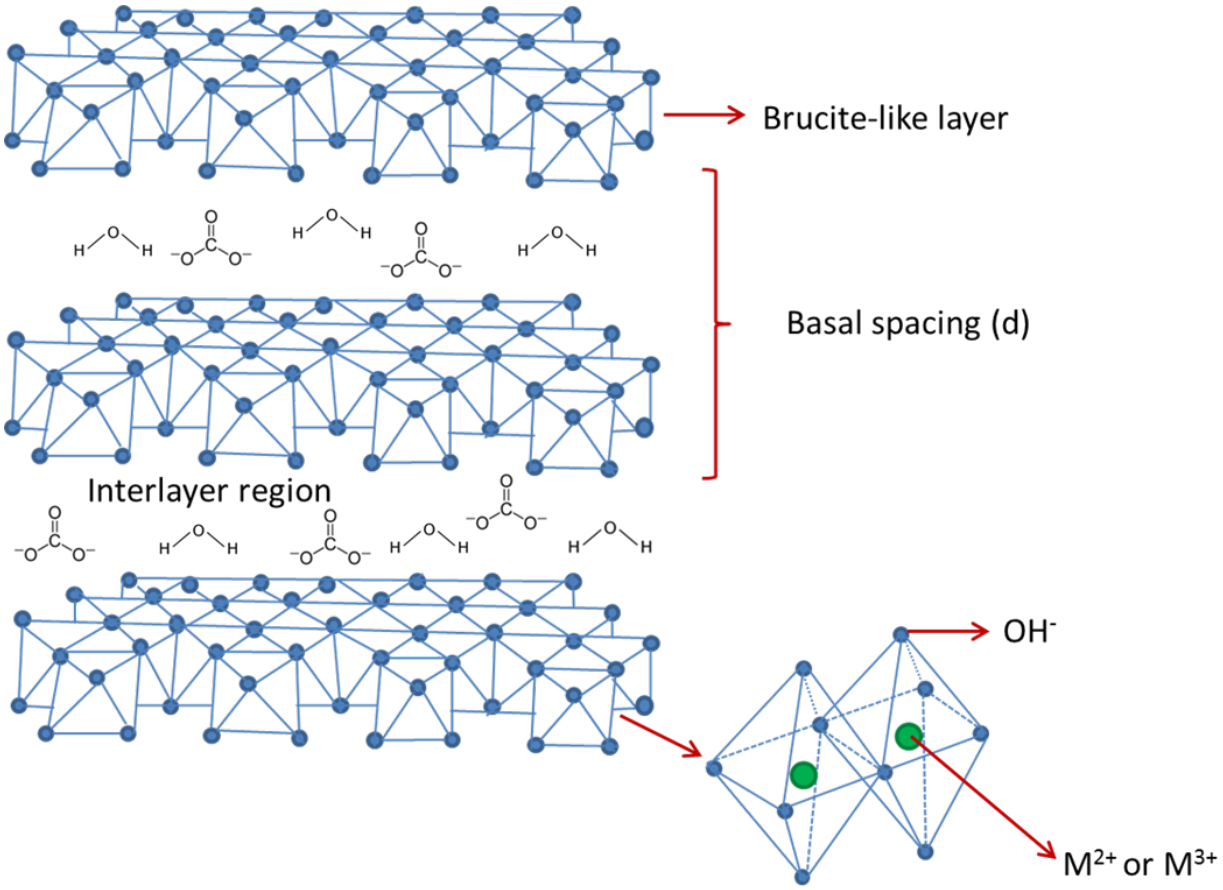

(b)

Figure 2.1 Structures of (a) brucite and (b) LDH [Redrawn and adapted from Benicio *et al.*, 2015].

The nature of the interlayer anions and presence of water in the interlayer regions results in an increase in basal spacing from 4.78 Å in brucite to 7.8 Å in HT [Brindley and Kikkawa, 1980; Wypych, 2004]. Generally, the thickness of the interlayer depends on the number, size, orientation and strength of the bonds between the anions and the hydroxyl groups of the brucite-like layers [Seftel *et al*., 2008].

2.2.1 ANION EXHANGE PROPERTY OF LAYERED DOUBLE HYDROXIDES

The anions in the LDH interlayer are relatively weakly bound and can be readily exchanged [Meyn *et al*., 1990]. The potential anion exchange capability for an LDH depends on its charge density (or unit charge per area) which is based on the different trivalent to divalent cation ratios. The formula for charge density is,

$$\text{Charge density} = xe/a^2\sin 60^o$$

where, **x** is the ratio of trivalent to total amount of metal, **a** is the distance between adjacent metal ions in the layer, **e** is the electronic charge, and **sin60°** is the angle between the **a** and **b** axes [Richardson, 2007].

Thus, a HT with Mg:Al ratio of 1:2 would have a higher charge density than one with a Mg:Al ratio of 1:3. The higher the trivalent cation content, the higher the positive charge density, and the higher the amount of anions that can be potentially adsorbed [Beavers, 1999].

A major advantage of LDHs over other anion exchangers is the “large space” between the brucite layers. This allows for a diverse array of anionic compounds to be exchanged using LDHs. Bish (1980) showed that anion exchange in the LDH interlayer can cause displacement of the brucite layers, resulting in a possible change in polytype.

2.2.2 ANION PREFERENCE

Miyata (1983) showed that selectivity of monovalent anions are in the order of $OH^- > Cl^- > Br^- > NO_3^- > I^-$, in slight contradiction to Bontchev and co-workers (2003), who showed that monovalent anion exchange preference was $Br^- > Cl^- > NO_3^- > I^-$. Generally, carbonate ($CO_3^{2-}$) is

the easiest to intercalate and the most difficult to exchange [Crosby *et al.,* 2014], whereas halides and nitrates are easy to intercalate and exchange. Therefore, most LDH materials are prepared using either nitrate or chloride as the initial anion. Divalent anions are more strongly adsorbed than monovalent anions [Forano *et al*., 2006], with the anion preference for divalent anions being $CO_3^{2-} > HPO_4^{2-} > CrO_4^{2-} > SO_4^{2-} > MoO_4^{2-}$ [Auerbach *et al*., 2004]. Multivalent anions are preferred by LDHs, due to stronger electrostatic interaction [Choy *et al*., 2007].

Naturally occurring LDHs usually contain carbonate as the interlayer anion, but synthetic LDHs may have a variety of anions of different geometries, sizes and charges incorporated within the layers, resulting in a large class of isostructural materials [Evans and Duan, 2006], with diverse physico-chemical properties [Miyata, 1975; Miyata and Okada, 1977]. Some of the reported anions incorporated within the interlayers of LDHs can be seen in Table 2.2.

For biological studies, the preferred anion for the synthesis of LDHs is the nitrate anion, which creates a non-toxic, biologically compatible form of LDH [Costantino *et al*., 2008]. The nitrate anion, being monovalent, is also a good precursor for exchange reactions [Choy *et al*., 2007].

Table 2.2 Some anions reported to have been incorporated into LDHs.

Class of Anion	Anion	Reference
Organic anions	Carboxylic acids	Carlino, 1997
	Alkoxides, naphthalene, β-napthol, phenol	Butenko *et al*., 2014
	Acetate, stearate, oleate	Kandare and Hossenlopp, 2006
	Tartarate, succinate	Prevot *et al*., 1998
	Oxalate	Prevot *et al.,* 1999
	Citrate	Kumar *et al*., 2006
	Sugar phosphates	Jellicoe and Fogg, 2012
	Cyclodextrins	Mohanambe and Vasudevan, 2006
	Unsaturated carboxylates	Takagi *et al*., 1993
Inorganic anions	Carbonate	Trujillano, 2006
	Nitrate, chloride, iodide, bromide	Bontchev *et al*., 2003; Miyata and Okada, 1977
	Chromate, dichromate, chlorate	Malherbe and Besse, 2000
	Chloride, percholate, sulphate	Brindley and Kikkawa,1980
	chlorate	Miyata, 1975
	Hydroxide	Newman *et al*., 2002
	Acetate, terephthalate, benzoate	Newman and Jones, 1999
	Metals and oxometalates	Rives and Ullibarri, 1999
	Hexacyanocobalt (III)	Suzuki *et al*., 1989
	$Mo_7O_{24}^{6-}$, $Cr_2O_7^{2-}$, SiO_3^{2-}	Misra and Perrotta, 1992
	Oxalate, $[Fe(CN)_6]^-$, bromide, chloride, carbonate, hydroxide, nitrate	Khan and O'Hare, 2002

Table 2.2 continued…

Surfactants	Sodium dodecylsulphate, sodium dodecylbenzenesulphate, sodium laurate, bis(2-ethylhexyl)phosphate	Costa *et al.,* 2008
	Octylsulphonate, octanebenzenesulphonate, dodecylbenzenesulphonate, octadecanesulphonate	Trujillano, 2006
	Alkyl sulphates, alkanesulphonates	Meyn *et al*., 1993
	Adipate, dodecylsulphate	Herrero *et al*., 2009
	Dodecylbenzenesulphonic acid, dodecylphosphonic acid, aleuritic acid, sebacic acid	Anbarasan *et al*., 2005
Drugs	Naproxen	del Arco[1] *et al*., 2004
	Indomethacin	del Arco[2] *et al*., 2004
	5-Fluorouracil	Wang *et al*., 2005
	Anti-inflammatory and/or anti-cancer drugs	Costantino *et al*., 2008; Zhang *et al*., 2014
	Camptothecin	Tyner *et al*., 2004
	Diclofenac	Perioli[1] *et al.,* 2011
	Flurbiprofen	Perioli[2] *et al*., 2011
Biomolecules	DNA	Balcomb *et al*., 2015; Kriven *et al*., 2004; Li *et al*., 2013; Choy *et al*., 2000; Xu *et al.,* 2007
	siRNA	Wong *et al*., 2010; Zhang *et al*., 2012; Chen *et al*., 2013; Ladewig[2] *et al*., 2010
	Antisense oligonucleotides	Kriven *et al*., 2004; Kwak *et al.,* 2002; Hibino 2004; Ikeda *et al*., 1984
	Amino acids and/or oligopeptides	Aisawa *et al*., 2001; Aisawa *et al*., 2006; Nakayama *et al.,* 2004; Stimpfling *et al*., 2016; Coelho *et al.,* 2012
	ATP, AMP, GMP, CMP	Choy *et al.,* 2001
Polymers	Various Polymers	Tronto *et al.,* 2013

2.2.3 CATIONS IN LAYERED DOUBLE HYDROXIDES

Various cations can be used to synthesize LDHs, with the main requirement being that the radii should not be too different from Mg^{2+} and Al^{3+} [Zhang *et al*., 2014; Sajid and Basheer, 2016]. Cavani and co-workers (1991) have suggested that cations with similar radii to that of Mg^{2+} and Al^{3+} can be better accommodated in the octahedral sites of the brucite-like layers of LDHs. The ionic radii of M^{2+} and M^{3+} should also ideally be close to each other [Miyata and Kumura, 1973]. Generally, the divalent and trivalent metal cations in LDHs belong mainly to the third, fourth, fifth and sixth periods of the periodic table. Table 2.3 shows some of the cations found in naturally occurring and/or synthetic LDHs. Khan and O'Hare (2002) have mentioned that all dipositive metal ions (except Cu^{2+}) and all trivalent metals (except Ti^{3+}) form LDHs.

Table 2.3 Cations in LDHs.

	PERIOD 3	PERIOD 4	PERIOD 5	PERIOD 6
DIVALENT	Mg^{2+}	Ca^{2+}, Mn^{2+}, Fe^{2+}, Co^{2+}, Ni^{2+}, Cu^{2+}, Zn^{2+}	Cd^{2+}	
TRIVALENT	Al^{3+}, Si^{3+}	Fe^{3+}, Sc^{3+}, V^{3+}, Cr^{3+}, Mn^{3+}, Ga^{3+}	Y^{3+}, Mo^{3+}, Ag^{3+}, In^{3+},	La^{3+}, W^{3+}, Au^{3+}
TETRAVALENT		Ti^{4+}, V^{4+}	Zr^{4+}, Pd^{4+},	Pt^{4+}

In most naturally occurring LDHs there is a partial replacement of divalent cations by trivalent cations, but there have been cases where tetravalent cations instead of trivalent cations have been reported [Saber and Tagaya[1], 2003; Intissar *et al.,* 2003].

There have also been reports of LDHs synthesized with three different cations, viz. Mg-Zn-Al and Zn-Cu-Al LDHs [Kooli *et al*.,1995], Zn-Al-Sn LDHs [Saber and Tagaya[2], 2003], Cu-Mn-Al LDHs [Velu and Swamy, 1996], Cu-Mg-Mn and Ni-Mg-Mn LDHs [Kovanda *et al.,* 2005], Mg-Zn-Al LDHs [Li *et al*., 2014], Mg-Fe-Al LDHs [Guo et al., 2003], and recently Ni-Co-Al LDHs [Si *et al*.,2017].

2.3 APPLICATIONS OF LAYERED DOUBLE HYDROXIDES

The highly tunable properties of LDHs lends itself to them being employed in a diversity of applications. Most of the applications are based on the LDHs high ion-exchange and adsorption capacity, low cost, their good biocompatibility and stability, combined with its large surface area. Some of the many applications of LDHs have been summarized in Table 2.4.

Table 2.4 Some application of LDH materials.

APPLICATION	REFERENCE
Catalysts	Vaccari, 1998; Newman and Jones,1998; Cavani *et al*., 1991; Xu *et al*., 2011; Fan *et al*., 2014; Wang[1] *et al*., 2015; Feng *et al.,* 2015; Valente *et al.,* 2010; Li *et al*., 2015; Zümreoglu-Karan and Ay, 2012; Abderrazek *et al.,* 2016; Liu *et al*., 1999; Senra *et al.,* 2017; Kuang *et al.,* 2010; Jabłońska *et al*., 2013
Agriculture	Benício *et al.,* 2015; Cardoso *et al*., 2006; Jaiswal *et al.,* 2014; Choy *et al*., 2007
Bio-medicine *(eg. drug delivery, gene delivery/*silencing*, biosensors, antacids)*	Shafiei *et al*., 2008; Wang *et al.,* 2005; Kura *et al*., 2014; Ladewig[1] *et al*., 2010; Ladewig *et al*., 2009; Li[1] *et al*., 2014; Xu *et al*., 2006; Mulens *et al*., 2013; Choy *et al*., 2004; Ha and Xanthos, 2011; Bi *et al*., 2014; Cunha *et al*., 2010; Kuang *et al*., 2010; Senapati *et al*., 2016; Mondal *et al*., 2016; del Arco[1] *et al*., 2004; del Arco[2] *et al*., 2004; del Arco *et al*., 2009; Vaccari 1998., Fong *et al*., 2011; Sarijo *et al*., 2017; Musumeci *et al.,* 2010; Yan *et al.,* 2014; Wei *et al*., 2015
Environmental and Industrial *(eg. Wastewater treatment, UV Absorption, Stabilization of polyesters, Sorbents for liquid radioactive waste, flame retardants)*	Kovanda *et al*., 2009; Cocheci *et al.,* 2010; Coelho *et al.,* 2012; Kulyukhin *et al*., 2014; Ruiz-Hitzky *et al*., 2010; Wang *et al.,* 2014; Kuang *et al*., 2010; Alexandrica *et al*., 2015; Wang *et al*., 2012; Sajid and Basheer, 2016; Zümreoglu-Karan and Ay, 2012; Kameda *et al*., 2017; Stimpfling *et al*., 2016; Sertsova *et al*., 2015
Cosmetics Industry	Choy *et al*., 2007; Perera *et al.,* 2015; Del Hoyo, 2007; Nalawade *et al*., 2009

2.3.1 GENE THERAPY

Gene therapy generally refers to the transfer of nucleic acids into a cell to either repair or correct defective genes. This is achieved by introducing either plasmid DNA (pDNA) to replace a defective gene, or small interfering RNA (siRNA) to silence an overexpressed gene.

Despite much research in the area of gene therapy in recent years, efficient gene delivery remains the greatest challenge for its practical application. Systemic delivery of naked nucleotides is ineffective due to their sensitivity to nuclease degradation, as well as the difficulty of crossing the cell membrane due to their negative charge. Hence, there is a need to develop carrier vectors. An ideal gene delivery vector should have the ability to deliver a therapeutic gene safely into a cell, have high loading capacity, exhibit little or no toxicity, be non-immunogenic, biodegradable, be stable during storage and after administration, have the ability to target specific cells and afford relatively efficient gene expression [Xu *et al*., 2007; Huang *et al*., 1999].

Carriers thus far have included viral vectors as well as a number of non-viral vectors such as cationic lipids, liposomes, cationic polymers, gold nanoparticles, magnetic nanoparticles, quantum dots, silica nanoparticles, fullerenes, carbon nanotubes and supramolecular systems [Smith *et al*., 1997; Lv *et al*., 2006; Ragusa *et al*., 2007; Ahmed *et al*., 2009; Pan *et al*., 2007; Gao *et al*., 2006; Pan *et al*., 2009]. Of these, viral vectors have been the most efficient, but they suffer the disadvantage of possible immunogenic responses, low DNA-loading capability, insertional mutagenesis as well as a lack of specific cell targeting. Cationic lipids and polymers may avoid such problems, but are often highly toxic to cells [Xu and Lu, 2006]. Inorganic nanoparticles appear more suitable for cellular delivery due to their wide availability, rich surface functionality, good biocompatibility, potential capability of targeted delivery and the ability for controlled release of genes/drugs [Xu *et al*., 2007].

Biocompatibility of the carrier is also of the utmost importance and is dependent on a number of factors (Table 2.5).

Table 2.5 Overview of nanoparticle characteristics which can be controlled to improve biocompatibility [adapted from Soenen *et al*., 2011].

Parameter	Advantage	Disadvantage
Size	Small (< 10 nm): greater cellular uptake	Small: higher cytotoxicity Large (> 200 nm): Too little cellular uptake
Shape	Spherical: highest uptake Rods: Reduced cytotoxicity Flat Platelets (eg. LDH): increased surface area resulting in increased carrying capacity	Spherical: highest cytotoxicity Rods: Diminished uptake
Purity	The presence of biologically compatible metals in suitable concentrations will not induce cytotoxic effects.	Certain metals or organic impurities present on the carrier may induce cytotoxic effects
Surface charge	Positively charged: better interaction with cell membrane	Positively charged: could be more cytotoxic as they have a tendency to interact with many biological components. Negatively charged: poor interaction with cell membrane

Ultimately an ideal gene delivery vector should be able to bind or condense nucleic acids forming nanocomplexes, protect nucleic acids from enzymatic degradation [Imami *et al*., 2015], promote cellular uptake, promote endosomal escape, and also enhance entry into the nucleus for strategies involving pDNA delivery [Dong *et al.,* 2013].

2.3.1.1 GENE THERAPY USING PLASMID DNA

In gene therapy strategies involving DNA transfection, functional or therapeutic DNA is delivered into cells to replace a missing or mutated gene [Morachis *et al*., 2012]. pDNA is generally used in gene therapy strategies since it is an inherently stable molecule, and is capable of withstanding changes in pH and ionic strength [Smith *et al*., 1997]. For successful gene therapy involving DNA transfection, the DNA needs to be effectively transported into the nucleus of the cell, where the exogenous gene must be integrated into the chromosome to obtain the desired level of expression to produce therapeutic effects [Liang and Lam, 2012; Dong *et al*., 2013].

There are a number of major obstacles to efficient pDNA delivery, including naked DNA's inability to cross the cell membrane, endosomal escape, nuclear uptake and de-complexation. pDNA is negatively charged and hydrophilic in nature and thus requires assistance to cross the plasma membrane. Non-viral DNA delivery into the cell proceeds via an endocytic pathway upon which the DNA-carrier complex would be trapped within an endosome. It is important that the complex be released from the endosome at an early stage to prevent lysosomal destruction of both the DNA and the carrier. Elouahabi and co-workers (1997) have reported that endosomal escape is a crucial and possibly the rate-limiting step for efficient transfection.

The process of nuclear uptake is not very clearly understood. It has been suggested that complexes may be internalized into cells during cell division, but non-dividing cells would probably require a receptor-mediated process for entry [Smith *et al*., 1997]. Smaller complexes appear to be able to diffuse through nuclear pores to gain entry into the nucleus [Elaesser and Howard, 2012]. Another possible mode of nuclear entry involves the endoplasmic reticulum, where the nanocomplex containing endosome fuses with the endoplasmic reticulum, releasing the DNA into the lumen of the reticulum, from where the DNA enters the nucleus through the nuclear membrane-reticulum network [Elouahabi and Ruysschaert, 2005].

De-complexation is also crucial for efficient gene expression. Partial de-complexation probably occurs in the lysosome, leaving the DNA in a partially condensed form. This allows for entry of the smaller, partially condensed DNA into the nucleus through basal leakage of the nuclear envelope [Smith *et al.,* 1997]. Zhang and co-workers (2012) have reported that de-complexation is pH dependent, where an acidic pH disrupts the complex to release the nucleic acid.

2.3.1.2 GENE SILENCING USING siRNA

Antisense therapy involves siRNA, a class of small 20-26 bp double-stranded (ds) RNA molecules [Valencia-Sanchez *et al*., 2006], that play an important role in RNA interference (RNAi). RNAi involves the silencing of expression of specific genes with nucleotide sequences complementary to that of the siRNA [Zhang *et al*., 2007]. This ultimately results in suppression of expression of the target (disease-causing) gene.

The RNAi pathway is triggered by the entry of a ds RNA molecule into the cell (Figure 2.2). The endonuclease DICER cuts the ds RNA molecule into smaller fragments (siRNAs) [Zhang *et al*., 2007]. These siRNA fragments integrate into a multi-subunit protein called the RNA-induced-silencing-complex (RISC) [Matranga *et al*., 2005]. The RISC complex contains Argonaute proteins that have a PAZ domain for miRNA/siRNA binding and a PIWI domain that functions in slicer activity [Valencia –Sanchez *et al*., 2006]. The Argonaute proteins cleaves the ds RNA into 2 strands: a guide or anti-sense strand (which remains bound to RISC), and the passenger or sense strand which is degraded. The anti-sense strand directs the sequence specific silencing of the target mRNA by cleaving the target mRNA with Argonaute 2. This leads ultimately to the inhibition of translation of the target mRNA [Ladewig[2] *et al*., 2010]. The DICER step may be bypassed by the addition of chemically synthesized siRNAs of the appropriate size.

As with DNA delivery, there are also a number of hurdles to successful siRNA delivery. Firstly, the net negative charge on siRNA molecules prevents entry into the cell [Chen *et al*., 2013]. Upon entry into the cell, the siRNAs are targeted by RNases and macrophages [Nguyen *et al*., 2008], and like DNA, the siRNA also needs to be released before it reaches the degradative environment of the lysosome. LDHs show great promise as siRNA carriers due to their high buffering capacity which not only protects the siRNA from the effects of the acidic environment but also contributes to bursting of the late endosome, and subsequent release of the siRNA, by the proton sponge effect.

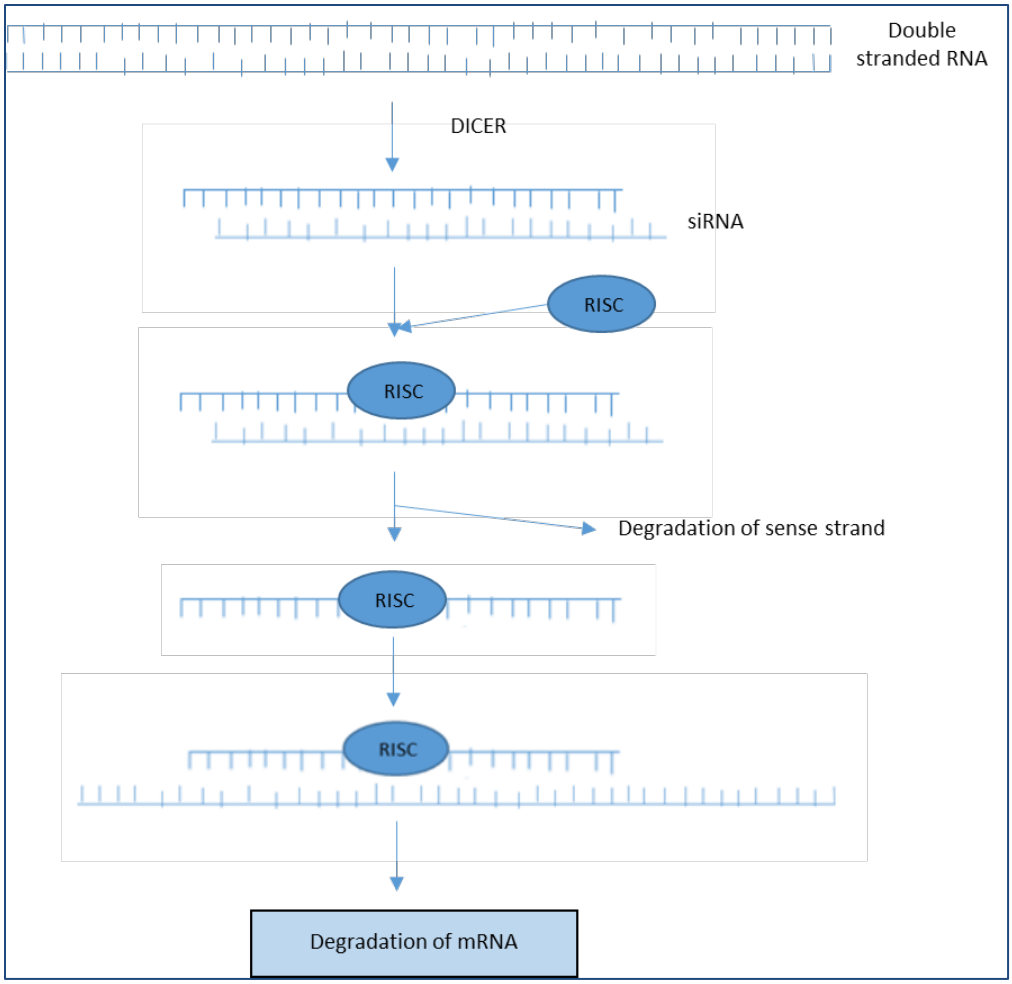

Figure 2.2 The RNAi mechanism.

Ladewig[2] and co-workers (2010) successfully employed LDHs as a siRNA carrier and reported fast and effective target gene knockdown. Gene knockdown was also successfully carried out in cortical neurons using LDH mediated siRNA delivery [Wong *et al*., 2010]. RNAi is an extremely promising technique and may prove to be the intervention method of choice for treatment of diseases in the future.

2.3.2 LAYERED DOUBLE HYDROXIDES IN GENE THERAPY

An ideal gene delivery vehicle needs to be able to adequately bind and protect the biomolecule being carried (DNA or siRNA), traverse the cell membrane, release its load in the appropriate region of the cell, achieve good transfection, and in doing so, not cause any harm (toxicity) to the cell [Imani *et al*., 2015].

The unique and highly tunable properties of LDHs lends itself to making them ideal gene delivery vehicles. Firstly, DNA or siRNA can be easily incorporated into/onto LDHs by either ion exchange, intercalation or adsorption [Rojas *et al*., 2015]. The nanocomplex thus formed gains extra stabilization energy due to the electrostatic interaction between the cationic brucite layers and the DNA/siRNA [Choy *et al*., 2000]. The positively charged atoms on the LDH surface interacts with the negatively charged cell membrane leading to the internalization of the LDH nanocomplex. Studies by Nagaraj and co-workers (2015) have shown that higher nanoparticle concentrations result in increased energy-dependent cellular uptake mechanisms.

This internalization occurs via clathrin-mediated endocytosis [Ladewig[2] *et al*., 2010; Wong *et al*., 2010; Chen *et al.,* 2013; Rojas *et al*., 2015]. A diagrammatic representation of this process is shown in Figure 2.3. Clathrin-mediated endocytosis involves the entrapment of the nanocomplex within an endosome, followed by either an exocytic pathway (endosome → Golgi apparatus) or an endocytic route (early endosome → late endosome → lysosome) [Chung *et al.,* 2012; Rojas *et al*., 2015]. The trafficking pathway followed is nanoparticle size dependent, with smaller particles generally following the endocytic route and larger particles taking the exocytic pathway [Chung *et al*., 2012]. The bursting of the endosome to release the nanocomplexes is facilitated initially by the ATPase mediated influx of H^+ ions into the late endosome, which partially dissolves the nanocomplexes, thus maintaining the pH at 5-6, and preventing formation of the lysosome [Wong *et al*., 2010]. This leads to an increase in the number of ions within the endosome which results in increased osmosis of water into the endosome. This culminates in the endosome bursting and releasing the free DNA/siRNA from the partially dissolved nanocomplexes and as well as the residual nanocomplexes into the cytoplasm [Rojas *et al*., 2015]. Another possible

release pathway of DNA/siRNA from the nanocomplex could be through ion exchange with cytoplasmic anions [Gu *et al*., 2008].

Release of the nucleic acid:LDH complex from the endosome, before the endosome can fuse with the lysosome is key to successful nucleic acid delivery. There are a number of endosomal escape mechanisms such as the 'proton sponge' hypothesis, the flip flop mechanism, the endosomal membrane fusion or destabilization mechanism, pore formation and photochemical internalization [Liang and Lam, 2012]. The 'proton sponge effect' causes endosomal bursting due to the influx of positive ions into the endosome, and this appears to be the mechanism of endosomal escape employed by LDHs.

The susceptibility of LDHs to changes in pH contributes to the controlled release properties exhibited by LDHs [Kriven *et al*., 2004; Zhang *et al*., 2012]. The pH dependent degradation of LDHs also prevents nanocarrier accumulation which could result in toxicity. Toxicity is also reduced due to the breakdown products of LDHs being biocompatible [Nagaraj *et al*., 2015]. Xu and Lu (2006) have indicated that LDH nanocomplexes undergo a reaction similar to the one shown below under physiological conditions:

$$MgAl\text{-}Cl\text{-}DNA + H^{+} \rightarrow Mg^{2+} + Al^{3+} + Cl^{-} + DNA + H_2O$$

The release of these cyto-friendly by-products aids in endosomal escape of the nanoparticles. The degradation products of LDHs, being small ions, may also leave the cell through "ion tunnels" and not accumulate in the cell thereby decreasing the possibility of cytotoxicity [Xu *et al*., 2006].

Overall the low cytotoxicity, high biocompatibility, controllable particle size, ease of availability, low cost, high loading capacity, effective load protection and controlled release properties, make LDHs an attractive gene therapy vehicle [Ladewig[2] *et al*., 2010; Chen *et al*., 2013].

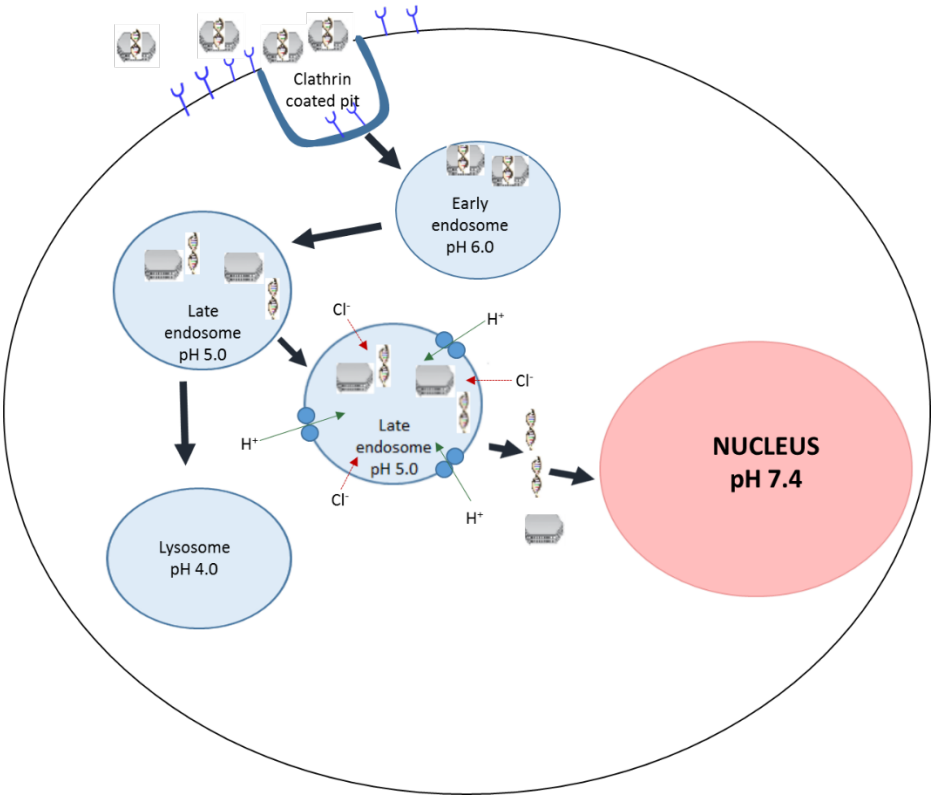

Figure 2.3 Diagrammatic representation of clathrin-mediated endocytosis [Adapted from Rojas *et al.,* 2015; Zhang *et al*., 2014; Choy *et al*., 2000].

2.3.3 FUNCTIONALIZATION OF HYDROTALCITE WITH AMINO ACIDS

The highly tunable surfaces of nanoparticles make them ideal scaffolds for various applications. Functionalization of nanoparticles is achieved by conjugating the vector with functional groups, which imparts either better payload binding capacity, enhanced intracellular delivery and/or targeted delivery. Cell targeting may be improved by the attachment of moieties such as ligands, which would deliver the payload to the intended cell by "homing in" to specific receptors on the target cell surface. There are a number of ways of functionalizing nano-carriers to achieve improved targeting, better membrane permeability or greater protection from degradation. Functionality may be provided by the attachment of a variety of ligands, oligonucleotides, proteins or antibodies [Mout *et al*., 2012]. Hu and co-workers (2013) have reported better condensation of pDNA, and higher levels of gene expression after functionalization of LDHs with disulfide-linked polycation brushes. Folic acid functionalization of siRNA-LDH complexes has

resulted in potent gene silencing *in vitro* and significantly high levels of tumor suppression *in vivo* [Park *et al*., 2016]. The preferential *in vivo* bio-distribution of chitosan functionalized LDHs to the lung paved the way for the development of organ-specific delivery systems [Kura *et al.,* 2014]. Kuo *et al*., (2015) have recently investigated LDHs as organ specific carriers with promising results.

Early endosomal escape appears to be the success-limiting step in gene therapy strategies. It may be possible to achieve better transfection by manipulation of the vector to cause faster endosomal escape, and one way of doing this is to functionalize the vector. Functionalization of vectors with arginine may have begun as a result of attempting to improve cellular internalization by bio-mimicking arginine-rich cell penetrating peptides [Zheng *et al*., 2015]. Arginine functionalized hydroxyapatites have displayed better transfection efficiency than non-functionalized hydroxyapatites [Wang *et al*., 2015]. Other arginine functionalized non-viral gene delivery systems such as chitosan and lipidosomes have also shown increased transfection efficiency and lower cytotoxicity when compared to non-functionalized chitosan [Gao *et al*., 2008; Wang *et al*., 2015]. Arginine is positively charged at physiological pH (Figure 2.4), which could enhance transfection is two ways. Firstly, the increased positive charge of the functionalized nanocomplex could lead to greater internalization of the complexes due to improved interaction between the complex and the negatively charged cell membrane. Secondly, the greater positive charge of the arginine-functionalized complex could also result in faster endosomal escape due to enhancement of the 'proton sponge' effect. This manipulation of the proton-sponge effect may also be applied to histidine, which is also positively charged at physiological pH. The incorporation of amino acids into LDHs is also relatively simple as amino acids act as anionic species above their isoelectric points, allowing for easy intercalation via ion exchange [Coelhoe *et al*., 2012]. Structures of arginine and histidine are shown in Figure 2.4. Xu and co-workers (2006) have also suggested that the addition of amino groups to a vector result in stronger interaction with the DNA chains. This indicates that the presence of amino acids on the LDH should lead to stronger interaction with DNA during complex formation, which could possibly result in better DNA protection and ultimately transfection.

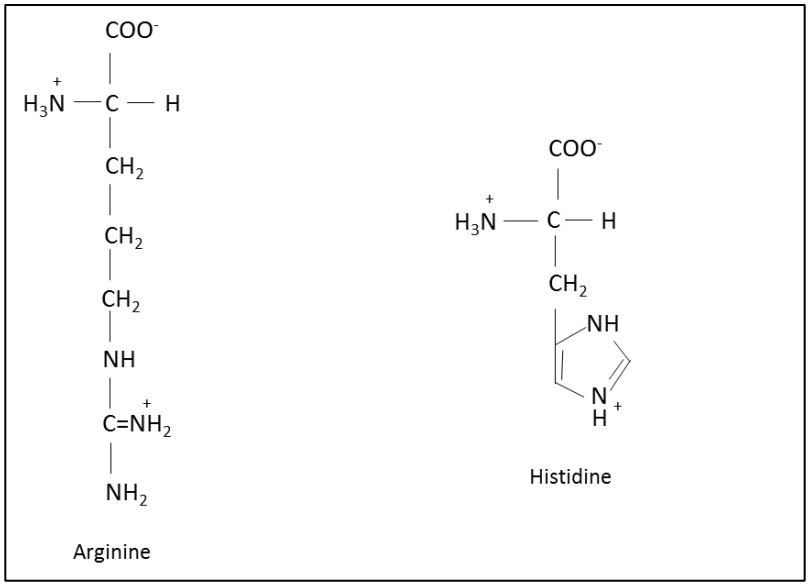

Figure 2.4 Amino acids arginine and histidine at physiological pH.

There have been a number of reports describing the functionalization of LDHs with amino acids [Aisawa *et al*., 2000; Aisawa *et al*., 2001; Nakayama *et al*., 2004; Aisawa *et al*., 2006]. Despite varying degrees of success in intercalating amino acids into LDHs, there has, as yet, not been any reports involving gene delivery using amino acid functionalized LDHs. This study therefore includes a comparison between the transfection efficiency of arginine or histidine functionalized HTs and non-functionalized HTs, in the delivery of DNA and siRNA.

CHAPTER THREE

3. PREPARATION AND CHARACTERISATION OF HYDROTALCITES AND HYDROTALCITE-LIKE COMPOUNDS

3.1 PREPARATION OF HYDROTALCITES AND HYDROTALCITE-LIKE COMPOUNDS

3.1.1 INTRODUCTION

Hydrotalcites (HT) and hydrotalcite-like (HT-like) compounds, also referred to as layered double hydroxides (LDHs) can be very easily synthesized in the laboratory by a number of methods. Synthetic LDHs may be composed of many different M^{II}/M^{III} cation combinations with different anions in the interlayer region. The particle shape and size can be controlled by adjusting synthesis conditions [Benito *et al*., 2010; Herrero *et al*., 2009; Oh *et al*., 2006; Xu *et al*., 2008; Zhao *et al* 2002].

Co-precipitation is the most commonly used method for the preparation of LDHs. In this method, aqueous solutions of M^{2+} and M^{3+} are slowly added to a solution containing the anion that is to be incorporated into the LDH, whilst maintaining a pH that is higher or equal to the pH at which the most soluble hydroxide is precipitated. Co-precipitation is also used in the preparation of organic anion-containing LDHs. Co-precipitation is followed by thermal or hydrothermal treatment to enhance yield and crystallinity of the prepared LDH.

There are two methods of co-precipitation, viz. precipitation at low supersaturation which involves addition of alkali to the reaction vessel (containing a solution of the anion to be intercalated) simultaneously to the addition of the metal salt solution, thus maintaining the pH at a selected value and precipitation at high supersaturation, where the metal salt solution is added to an alkaline solution containing the desired anion. Co-precipitation at low supersaturation has the advantage of forming more uniform LDHs with a higher crystallinity than that produced by co-precipitation at high supersaturation [He *et al*., 2005].

A co-precipitation method involving separate nucleation and aging steps reported by Zhao and co-workers in 2002 is a very rapid mixing and nucleation process in a colloid mill followed by a

separate aging process resulting in the production of small, uniform and highly crystalline product. Dong and co-workers (2014) prepared LDH nanoparticles by non-aqueous co-precipitation. Another modified co-precipitation method for the preparation of LDHs is referred to as the urea hydrolysis method. Costantino and co-workers (1998) prepared MgAl-carbonate, ZnAl-carbonate and NiAl-carbonate LDHs using the urea hydrolysis method. This method involves dissolving solid urea in a solution of the chosen metal chlorides and then maintaining this solution at 100 °C for 36 hours. The LDHs produced by this method have a larger particle sizes and higher charge density than those prepared by the other co-precipitation methods. The intercalated carbonate anions can be replaced with chloride by treating the LDH with gaseous or liquid HCl. Thereafter, chloride can be replaced quite easily by organic anions [Costantino *et al*., 1998]. Pérez-Bernal and co-workers (2009) prepared layered double hydroxides via the co-precipitation method in the presence of a surfactant, which controlled aggregation of particles through the formation of mixed micelles. The resultant crystals were larger and more ordered than those prepared by normal co-precipitation.

The interlayer anions of preformed LDHs can be replaced with guest anions by ion exchange. Ion-exchange may be carried out in one of two ways. Firstly, the precursor LDH would contain anions such as chloride, nitrate or perchlorate which would have a weak interaction with the LDH layers. The second method involves LDHs containing anions which are susceptible to acid attack such as carbonate or carboxylates [He *et al*., 2005]. The extent of ion-exchange depends on the affinity for the incoming anion, the nature of the exchange medium, the pH of the reaction solution and the chemical composition of the layers. Bontchev *et al*., (2003) showed that monovalent anion exchange preference is $Br^- > Cl^- > NO_3^- > I^-$ and was independent of the method of synthesis.

Upon calcination, i.e. heating LDHs to about 500 °C, the interlayer water, interlayer anions and the hydroxyl groups are removed. Calcined LDHs are able to regenerate its layered structure through the "memory effect" when exposed to water and anions [Bontchev *et al*., 2003; Klemkaite *et al*., 2011; Tao *et al*., 2006]. The anion does not have to be the same as the one that was present in the original sample, thus this is a method which can be used to introduce various other types of organic or inorganic anions into the interlayer. The reconstruction process is

carried out under nitrogen for incorporation of a non-carbonate anion since the carbonate LDH is preferentially formed in the presence of atmospheric carbon dioxide [He *et al.,* 2005]. Wang and co-workers (2005) preferentially intercalated 5-fluorouracil into an MgAl LDH using this restructure method.

Other methods for the preparation of LDHs include hydrothermal methods [Cavani *et al.,* 1991; Wang *et al*., 2013], secondary intercalation, salt-oxide method, non-equilibrium aging method, surface synthesis, templated synthesis, non-conventional aging methods, the sol-gel method and electrosynthesis [He *et al*., 2005]. Xu and co-workers (2010) have devised an atom-economic method of preparing LDHs, where the reactants are completely incorporated into the target product and there is no need for washing or filtering of the LDHs as there are no by-products. Modifications in the synthesis procedure has led to the production of LDHs with sheet-like morphology [Kelkar and Schutz, 1997], needle-shaped morphology [Kelkar and Schutz, 1997], LDH nanoscrolls [Ren *et al*., 2007; Lv *et al.,* 2015], LDH films [Kuang *et al*., 2010] and LDH nanorattles [Liu *et al*., 2011]. Another recent development involved the synthesis of LDHs using a mechano-chemical method to prepare highly dispersed LDH nanoparticles [Qu *et al*., 2016]. This mechano-chemical method is reported to produce less aqueous waste and requires less energy than conventional LDH preparation methods.

3.1.2 MATERIALS AND METHODS

$Mg(NO_3)_2.6H_2O$, $Al(NO_3)_3.9H_2O$, $Fe(NO_3)_3.9H_2O$, $Zn(NO_3)_2.6H_2O$, NaOH and Na_2CO_3 were all of analytical grade purchased from *Merck* (Darmstadt, Germany). L-Arginine and L-Histidine were obtained from *Sigma-Aldrich* (St Louis, USA).

The HT and HT-like compounds were prepared using the co-precipitation technique at low supersaturation. HT and HT-like compounds were prepared using M^{II}:M^{III} ratios of 2:1 and 3:1. To prepare a Mg-Al HT with a M^{II}:M^{III} ratio of 2:1 (denoted MgAl 0.33), 25.6 g (0.1 mol) $Mg(NO_3)_2.6H_2O$ and 18.75 g (0.05 mol) $Al(NO_3)_3.9H_2O$ were dissolved in 200 mL deionized water. The mixed metal solution was added dropwise to 1 L of a 0.5 M solution of Na_2CO_3, with vigorous stirring. The pH was maintained at 11 by addition of a 1 M NaOH solution as required. After

complete addition of the mixed cation solution, the suspension was transferred to a flat-bottomed flask, and heated to 80 °C under reflux for 18-20 hours. Thereafter, the precipitate was filtered and washed thoroughly until the filtrate had a pH of 7. The precipitate was then dried in an oven at 110 °C overnight. The resulting dry precipitate was ground to a fine powder (talc-like consistency) using a mortar and pestle.

Similarly, the Mg-Al HT with $M^{II}:M^{III}$ = 3:1 (denoted MgAl 0.25), was prepared using a mass of 25.6 g (0.1 mol) $Mg(NO_3)_2.6H_2O$ and 12.38 g (0.033 mol) $Al(NO_3)_3.9H_2O$. The arginine and histidine functionalized HTs were also prepared using the co-precipitation method. To prepare the arginine functionalized HT in the molar ratio Mg:Al:Arg of 2:1:1 (denoted MgAlArg 0.33), a mass of 5.12 g (0.02 mol) $Mg(NO_3)_2.6H_2O$, 3.76 g (0.01 mol) $Al(NO_3)_3.9H_2O$ and 2.11 g (0.01 mol) L-arginine hydrochloride was used.

The masses of all the precursors used in the preparation of the HTs and HT-like compounds (LDHs) in this study is shown in Table A1 (Appendix). The masses of the metal precursors and amino acids that were used to prepare amino acid-functionalized HT are shown in Table A2 (Appendix).

3.2 CHARACTERIZATION OF HYDROTALCITE AND HYDROTALCITE-LIKE COMPOUNDS

The prepared HT and HT-like compounds (LDHs) were characterized using powder X-ray diffraction (XRD), inductively coupled plasma-optical emission spectroscopy (ICP-OES), Fourier transform infrared spectroscopy (FTIR), transmission electron microscopy (TEM), scanning electron microscopy (SEM) and nanoparticle tracking analysis (NTA).

3.2.1 X-RAY DIFFRACTION

Single crystal X-ray diffraction (XRD) is usually the technique of choice for crystalline samples, but obtaining a single crystal sample from synthesized LDH is almost impossible due to the polycrystalline nature of the sample [Ennadi *et al*., 2000]. Powder XRD is therefore used to elucidate much of the structural information for LDHs.

Powder X-ray diffraction (PXRD) patterns were obtained using a Bruker D8 Advance diffractometer equipped with a graphite monochromator operating at 40 kV and 40 mA. The radiation source was a CuKα X-ray source with λ = 1.5406 Å. Data was collected at a step of 0.021 ° and at a scanning speed of 0.454 $°s^{-1}$.

3.2.2 INDUCTIVELY COUPLED PLASMA-OPTICAL EMISSION SPECTROSCOPY

Inductively coupled plasma- optical emission spectroscopy (ICP-OES) is used to detect and quantify elements in a solution.

The samples were analyzed on a Perkin Elmer Optical Emission Spectrometer Optima 5300 DV. The instrument was calibrated using a mixed metal standard solution. The standard solutions with concentrations of 20 ppm, 40 ppm, 60 ppm, 80 ppm and 100 ppm were prepared using ICP and atomic absorption spectroscopy standards of 1000 ppm (1000 Magnesium 1000, 1000 Aluminium 1000, 1000 Iron 1000 and 1000 Zinc 1000), which were obtained from Polychem Supplies cc (South Africa). Samples were prepared by dissolving 10 mg of the powdered compound in 10 mL of 0.1 M HNO_3. This solution was then diluted to 100 mL with double distilled water. Approximately 14 mL of each sample was transferred to ICP tubes and analyzed.

3.2.3 FOURIER-TRANSFORM INFRA-RED SPECTROSCOPY

Fourier-transform infrared spectroscopy (FTIR) is one of the principal tools for LDH characterization, used primarily for functional group identification. Each functional group absorbs specific IR radiation at different frequencies, making FT-IR a useful tool for indicating the presence or absence of a specific functional group in a compound. FT-IR is usually carried out in the infrared region (4000-250 cm^{-1}).

The samples were analyzed on a Perkin Elmer Spectrum Universal ATR 100 FT-IR Spectrometer. The crystal area was cleaned with methanol prior to analysis of each sample. Approximately, 0.5 g of each LDH sample was placed on the crystal area, the pressure arm was locked into place and the sample was then analysed.

3.2.4 SCANNING AND TRANSMISSION ELECTRON MICROSCOPY

Transmission electron microscopy (TEM) is an extremely useful nanoparticle characterization tool for the determination of particle distribution and ultrastructural morphology. Scanning electron microscopy (SEM) was carried out to determine the surface topography of the LDH samples.

For TEM, the samples were prepared by suspending 1 mg of the powdered sample in about 1 mL of double distilled water and sonicating the mixture for 15-20 minutes. About 1 µL of the suspended sample was placed on a copper grid, air-dried and then viewed under a JEOL 1010 Megaview 3 Soft Imaging TEM system. For SEM, a strip of double sided carbon tape (Nisshin EM, Co Ltd) was placed onto an SEM stub. The LDH sample was placed onto the stub and coated with gold particles using a Polaron SC500 Sputter Coater. The stub was placed in a LEO 1450 SEM, and analyzed using SmartSEM software version 5.03.05.

3.2.5 NANOPARTICLE TRACKING ANALYSIS

Particle size and zeta potentials are accurately determined using nanoparticle tracking analysis (NTA). Zeta (ζ) potential refers to the electric potential present in the double layer between the surface of a particle and the solvent/fluid in which the particle is suspended (Figure 3.1).

NTA was used to obtain both particle size and ζ-potential. A 1:1000 dilution of the LDH sample in double distilled water was analyzed in a NanoSight NS500 system (Malvern Instruments Ltd., Worcestershire, UK), using NanoSight nanoparticle tracking analysis software v3.2.

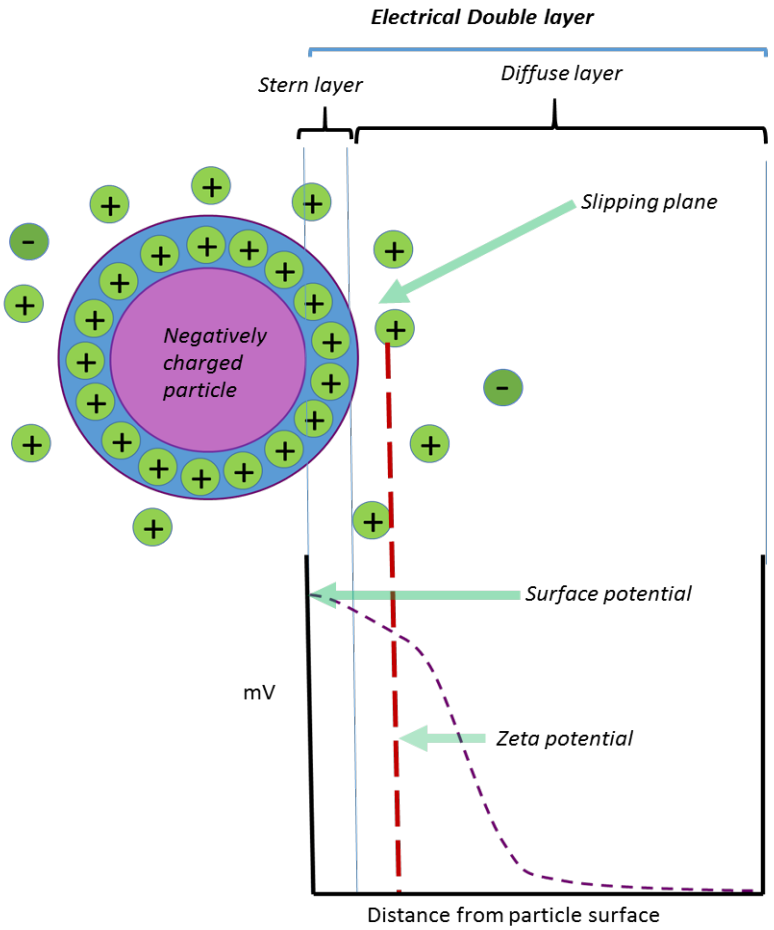

Figure 3.1 Diagrammatic representation of zeta potential [adapted from http://www.pharmainfo.net/book/emerging-trends-nanotechnology-pharmacy-physicochemical-characterization-nanoparticles/zeta Date accessed: 31st August 2017).

3.2.6 IDENTIFICATION OF AMINO ACIDS

The ninhydrin test is a very simple and inexpensive test to confirm the presence of amino groups in a sample. Ninhydrin reacts with the amines of amino acids to produce a blue or purple color. The ninhydrin test for this study was conducted using a chromatographic method. Standard samples of arginine and histidine as well as solutions of the amino acid-functionalized LDHs were spotted onto cellulose paper and then developed in a solvent system composed of n-butanol:acetic acid:water (5:2:2) containing 0.2 g of ninhydrin. Qiu *et al* (2010) have reported

that adding ninhydrin to the solvent system resulted in a cleaner and more rapid method for amino acid detection than the conventional post-staining method.

The actual amount of arginine present in the prepared samples (MgAlArg 0.25 and MgAlArg 0.33) was determined using a spectrophotometric method developed by Wang and co-workers (2008). This method involved the use of solutions of 8-hydroxyquinoline (0.2 % (w/v) in 95 % ethanol), 2 M sodium hydroxide and sodium hypobromite (2 % bromine (v/v) in 5 % sodium hydroxide). An arginine stock solution (100 μg/mL) was made up in 1 M sodium hydroxide. The arginine-functionalized LDH samples (0.01 g) were each dissolved in 1 mL of 10 M hydrochloric acid and this was made up to 5 mL in deionized water. The test samples contained 100 μL of the arginine-functionalized LDH samples in 2.4 mL of deionized water. Standard arginine samples (containing 10 μg – 60 μg) were prepared to a volume of 2.5 mL with deionized water. To a tube containing 2.5 mL of arginine solution, was added 0.5 mL of 8-hydroxyquinoline solution and 0.5 mL of 2 M sodium hydroxide. The solutions were thoroughly mixed and placed on ice for 10 minutes. Thereafter, 0.25 mL of cold sodium hypobromite and 0.5 mL of 40 % urea was added, thoroughly mixed and the optical density was measured at 500 nm using an Irmeco V1200 spectrophotometer. A deionized water blank solution was prepared in a similar manner.

Quantification of histidine in the prepared samples (MgAlHist 0.25 and MgAlHist 0.33) was conducted by adapting a method described by Patel and co-workers (2009). The color reagent was prepared by dissolving 200 mg sodium nitrite in 60 mL deionized water, followed by the addition of 1 mL concentrated hydrochloric acid. This solution was allowed to stand for 1 hour, after which 500 mg of sulphanilic acid was added and the final volume made up to 100 mL. The solution was allowed to stand for a further 30 minutes prior to use. A stock solution of standard histidine was prepared (100 μg/mL) in 1 M sodium hydroxide. Standard histidine samples (containing 10 μg – 50 μg) were prepared from the stock solution to a volume of 2.5 mL with deionized water. The histidine functionalized LDH samples (0.01 g) were each dissolved in 1 mL of 10 M hydrochloric acid and then made up to 5 mL with deionized water. The test samples comprised of 100 μl of the histidine-functionalized LDH samples added to 2.4 mL of deionized water and 100 μL 1 M sodium hydroxide. To a tube containing 2.5 mL of histidine solution, 5 mL

of colour reagent was added and allowed to stand for 5 minutes. The absorbance was measured at 405 nm using an Irmeco V1200 spectrophotometer with 1 M sodium hydroxide used as a blank.

3.3 RESULTS AND DISCUSSION

3.3.1 PHYSICAL PROPERTIES OF SYNTHESIZED LAYERED DOUBLE HYDROXIDES

All the LDHs synthesized were obtained in the form of smooth, finely textured powders. The prepared compounds denoted with "0.25" indicate a mole ratio of 3:1 (M^{2+}:M^{3+}) and those denoted with "0.33" indicate a mole ratio of 2:1 (M^{2+}:M^{3+}). The MgAl 0.25, MgAl 0.33, MgAlArg 0.25, MgAlArg 0.33, MgAlHist 0.25, MgAlHist 0.33, ZnAl 0.25 and ZnAl 0.33 samples were all pristine white, talc-like powders. The MgFe 0.25 sample appeared as a smooth, fine cream-coloured powder while the MgFe 0.33 sample had a similar texture, but appeared reddish-brown in color. The LDH samples were insoluble in water, but formed suspensions when vortexed or sonicated. Only the MgAl 0.33, MgAlArg 0.33 and ZnAl 0.33 samples remained in suspension indefinitely, whilst all the other samples eventually settled out in the water solution within 24 hours (Figure 3.2). This observation suggests partial dissolution of these LDH nanoparticles, a phenomenon confirmed to occur with HTs prepared in a Mg:Al ratio of 2:1 by aqueous stability studies [Nagaraj *et al*., 2015].

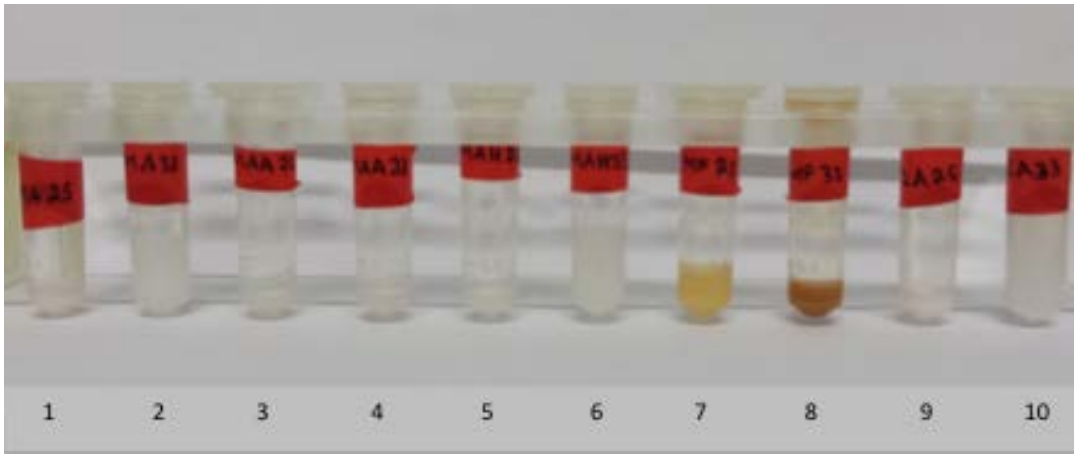

Figure 3.2 Solubility of HTs and LDHs in distilled water (1) MgAl 0.25, (2) MgAl 0.33, (3) MgAlArg 0.25, (4) MgAlArg 0.33, (5) MgAlHist 0.25, (6) MgAlHist 0.33, (7) MgFe 0.25, (8) MgFe 0.33, (9) ZnAl 0.25, (10) ZnAl 0.33.

3.3.2 CHARACTERIZATION OF LAYERED DOUBLE HYDROXIDES

3.3.2.1 POWDER X-RAY DIFFRACTION

Powder XRD is used to elucidate structural information about the LDHs, such as whether the sample is crystalline or amorphous, the size, lattice parameters, shape and orientation of a unit cell for a specific compound [Cullity and Stock, 2001.; Dinnebier and Billenge, 2008]. It is an important characterization tool as all crystalline solids have a unique, characteristic XRD pattern that may be used as a "fingerprint" in identification of a crystalline sample [Wilson, 1947].

All of the synthesized compounds displayed XRD patterns that were characteristic of LDHs, as exemplified by the XRD pattern of MgAl 0.33 shown in Figure 3.3. The individual XRD diffractograms of all the other LDHs synthesized are shown in Figures A1-A9 (Appendix).

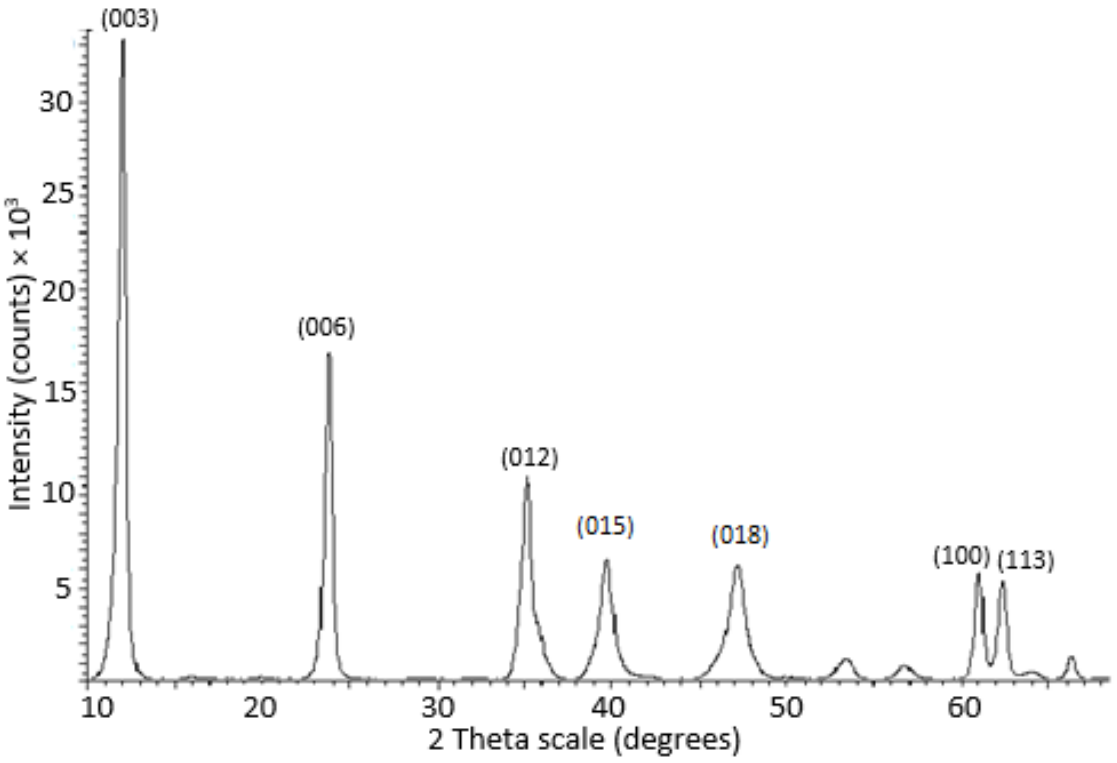

Figure 3.3 XRD pattern of MgAl 0.33.

All HT samples (Figures 3.4 and 3.5) displayed XRD patterns corresponding to hydrotalcite (ICDD 01-089-5434), where ICDD refers to "The international Centre for Diffraction Data". They all show sharp, symmetrical, intense peaks at the lower 2θ values [(003), (006)] and the broader, asymmetric and less intense peaks at the higher 2θ values [(012), (015), (018)] similar to XRD patterns of HTs reported in literature [Carja *et al.,* 2006; Kloprogge *et al*., 2002; Mora *et al*., 2014; Kloprogge and Frost, 1999; Kagunya *et al*., 1998; Li *et al*., 2014]. The samples prepared were also crystalline in nature as indicated by the sharpness and intensity of the peaks. Another characteristic of the XRD patterns of LDHs, clearly visible in Figure 3.3 is the doublet peak designated the (110) and (113) reflections at a 2θ value of approximately around 61- 63 °.

The diffraction peaks of the amino acid functionalized HTs exhibit a slight shift to lower 2θ angles, a phenomenon commonly observed after intercalation of amino acids into LDHs [Jiao *et al*., 2009]. The non-functionalized MgAl 0.25 sample displayed a $d_{(003)}$ basal spacing of 7.61, which was identical to the $d_{(003)}$ basal spacing of the arginine functionalized MgAlArg 0.25 sample. There was a very slight increase in basal spacing with the corresponding histidine functionalized sample (Table 3.1), where MgAlHist 0.25 displayed a $d_{(003)}$ basal spacing of 7.63. A similar trend was observed with the MgAl 0.33 samples. These results indicate that the arginine and histidine were most probably adsorbed onto the outer surface of the basal layer, as intercalation of the amino acid into the LDH interlayer would have resulted in a much greater increase in d-basal spacing as observed by Aisawa *et al* (2000), Aisawa *et al* (2001) and Coelho *et al* (2012). Similarly, Nakayama and co-workers (2004) have reported results showing intercalation of histidine into the interlayer of an MgAl LDH with a corresponding increase in basal spacing.

The MgFe 0.25 and MgFe 0.33 samples both showed XRD patterns corresponding to the LDH, pyroaurite (ICDD 01-070-2150) while the diffractograms of the ZnAl 0.25 and ZnAl 0.33 samples corresponded exactly to patterns referenced in ICDD 00-048-1025 and ICDD 00-048-1024, respectively.

The XRD patterns obtained for the ZnAl LDHs exhibit the characteristic sharp, intense peaks at low 2θ values with the doublet peak at around 60 ° similar to those obtained by Kooli and co-workers (1997) and Nagaraj and co-workers (2015).

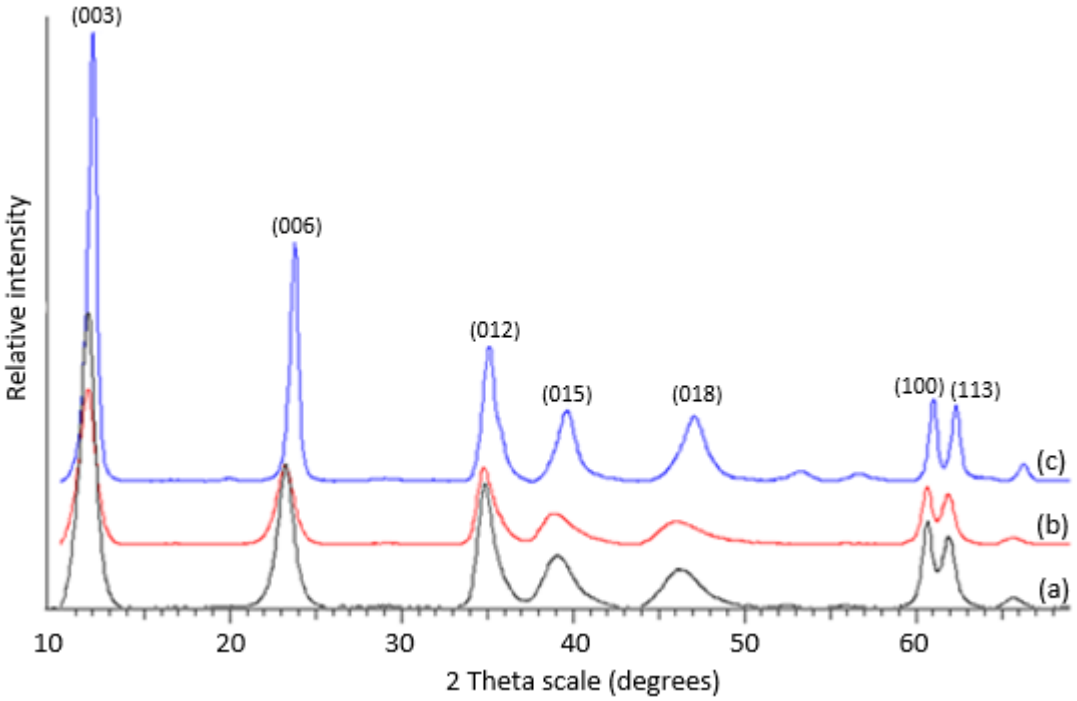

Figure 3.4 XRD patterns of (a) MgAlArg 0.25, (b) MgAlHist 0.25 and (c) MgAl 0.25.

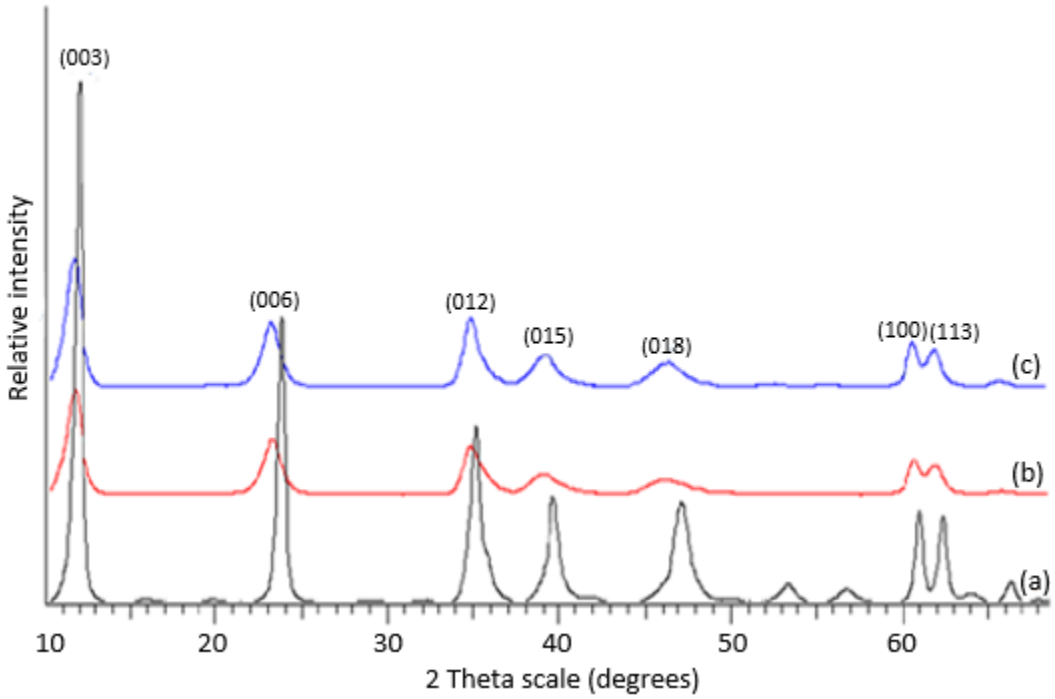

Figure 3.5 XRD patterns of (a) MgAl 0.33, (b) MgAlArg 0.33 and (c) MgAlHist 0.33.

Table 3.1 d-basal spacing for LDH compounds.

		Basal Spacing / Å						
Compound	**$M^{II}:M^{III}$**	**$d_{(003)}$**	**$d_{(006)}$**	**$d_{(012)}$**	**$d_{(015)}$**	**$d_{(018)}$**	**$d_{(110)}$**	**$d_{(113)}$**
MgAl 0.25	0.25	7.61	3.83	2.57	2.30	1.96	1.52	1.49
MgAl 0.33	0.33	7.42	3.75	2.55	2.26	1.92	1.51	1.48
MgAlArg 0.25	0.25	7.61	3.83	2.57	2.30	1.97	1.52	1.50
MgAlArg 0.33	0.33	7.61	3.84	2.58	2.31	1.97	1.52	1.50
MgAlHist 0.25	0.25	7.63	3.84	2.57	2.34	1.96	1.52	1.50
MgAlHist 0.33	0.33	7.42	3.75	2.55	2.27	1.93	1.51	1.49
MgFe 0.25	0.25	7.61	3.84	2.60	2.32	1.97	1.54	1.52
MgFe 0.33	0.33	7.49	3.78	2.59	2.30	1.95	1.54	1.51
ZnAl 0.25	0.25	7.46	3.75	2.57	2.28	1.93	1.53	1.50
ZnAl 0.33	0.33	7.36	3.72	2.56	2.27	1.93	1.53	1.50

As previously mentioned, the prepared compounds denoted with “0.25” indicate a mole ratio of 3:1 ($M^{2+}:M^{3+}$) and those denoted with “0.33” indicate a mole ratio of 2:1 ($M^{2+}:M^{3+}$), the latter having more trivalent metals present. Brindley and Kikkawa (1979) reported that an increase in the amount of trivalent metal results in a decrease in both lattice parameters, *a* and *c*. Lattice parameter c decreases because as M^{3+} ions increase, the electrostatic attraction between the positive and negative interlayers also increases. Lattice parameter *a,* decreases with increasing M^{3+} ions because M^{3+} are generally smaller in size than M^{2+} ions and the higher charge of the trivalent ion combined with the smaller ionic radii leads to shorter bond lengths. This trend can be clearly seen in Table 3.2.

Table 3.2 The *a*, *c* and c_0 parameters of the prepared LDHs in angstroms.

Compound	$d_{(003)}$	*c*	$d_{(110)}$	*a*
MgAl 0.25	7.61	22.83	1.52	3.04
MgAl 0.33	7.42	22.26	1.51	3.02
MgAlArg 0.25	7.61	22.83	1.52	3.04
MgAlArg 0.33	7.61	22.83	1.52	3.04
MgAlHist 0.25	7.63	22.89	1.52	3.04
MgAlHist 0.33	7.42	22.26	1.51	3.02
MgFe 0.25	7.61	22.83	1.54	3.08
MgFe 0.33	7.49	22.47	1.54	3.08
ZnAl 0.25	7.46	22.38	1.53	3.06
ZnAl 0.33	7.36	22.08	1.53	3.06

The interlayer spacing of LDHs containing carbonate is 7.8 Å [Kloprogge and Frost, 1999], the same as the interlayer spacing for chloride containing LDHs [Rossi *et al.*, 2005]. The replacement of carbonate by nitrate anions should result in a slight increase of interlayer space to between 8.1 Å [Kloprogge *et al*., 2002] to 8.8 Å [Nagaraj *et al*., 2015], thus the lower interlayer spacing of prepared samples suggests that some carbonate may have been incorporated into the interlayers during LDH preparation. This was expected as the LDHs were not prepared under nitrogen, which would have aided in decreasing the level of contamination by atmospheric carbonate anions. The results in Tables 3.1 and 3.2 shows a decreased interlayer spacing closer to 7.6 Å for the Mg/Al LDHs which seems to agree more with the values reported by Bookin and Drits (1993) and Li and co-workers (2014), indicating the presence of carbonate anions in the interlayer region of the prepared LDHs. This may have an effect on the ion exchange capacity of the LDHs prepared as carbonate anions have a high affinity for the hydroxide layers in LDHs [Kloprogge *et al*., 2002]. The basal spacings for ZnAl 0.25 and ZnAl 0.33 was 7.46 and 7.36 Å respectively which was quite

different from previously reported values of 8.53 – 8.92 Å [Salak *et al*., 2012]. This suggests that carbonate was incorporated as the interlayer anion instead of nitrate in the ZnAl LDHs as well.

3.3.2.2 INDUCTIVELY COUPLED PLASMA-OPTICAL EMISSION SPECTROSCOPY

The ICP results are shown in Table 3.3.

Table 3.3 ICP data for LDHs.

Compound	**Stoichiometry**	**M^{II}:M^{III}**	
		Calculated ratio	**Actual ratio**
MgAl 0.25	0.25	3:1	3.04 : 1
MgAl 0.33	0.33	2:1	2 : 1
MgAlArg 0.25	0.25	3:1	2.94 : 1
MgAlHist 0.25	0.25	3:1	2.98 : 1
MgAlArg 0.33	0.33	2:1	2.46 : 1
MgAlHist 0.33	0.33	2:1	2.07 : 1
MgFe 0.25	0.25	3:1	3.32 : 1
MgFe 0.33	0.33	2:1	1.96 : 1
ZnAl 0.25	0.25	3:1	3.49 : 1
ZnAl 0.33	0.33	2:1	2.16 : 1

The actual ratio of M^{II}:M^{III} for HT and HT-like compounds were very similar to the calculated ratios. This indicates that the desired products were most likely formed. Both MgAlArg 0.33 and ZnAl 0.25 also showed a substantial deviation from the desired M^{II}:M^{III} ratio. ICP results indicate a higher concentration of the divalent cation in both cases. A possible reason for this is that the greater repulsion between trivalent ions resulted in more spaces being available for the divalent ions to occupy.

3.3.2.3 FOURIER-TRANSFORM INFRARED SPECTROSCOPY

Analysis of the infrared spectra of the LDHs revealed three major types of vibrations, viz. vibrations as a result of the interlayer anions, vibrations due to the hydroxyl groups (molecular vibrations) and vibrations due to the octahedral layers (lattice vibrations) [Hernandez-Moreno *et al*., 1985].

The FTIR spectra of the HTs are shown in Figures 3.6 and 3.7. The v(OH) stretching modes can be seen at around 3440 cm^{-1}, presenting at slightly lower wavenumbers than free hydroxyl groups which have an average v(OH) value of 3620 cm^{-1} [Kagunya *et al*., 1998]. This may be attributed to the hydroxyl groups in the samples being hydrogen bonded to lattice water. The band occurring at around 1650 is due to interlayer water bending modes [Kloprogge and Frost, 1999]. Water is strongly bonded to both the anions and the hydroxyl surfaces of the LDHs and the presence of the water bending modes indicate that water plays an important role in the structure of the LDHs [Palmer *et al*., 2009].

Vibrations occurring below 800 cm^{-1} are assigned v(M-O) or metal-oxygen absorption bands [Kooli *et al*., 1997., Wu *et al*., 2014., Mallakpour and Dinari, 2016]. The bands appearing around 500 cm^{-1} can be assigned to the translational modes of hydroxyl groups influenced by trivalent aluminium, while the bands around 600 cm^{-1} are due to translational modes of hydroxyl groups influenced by divalent magnesium [Millange *et al*., 2000].

Bands due to intercalated and adsorbed anions are observed between 1800-1000 cm^{-1} [Medina-Juárez *et al*., 2016]. The strong reflection between 1300 and 1400 cm^{-1} is associated with the asymmetric stretching modes of the interlayer carbonate ions (v_3 vibrational mode of CO_3^{2-}) [Kooli *et al*., 1997; Millange *et al*., 2000; Frost *et al.,* 2003]. A band associated with the CO_3^{2-} - H_2O bridging mode in the interlayer at around 3000 cm^{-1} [Kloprogge *et al.,* 2002; Kloprogge and Frost, 1999; Millange *et al*., 2000], would have confirmed incorporation of carbonate within the interlayer. The absence of this band suggests that perhaps some nitrate and amino acid residues (in the case of the amino acid functionalized HTs) may have also been incorporated into the interlayer.

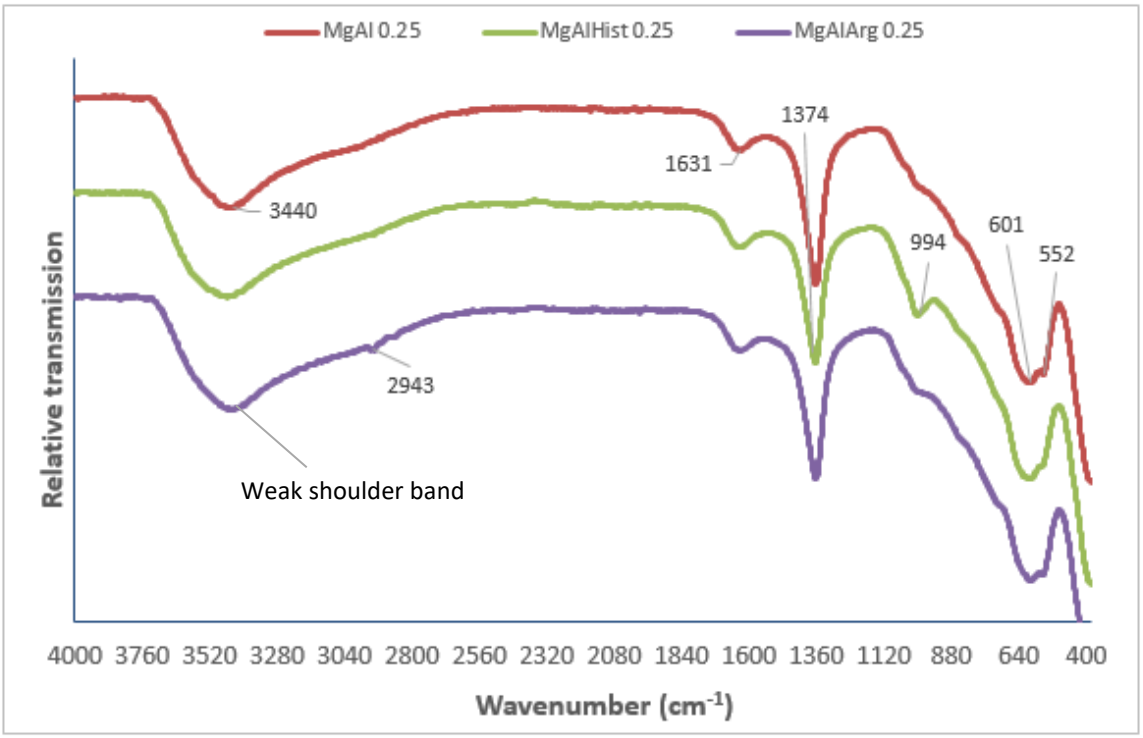

Figure 3.6 FTIR patterns of MgAl 0.25, MgAlArg 0.25 and MgAlHist 0.25.

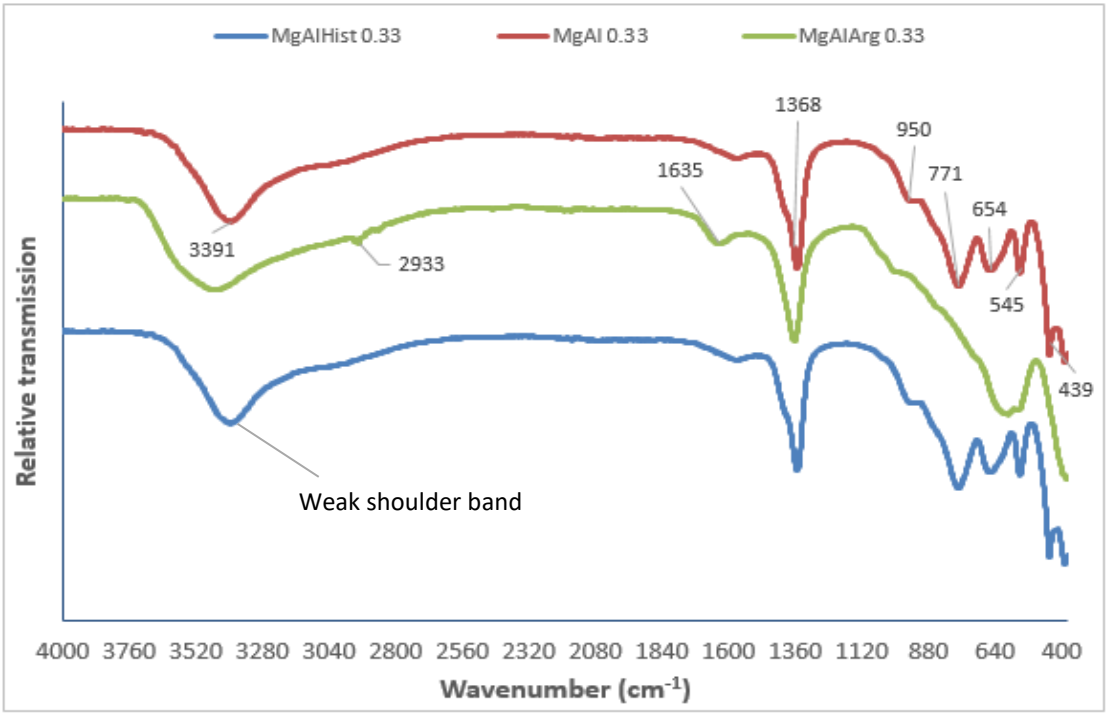

Figure 3.7 FTIR patterns of MgAl 0.33, MgAlArg 0.33 and MgAlHist 0.33.

The weak shoulder at around 3100 cm^{-1} (shown in figures 3.6 – 3.8) is ascribed as the stretching modes of hydroxyl groups linked to carbonate ions [Kagunya *et al*., 1998]. Weak CO_3^{2-} vibrational modes are also present between 700 and 1100 cm^{-1}, with v_4 vibrational modes of CO_3^{2-} generally occurring at around 730 cm^{-1}, v_2 at around 850 cm^{-1} and v_1 at around 1000 cm^{-1} [Kloprogge *et al.,* 2001].

FTIR spectra of the aa-functionalized hydrotalcites all exhibit O-H stretching modes between 3400 cm^{-1} and 3600 cm^{-1}, strong reflections between 1300 cm^{-1} and 1400 cm^{-1} due to asymmetric stretching of carbonate ions and low frequency vibrations between 400 cm^{-1} and 800 cm^{-1} attributed to M-O and M-O-M vibrations of the LDH lattice [Kooli *et al*., 1997; Kagunya *et al*., 1998; Millange *et al*., 2000; Li[1] *et al.,* 2014; Choi *et al*., 2015].

Bands attributed to symmetric and asymmetric stretching of the COO^- groups of the amino acids usually occur between 1400 cm^{-1} and 1600 cm^{-1}, but these bands are not clearly visible in the spectra shown possibly due to the low levels of incorporation of the amino acids into the HTS [Aisawa *et al*., 2000; Aisawa *et al*., 2001; Kumar and Rai, 2010; Choi *et al.,* 2015]. The band at 2943 cm^{-1} for MgAlArg 0.25 and at 2933 cm^{-1} for MgAlArg 0.33 are characteristic for arginine FTIR spectra and correspond to asymmetric stretching of the methyl group [Kumar and Rai, 2010]. Bands due to a mixed vibration of COO^- asymmetric stretching and NH bending modes of the histidine moiety usually occur at around 1630 cm^{-1} [Kumar *et al*., 2010] and the band due to guanidine C=N stretching and C=O carbonyl stretching which would normally be seen at around 1700 cm^{-1} [Imani *et al.,* 2015; Barth, 2000] but these appear to be masked here by the interlayer water bending modes.

The infrared spectra of of HT-like compounds (MgFe 0.35, MgFe 0.33, ZnAl 0.25 and ZnAl 0.33) show similar patterns to the spectra of the HTs (see Figure 3.8). The spectra are characteristic of LDHs. The O-H stretching of water molecules appear at around 3440 cm^{-1}, the H-OH bands occur at around 1650 cm^{-1}, the peak at around 1300 corresponds to the intercalated carbonate anions and the M-O (metal-oxygen) absorption bands occur below 800 cm^{-1} [Frost[1] *et al*., 2003; Choi *et al*., 2015; Komarala *et al*., 2016].

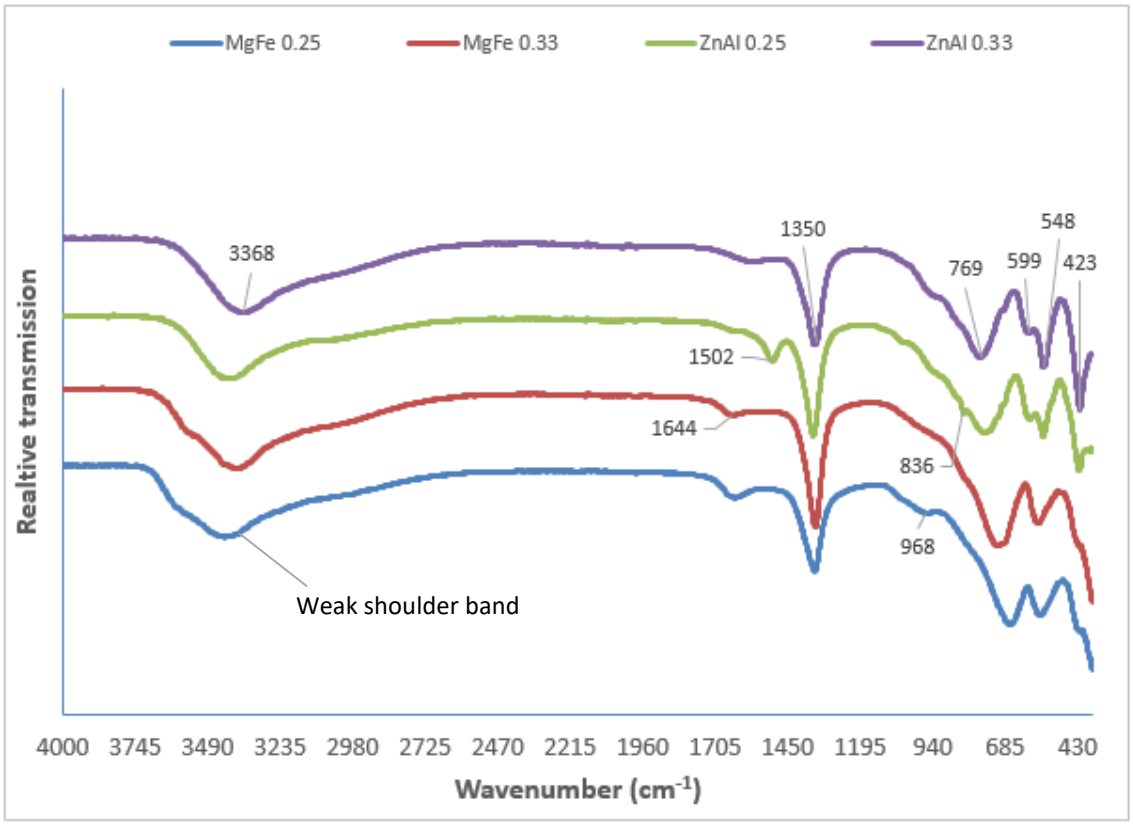

Figure 3.8 FTIR patterns of MgFe 0.25, MgFe 0.33, ZnAl 0.25 and ZnAl 0.33.

3.3.2.4 SCANNING AND TRANSMISSION ELECTRON MICROSCOPY

The TEM and SEM images of the hydrotalcite, MgAl 0.25 are shown in Figure 3.9. The crystals generally appear as hexagonal platelets, tending to agglomerate, resulting in the platelets being piled on top of each other. TEM analysis at 150 000X magnification shows irregularly shaped crystals with most being in the size range of less than 50 nm. It has been suggested that irregularity in shape occurs due to crystal defects [Wang *et al*., 2012]. SEM analysis at a much lower magnification (42.61 K X), also shows some larger particles with a lateral width of about 100 nm. This indicates a large size distribution of the LDH nanoparticles. The morphology observed for MgAl 0.25 was similar to that reported by Mondal and co-workers (2016).

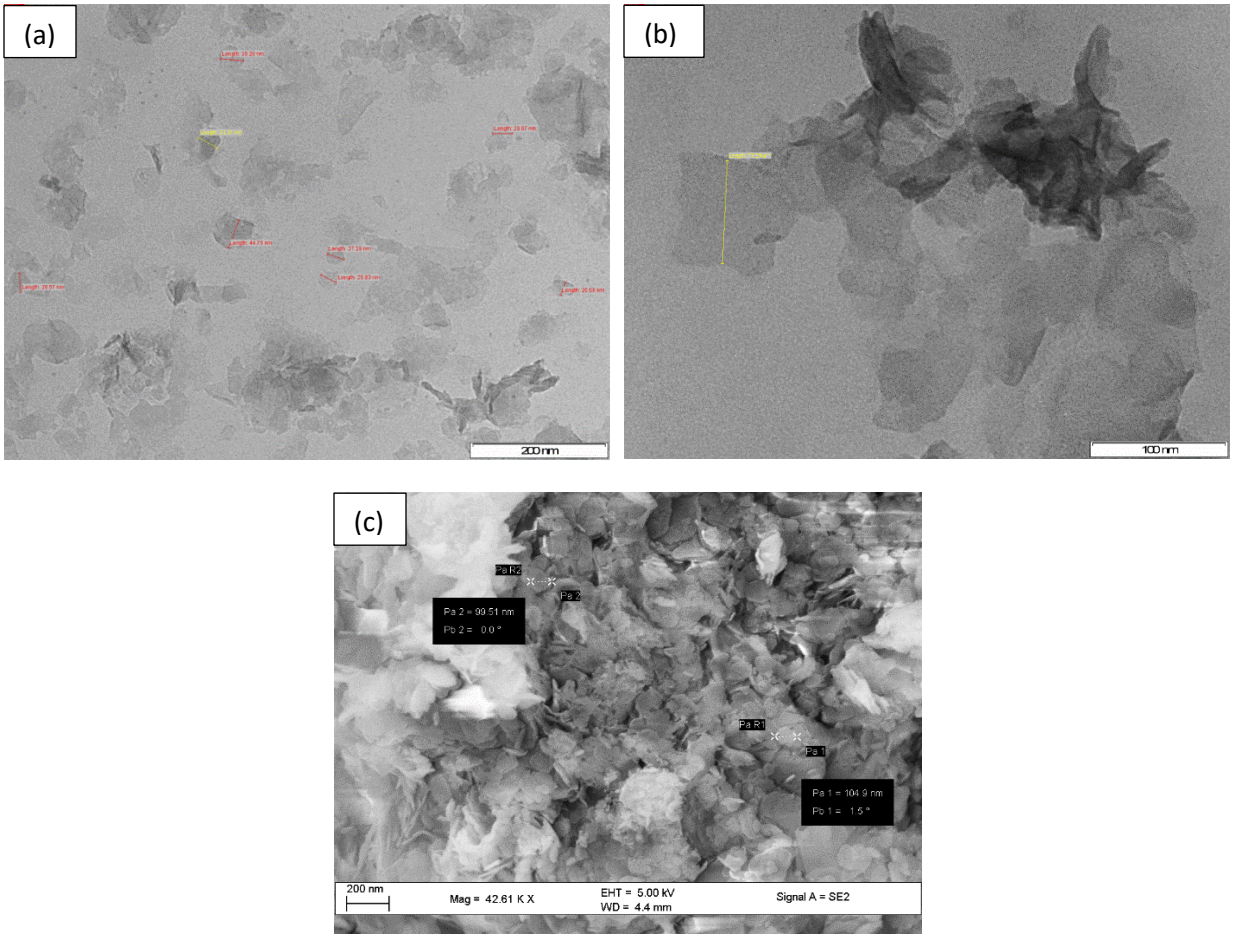

Figure 3.9 Electron microscopy images of MgAl 0.25 (a) TEM at 150K magnification, (b) TEM at 300K magnification and (c) SEM at 42.61K magnification. The bars represent (a) 200 nm, (b) 100 nm and (c) 200 nm respectively.

The MgAl 0.33 hydrotalcite sample shows a similar flat platelet type structure, typical of layered double hydroxides (Figure 3.10). The particles appear more uniform in shape when compared to the MgAl 0.25 sample. Both TEM and SEM indicate a more even particle size distribution with most of the particles within the 20-70 nm range. The rod-like structures visible on the TEM micrographs are most likely particles lying on either sides or in a position not in the direct plane of view.

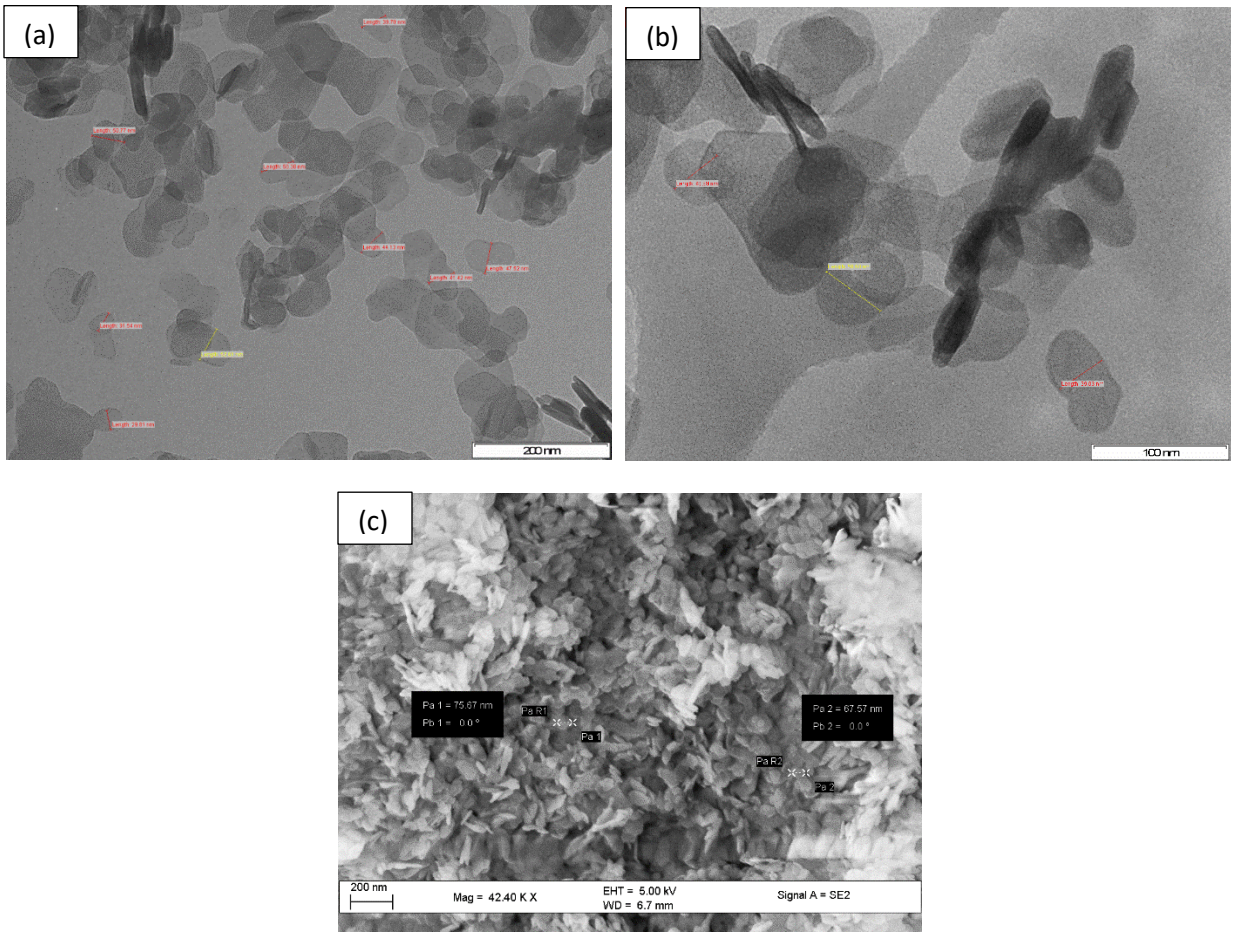

Figure 3.10 Electron microscopy images of MgAl 0.33 (a) TEM at 150K magnification, (b) TEM at 300K magnification and (c) SEM at 42.40K magnification. The bars represent (a) 200 nm, (b) 100 nm and (c) 200 nm respectively.

TEM and SEM analysis of the aa-functionalized LDHs are shown in Figures 3.11 and 3.12. These LDHs exhibit the characteristic flat platelet like structure of the non-functionalized LDHs. Although XRD analysis of the aa-functionalized LDHs suggest that the amino acid groups are most probably attached to the external surfaces of the LDH molecules, it is not possible for the amino acid moieties to be viewed at the magnifications used here for TEM and SEM, due to their very small size. The sizes of the arginine functionalized LDHs ranged between 20 and 50 nm. The size of the histidine functionalized LDH MgAlHist 0.25 appear to average around 70 nm, while the MgAlHist 0.33 particles appear much smaller, and range between 15 and 50 nm.

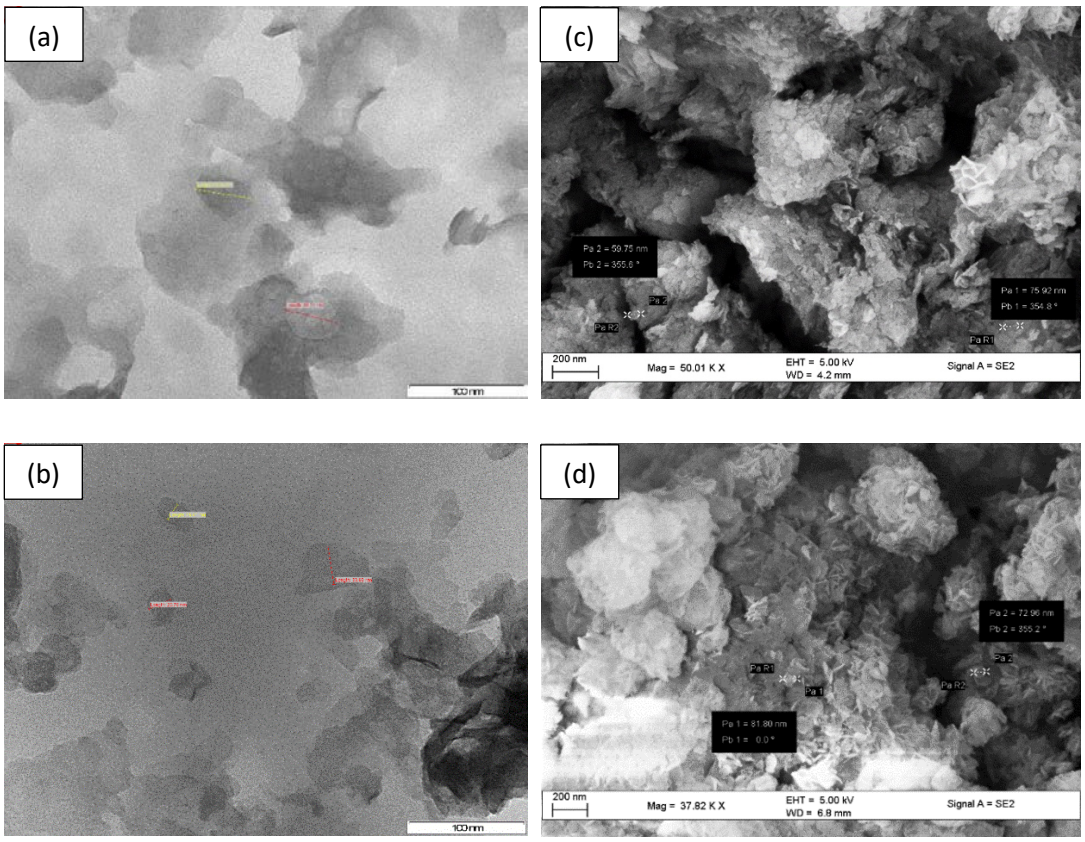

Figure 3.11 Electron micrographs showing TEM images of arginine functionalized LDHs (a) MgAlArg 0.25 and (b) MgAlArg 0.33 at 300K magnification, and SEM images of (c) MgAlArg 0.25 and (d) MgAlArg 0.33 at 50.01K and 37.82K magnification respectively. The bars represent (a) 100 nm, (b) 200 nm, (c) 100 nm and (d) 200 nm respectively.

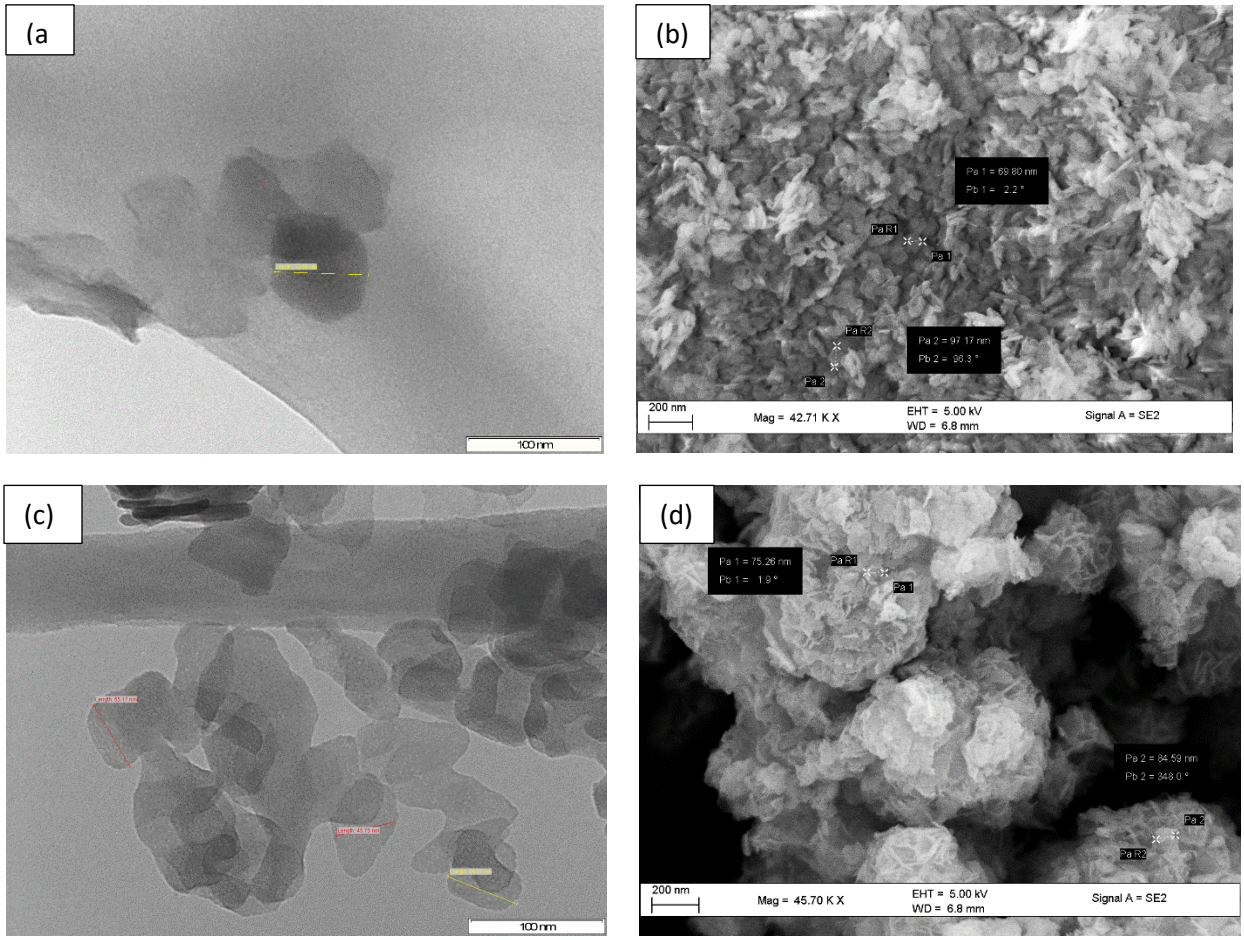

Figure 3.12 Electron micrographs showing TEM images of histidine functionalized LDHs (a) MgAlHist 0.25 and (b) MgAlHist 0.33 at 300K magnification, and SEM images of (c) MgAlHist 0.25 and (d) MgAlHist 0.33 at 42.71K and 45.70K magnification respectively. The bars represent (a) 100 nm, (b) 200 nm, (c) 100 nm and (d) 200 nm respectively.

The particle morphology of the MgFe 0.25 and MgFe 0.33 LDHs appear very similar to each other (Figures 3.13 and 3.14). Typical hexagonal flat platelets are observed with a wide size distribution. The lateral particle size range for MgFe 0.25 was 40-80 nm, whilst that of MgFe 0.33 ranged from 70-200 nm. SEM at low magnification also revealed the presence of some larger particles in the 150-300 nm range, once again emphasizing the wide particle size distribution of the samples.

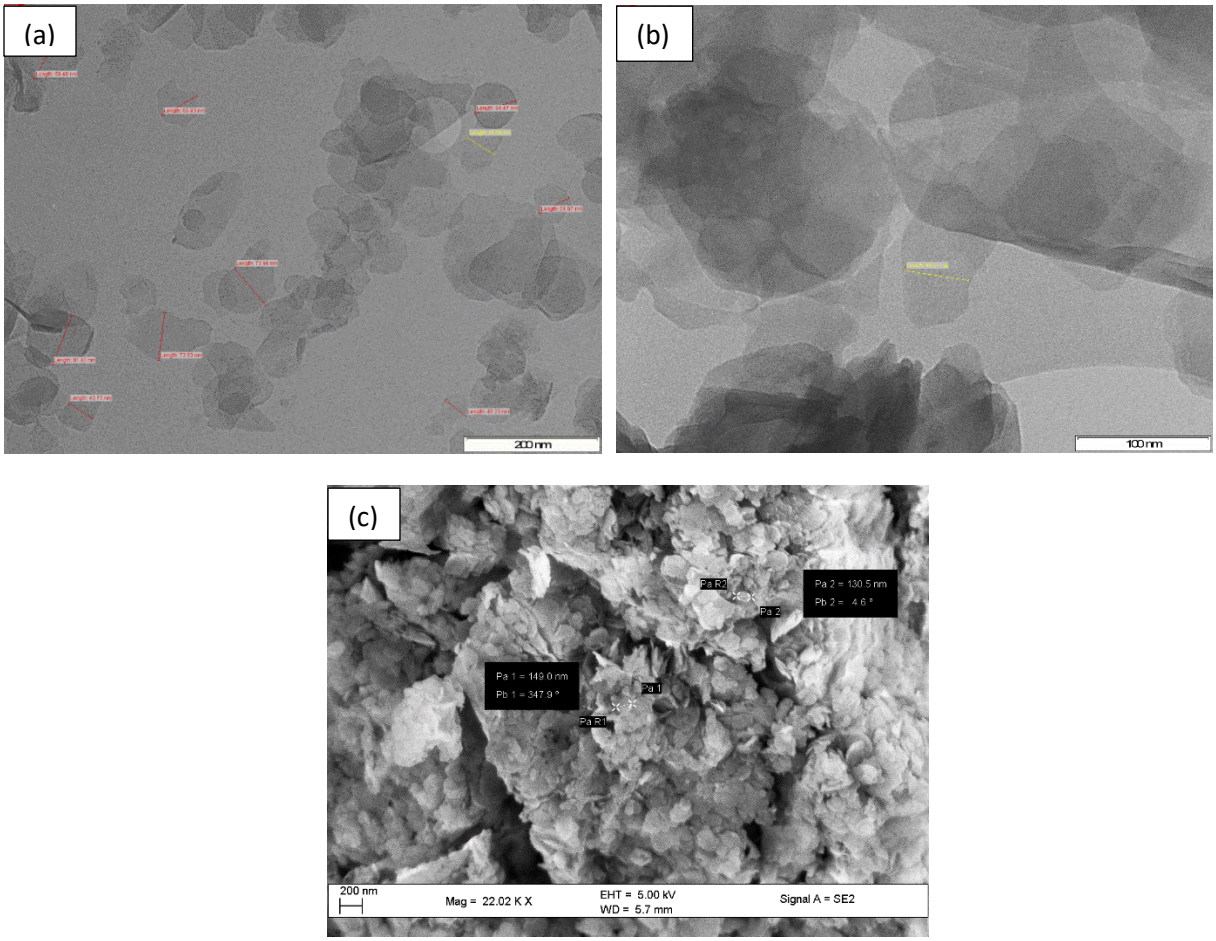

Figure 3.13 Electron microscopy images of MgFe 0.25 (a) TEM at 150K magnification, (b) TEM at 300K magnification and (c) SEM at 22.02K magnification. The bars represent (a) 200 nm, (b) 100 nm and (c) 200 nm respectively.

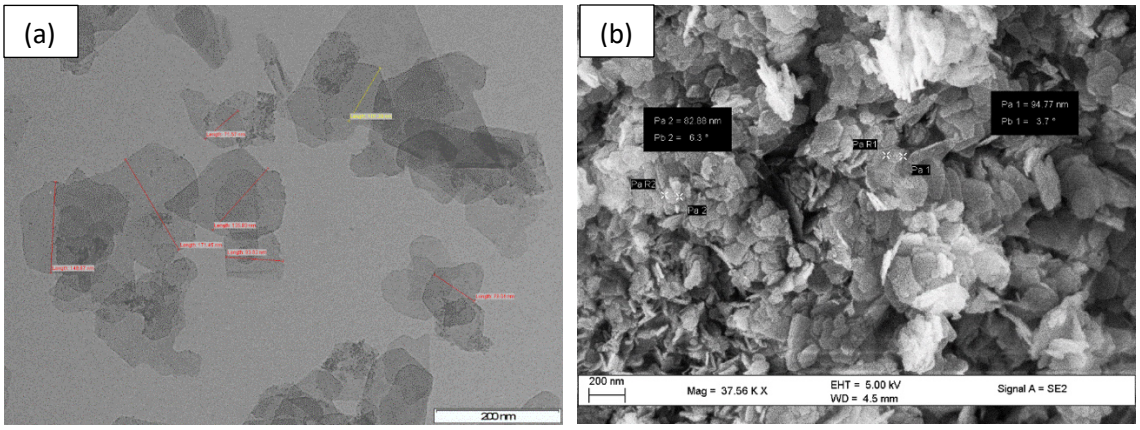

Figure 3.14 Electron microscopy images of MgFe 0.33 (a) TEM at 150K magnification and (b) SEM at 37.56K magnification. The bars represent 200 nm.

The ZnAl 0.25 and ZnAl 0.33 LDHs also exhibited the typical hexagonal shaped flat platelet structure, clearly visible in both the TEM and SEM micrographs (Figures 3.15 and 3.16). These platelets appear much denser (opaque) than the MgAl and MgFe LDHs. The lateral size distribution ranged from 50 nm to 200 nm. Nagaraj and co-workers (2015) have synthesized ZnAl LDHs in a ratio of Zn:Al (2:1) and have reported similar particle morphology and size, as have Kloprogge and co-workers (2004).

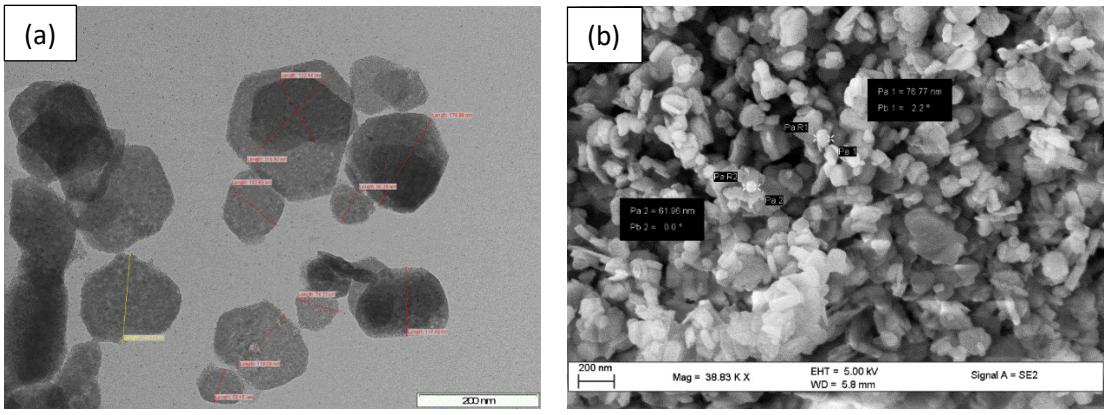

Figure 3.15 Electron microscopy images of ZnAl 0.25 (a) TEM at 150K magnification, and (b) SEM at 38.83K magnification. The bars represent 200 nm.

The general appearance of the LDHs obtained in this study is very similar to that in recent reports [Rojas *et al*., 2015; Kriven *et al*., 2004; Chen *et al*., 2013], and is typical of LDHs aged in the supernatant resulting from the nucleation step, with larger particles of a wide size distribution. Separate nucleation and aging steps would have resulted in more symmetrical and smaller sized particles [Zhao *et al*., 2002; Xu *et al*., 2006]. The size of the LDH nanoparticles is significant for biological applications, as reports suggest that LDHs display size-dependent toxicity. Choi and co-workers (2008) have reported that LDH particles less than 50 nm in length was more toxic than larger particles within the size range of 100-200 nm. There is a wide size distribution of the LDHs prepared in this study, with most of the particles being within the 'safe' or low cytotoxicity size range.

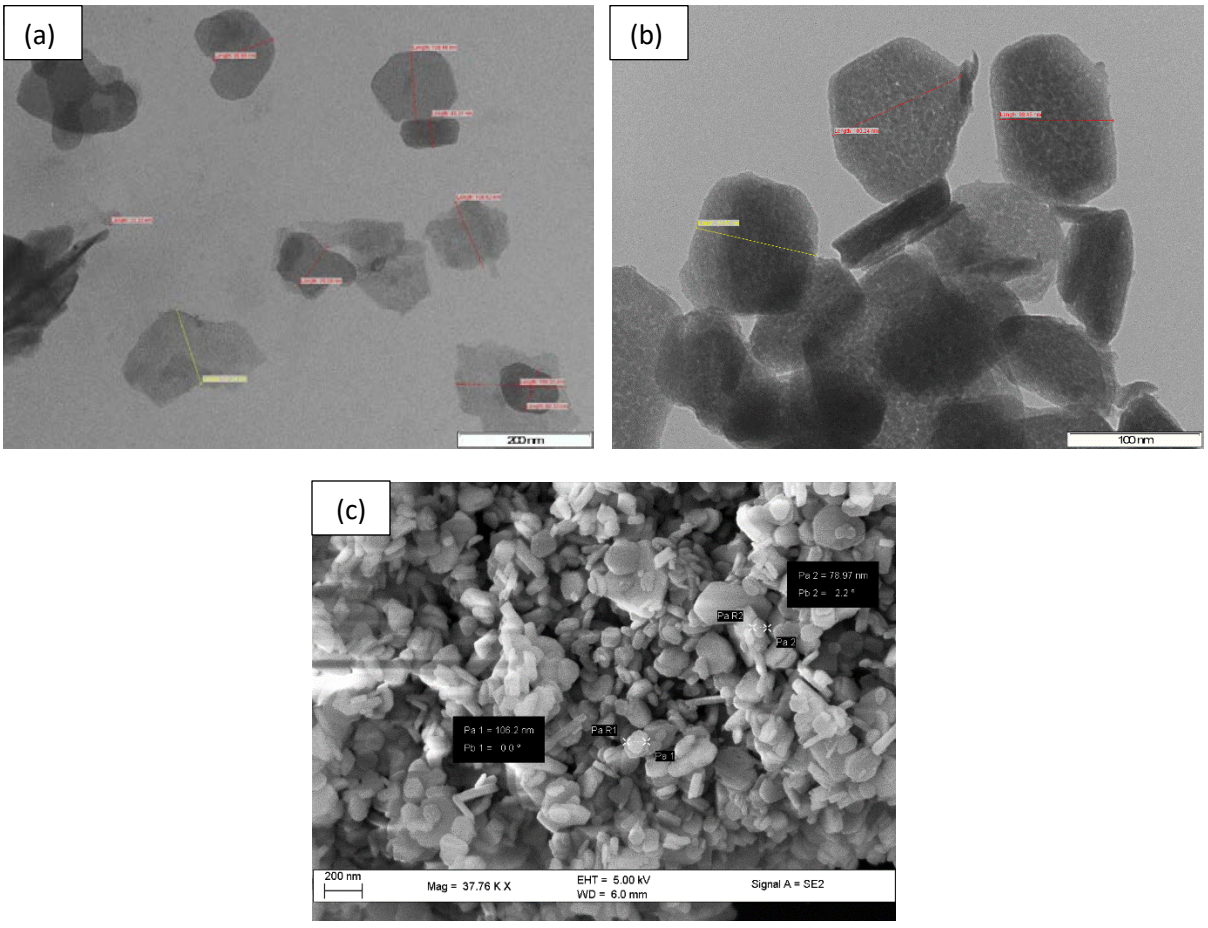

Figure 3.16 Electron microscopy images of ZnAl 0.33 (a) TEM at 150K magnification, (b) TEM at 300K magnification and (c) SEM at 37.76K magnification. The bars represent (a) 200 nm, (b) 100 nm and (c) 200 nm respectively.

3.3.2.5 NANOPARTICLE TRACKING ANALYSIS (NTA)

The efficacy of nanoparticle mediated delivery is affected by physicochemical properties such as size, shape and surface charge [Dong *et al*., 2015]. The size of nanoparticles greatly affects its interaction with cells, and influences cellular uptake efficiency, route of internalization, localization within the cell as well as cytotoxicity [Shang *et al*., 2014; Rojas *et al*., 2015].

Zeta potential provides an indication of the stability of a colloidal dispersion. Zeta potential depends not only on the properties of the nanoparticle but also on its environment and is thus affected by both pH and ionic strength of the suspension fluid [Xu, 2008]. It is extremely important to assess the ζ-potential of nanoparticles to be used for biological studies, as it greatly affects interactions between the nanoparticles themselves, the interactions between cells and nanoparticles, and also affects the cell targeting ability of the nanoparticles.

The modal size and ζ-potential values are recorded in Table 3.4. The large particle size distribution observed by TEM and SEM was confirmed by NTA, which revealed size variations of up to ± 100 nm of the modal size value.

Table 3.4 Size and zeta potential of LDHs.

LDH	SIZE (nm)	ZETA POTENTIAL (mV)
MgAl 0.25	148.4	-11.6
MgAl 0.33	72.4	15.0
MgAlArg 0.25	193.1	-19.8
MgAlArg 0.33	123.7	6.7
MgAlHist 0.25	60.8	-24.6
MgAlHist 0.33	44.5	22.7
MgFe 0.25	307.4	1.2
MgFe 0.33	27.9	-12.8
ZnAl 0.25	30.0	-7.2
ZnAl 0.33	67.9	29.7

TEM analysis of MgAl 0.25 showed most of the nanoparticles to be in the ±50 nm size range, whereas NTA analysis revealed a modal size of 148.4 nm. This could be as a result of particle aggregation. Generally, ζ-potential values much greater or less than zero indicate high colloidal stability whereas ζ-potential values closer to zero represent lower stability and thus greater aggregation of the nanoparticles. This phenomenon is well represented by the MgFe 0.25 LDHs (Table 3.4), where rather large particle size was observed (307.4 nm) with the ζ-potential value close to zero (1.2 mV). The larger particle size observed may be attributed to aggregation of smaller particles. This theory is well supported when considering that the particle size seen for MgFe 0.25 LDHs using TEM was 40-50 nm. The sizes of the other non-functionalized LDHs appear to be similar to that observed by TEM analysis.

The sizes of the arginine functionalized HTs were generally larger than their histidine functionalized counterparts. The ζ-potential values suggest the possibility of aggregation resulting in the larger observed particle size. TEM analysis showed the arginine functionalized LDHs as having particle size ranging between 20 to 50 nm, thus the modal value obtained by NTA (193.1 nm) is most probably due to aggregation. This theory is supported by the ζ-potential values obtained for the arginine functionalized LDHs, especially MgAlArg 0.33 which had a ζ-potential value of 6.7. The sizes of the histidine functionalized HTs as determined by NTA was similar to the results obtained by TEM analysis. Here again, as with the non-functionalized LDHs, there was no particular trend in the zeta potential values obtained, except that the aa-LDHs prepared in the ratio M^{2+}:M^{3+}:aa of 2:1:1 show positive ζ-potentials, whereas the aa-LDHs prepared in the ratio M^{2+}:M^{3+}:aa of 3:1:1 show negative ζ-potential values.

The ζ-potential values were negative for five of the samples (MgAl 0.25, MgAlArg 0.25, MgAlHist 0.25, MgFe 0.33 and ZnAl 0.25) and positive for the other five samples (MgAl 0.33, MgAlArg 0.33, MgAlHist 0.33, MgFe 0.25 and ZnAl 0.33).

3.3.2.6 IDENTIFICATION OF AMINO ACIDS

The co-precipitation of amino acids with LDHs is dependent on pH as well as the nature of the side chain groups [Aisawa *et al*., 2000; Aisawa *et al*., 2006]. The presence of amino acid in/on the functionalized LDHs was confirmed by the ninhydrin test (Figure 3.17).

Aisawa and co-workers (2000) reported a 42 % co-precipitation of histidine with a ZnAl LDH with molar ratios of Zn^{2+}:Al^{3+}:Histidine of 2:1:1 at pH 8 (where most of the histidine would exist as a zwitterion). The preparation of the LDHs for this study was carried out at a pH of 10 to 11. At this pH, histidine would be expected to have a negative charge (anionic in nature) and thus a significant amount of histidine would be expected to be incorporated within the LDH interlayer. However, the rather small change in $d_{(003)}$ basal spacing in the histidine functionalized hydrotalcites compared to the non-functionalized hydrotalcites (Figures 3.4 and 3.5), indicates that this was not the case. The amount of histidine present in the MgAlHist 0.25 and MgAlHist 0.33 samples was found to be 1.80 µg and 3.77 µg histidine per 200 µg LHD sample respectively. These values were obtained using the standard curve for histidine (see Figure A10 in Appendix). These values corresponds to the degree of incorporation of histidine in MgAlHist 0.25 being 0.90 % and in MgAlHist 0.33 being 1.89 %. The lower than anticipated degree of histidine incorporation within the LDH interlayer, is most likely as a result of the preparation of the LDHs not being carried out under nitrogen, which probably resulted in atmospheric carbonate being incorporated into the interlayer instead of the amino acid.

A much lower degree of co-precipitation of arginine has been reported thus far [Aisawa *et al*., 2001; Hibino, 2004]. Aisawa and co-workers (2001) have reported a 9 % co-precipitation of arginine into LDHs, which could be attributed to the repulsion of the positive charges between the arginine side chain and the LDH basal layers, at the pH used for the preparation of the arginine-functionalized LDHs. The amount of arginine present in the MgAlArg 0.25 and MgAlArg 0.33 samples was found to be 2.53 µg and 5.23 µg arginine per 200 µg LHD sample, respectively. These values were obtained using the standard curve for arginine (Figure A11 in Appendix). The degree of incorporation of arginine was calculated to be 1.27 % and 2.62 % for MgAlArg 0.25 and MgAlArg 0.33 respectively.

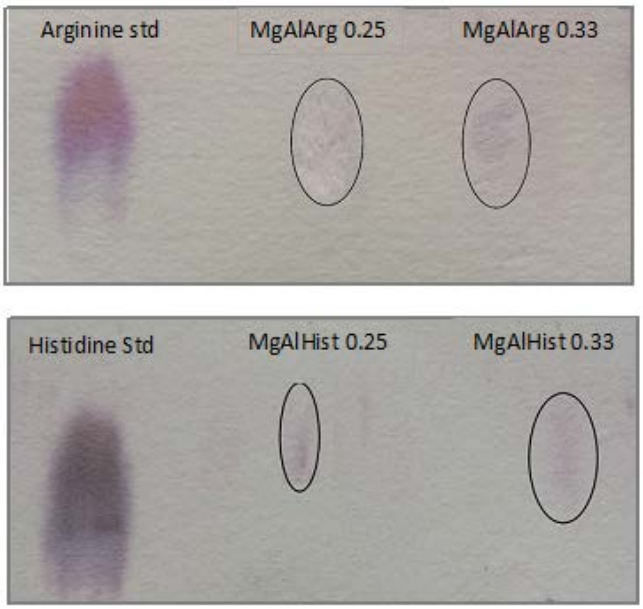

Figure 3.17 Ninhydrin test for amino acid functionalized LDHs.

3.4 CONCLUSION

The desired LDHs and aa-functionalized HTs were successfully synthesized using the co-precipitation method and characterized by XRD, ICP-OES, FTIR, SEM, TEM and NTA. XRD diffractograms for the various synthesized LDHs and aa-functionalized HTs were consistent with data reported in literature. The ratios of M^{2+}:M^{3+} cations and vibrational profiles of the compounds were confirmed by ICP-OES and FTIR respectively. SEM and TEM analysis revealed that morphologies of the synthesized compounds were typical of LDHs and HTs. Sizes of the nanoparticles varied between 30 and 200 nm and the zeta-potential values ranged from -24.6 to 29.7 as determined by NTA analysis. The attachment of arginine and histidine in the aa-functionalized HTs was confirmed by the ninhydrin test and the degree of incorporation of amino acid was calculated to be 0.90% in MgAlHist 0.25, 1.89% in MgAlHist 0.33, 1.27 % in MgAlArg 0.25 and 2.62 % in MgAlArg 0.33.

CHAPTER FOUR

4. NUCLEIC ACID BINDING AND PROTECTION STUDIES

4.1. INTRODUCTION

Nucleic acids are negatively charged and would therefore bind to LDHs as any other anion would. The degree of binding can be assessed using the electrophoretic mobility shift assay (EMSA), also known as the gel retardation assay. It was first described in the 80's by Garner and Revzin (1981) and Fried and Crothers (1981), two groups working independently on DNA-protein interactions. EMSA is a simple, efficient and widely used method for detection of binary changes such as the presence or absence of binding of nucleic acids [Holden and Tacon, 2011]. The method has since been adapted to study the interactions of nucleic acids with various compounds such as drugs and carrier vectors in gene delivery studies. The rationale behind EMSA is that free/unbound nucleic acids would have a different electrophoretic mobility in a gel matrix than nucleic acid that is bound to a carrier. In this study, the migration of DNA:LDH or siRNA:LDH complexes would be 'retarded' when compared to the migration of free/unbound DNA or siRNA.

This assay is used to determine the optimal binding ratio, which refers to the lowest ratio of nucleic acid:LDH, where complete binding of the nucleic acid occurs. The optimal binding ratio is very important, as it plays a key role in determining whether a vector would be suitable for gene therapeutic applications *in vivo*.

When unbound 'naked' DNA is exposed to agarose gel electrophoresis, a typical band pattern is observed. Depending on the forms of DNA present in the sample, three bands may be observed. The supercoiled form of DNA is more compact and migrates the furthest of the three forms of DNA. The circular form of DNA migrates much slower than the other two forms, most probably due to stearic hindrance, whilst the linear form of DNA migrates at a rate intermediate to the supercoiled and circular forms. When DNA is bound to a vector such as LDH, the mobility of the DNA:LDH is retarded and the complex would remain in the well.

The 6.2 kilobase pair pCMV-*luc* DNA plasmid was used for this study (Figure 4.1). In addition to the luciferase gene, this plasmid contains a cytomegalovirus (CMV) promoter from pcDNA3, a

simian virus promoter, enhancer and late polyadenylation site, as well as an ampicillin resistance gene and bacterial origin of replication.

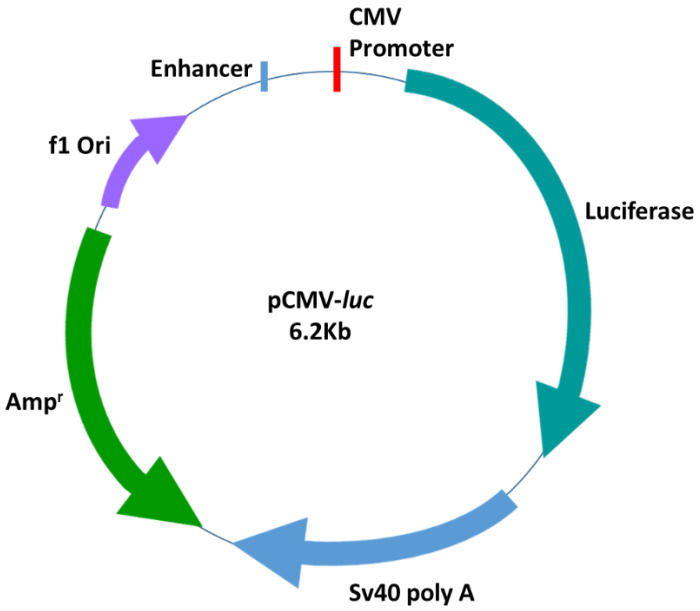

Figure 4.1 Map of the pCMV-*luc* vector [Plasmid Factory, Bielefeld, Germany].

Small interfering RNA (siRNA) are short (20-25 base pairs long) double stranded RNA molecules which generally migrate as a single band when exposed to gel electrophoresis. The anti-*luc* siRNA targeting the luciferase gene was used for the gene knockdown/silencing studies.

4.2. MATERIALS AND METHODS

DNA grade agarose was obtained from *Bio-Rad Laboratories*, Richmond, USA. pCMV-*luc* plasmid DNA was supplied by *Plasmid Factory* (Bielefeld, Germany). Anti-luciferase siRNA [5'-GAUUAUGUCCGGUUAUGUA-3'] was purchased from *Dharmacon* (Lafayette CO, USA). Ethidium bromide and ethylenediaminetetraacetic acid (EDTA) (disodium salt, dihydrate) were acquired from *Merck*, Darmstadt, Germany. All other reagents were of analytical grade.

4.2.1. PREPARATION OF NUCLEIC ACID-LDH COMPLEXES

To find the optimal binding ratios, 0.5 µg of pCMV-*luc* DNA was added to the respective LDH samples at varying weight ratios in a total volume of 10 µl HEPES buffered saline [HBS (20 mM HEPES and 150 mM NaCl, pH 7.5)] (Table 4.1). This mixture was vigorously vortexed for 10 minutes and then allowed to stand at room temperature for 30 minutes.

Table 4.1 Ratios used for nucleic acid:LDH complex formation.

Lane	Ratio nucleic acid :LDH	Nucleic Acid (µg)	LDH (µg)
1	1:0	0.5	0
2	1:10	0.5	5
3	1:20	0.5	10
4	1:30	0.5	15
5	1:40	0.5	20
6	1:50	0.5	25
7	1:60	0.5	30
8	1:70	0.5	35

The siRNA-LDH complexes were prepared in a similar manner as the DNA-LDH complexes using anti-luciferase siRNA. The siRNA-LDH-HBS mixtures were briefly vortexed and then incubated overnight at 60 °C to allow for optimal binding to occur.

4.2.2 AGAROSE GEL ELECTROPHORESIS

A 1 % agarose gel was prepared by dissolving (with heating) 0.2 g of agarose in 18 ml distilled water. The solution was cooled to approximately 75 °C, after which 2 ml of 10x electrophoresis buffer (0.36 M Tris-HCl; 0.3 M Na_2HPO_4 and 0.1 M EDTA in 1 litre 18 Mohm water, pH 7.5) and 3 µl of ethidium bromide (10 mg/ml) were added to it. The solution was cooled further to approximately 60 °C, and then poured onto an electrophoresis gel tray fitted with an 8-well comb. The agarose gel was allowed to set for ± 1 hour, after which the comb was removed and the gel placed in an electrophoresis tank (*Bio-Rad Mini-Sub®Cell GT*) containing 1x electrophoresis buffer. A volume of 3 µL of gel loading buffer [glycerol 50 %, bromophenol blue 0.05 % and xylene

cyanol (0.05 %)] was added to the complexes, and 10 µL of each sample was loaded onto the agarose gel and exposed to electrophoresis at 50 volts for 90 minutes. The gel was then viewed under UV light using a *Syngene* G-Box documentation system (Syngene, Cambridge, UK).

4.2.3 CHARACTERIZATION OF NUCLEIC ACID:LDH COMPLEXES

The ultrastructural morphology and size and ζ-potential of the DNA:LDH and the siRNA:LDH complexes was determined using TEM and NTA, respectively. The mechanism of DNA binding was evaluated by XRD analysis of the DNA:LDH complex. For this aspect of the study MgAl 0.33 was selected as an ideal representative of all the LDHs prepared. XRD analysis required a substantial amount of sample and budgetary constraints did not allow for the preparation of such large quantities of the siRNA:LDH complexes. This analysis was therefore not carried out on the siRNA:LDH complex. The methods employed are as described in Chapter 3, sections 3.2.1, 3.2.4 and 3.2.5.

4.2.4 NUCLEASE DIGESTION AND NUCLEIC ACID RELEASE ASSAY

This assay was performed using only the DNA:MgAl 0.33 complex as all the nucleic acid:LDH complexes would be expected to react similarly when exposed to serum nucleases. A DNA:LDH (10 µl) complex was prepared at the optimal binding ratio determined from the electrophoretic mobility shift assay. Two control samples were also prepared; a positive control containing only the DNA and a negative control containing DNA and 10 % v/v foetal bovine serum (FBS). The 10 % v/v FBS was also added to the DNA:LDH complex, and all samples were incubated at 37 °C for 4 hours. The nuclease digestion reaction was stopped by the addition of ethylenediamine tetraacetic acid (EDTA), to a final concentration of 1 mM. The sample was then centrifuged, the supernatant discarded, and 0.1 M HCl (1 µl) was added, and sample incubated at 37 °C for 1 hour. Thereafter, 2 µl of gel loading buffer was added to each sample and they were subjected to electrophoresis at 50 V for 90 minutes. The gels were viewed under UV light using a *Syngene* G-Box documentation system (Syngene, Cambridge, UK).

This process was also conducted for the siRNA:MgAl 0.33 complex, with electrophoresis for 30 minutes instead of 90 minutes.

4.3 RESULTS AND DISCUSSION

4.3.1 NUCLEIC ACID BINDING STUDIES

Various incubation times and temperatures have been reported by investigators in the preparation of DNA:LDH complexes [Choy *et al.,* 2000; Xu *et al*., 2007; Xu *et al*., 2008]. Balcomb and co-workers (2015) have reported incubation times of up to 72 hours at 60 °C for optimal DNA:LDH binding to occur.

A number of different incubation times and temperatures (30 minutes/1 hour/ 6 hours at room temperature/37 °C /60 °C) were initially investigated (data not shown) with limited success. In some cases partial binding was observed but in most cases the experimental conditions did not result in the complete formation of DNA:LDH complexes. Eventually, a 24 hour incubation period at 60 °C was attempted, with promising results. MgAl 0.25, MgAlArg 0.25, MgAlHist 0.25 and MgAlHist 0.33 all displayed complete binding with DNA at ratios of DNA:LDH of 1:30, 1:30, 1:10 and 1:30 respectively (Figure 4.2). MgAl 0.33, MgAl Arg 0.33, MgFe 0.25, MgFe 0.33, ZnAl 0.25 and ZnAl 0.33 all showed partial retardation, which corresponded to incomplete binding [Figures 4.2 (A,B and C) and 4.3 (D and E)]. ZnAl 0.33 showed complete binding at a ratio of DNA:LDH of 1:60. Smears observed in Figure 4.2 could be due to the presence of nucleases in the buffer.

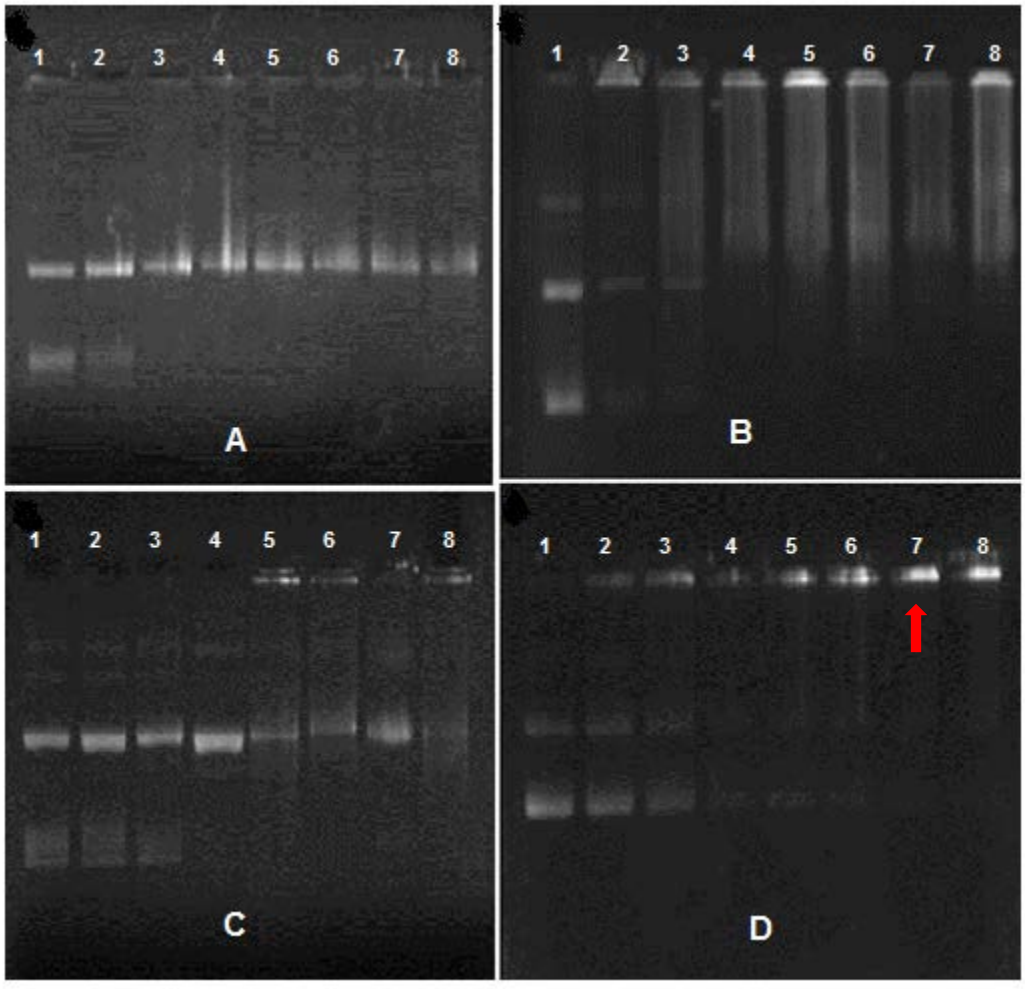

Figure 4.2 Gel retardation patterns of (A) MgFe 0.25, (B) MgFe 0.33, (C) ZnAl 0.25, (D) ZnAl 0.33 after a 24 hour incubation period. Lane 1 of all the gels contain DNA only. Lanes 2-8 contain DNA:LDH ranging in ratios from 1:10 to 1:70 (w/w). The arrow indicates the point of complete retardation. (A) MgFe 0.25, (B) MgFe 0.33, (C) and ZnAl 0.25 show partial retardation.

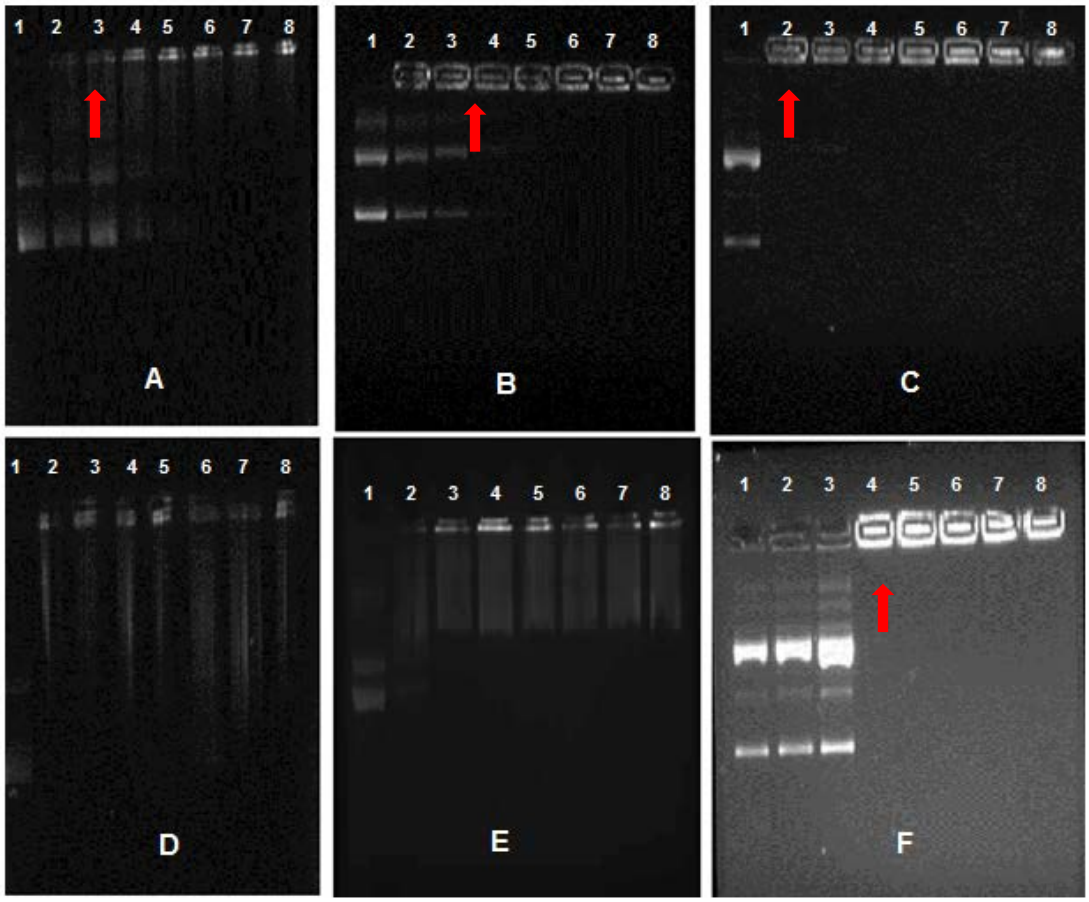

Figure 4.3 Gel retardation patterns of (A) MgAl 0.25, (B) MgAlArg 0.25, (C) MgAlHist 0.25, (D) MgAl 0.33, (E) MgAlArg 0.33, (F) MgAlHist 0.33 after a 24 hour incubation period. Lane 1 of all the gels contain DNA only. Lanes 2-8 contain DNA:LDH ranging in ratios from 1:10 to 1:70 (w/w). The arrows indicate the point of complete retardation. (D) MgAl 0.33 and (E) MgAlArg 0.33 show partial retardation.

Barichello *et al* (2012) reported that agitation by vortex resulted in enhanced binding between siRNA and cationic liposomes, resulting in superior gene knockdown. This methodology was then applied to the formation of the DNA:LDH complexes. The components required to make up the DNA:LDH complexes were vortexed at high speed for 10 minutes followed by a 10 minute incubation at room temperature. This method resulted in complete binding of the DNA to LDH, as confirmed by the gel retardation (Figure 4.4). It has been further suggested that the high energy transmitted during vortexing harmonizes the interaction between the nucleic acid and the carrier vector [Barichello *et al*., 2012].

Figure 4.4 Gel retardation patterns of DNA only (lane 1), DNA:MgAl 0.25 (lane 2), DNA:MgAlArg 0.25 (lane 3), DNA:MgAlHist 0.25 (lane 4), DNA:MgAl 0.33 (lane 5), DNA:MgAlArg 0.33 (lane 6), DNA:MgAlHist 0.33 (lane 7), DNA:MgFe 0.25 (lane 8), DNA:MgFe 0.33 (lane 9), DNA: ZnAl 0.25 (lane 10) and DNA:ZnAl 0.33 (lane 11)after vigorous vortexing for 10 minutes followed by a 10 minute incubation period at room temperature. Results indicate complete complexation of the LDH with DNA under these conditions. All complexes were prepared in a ratio of DNA:LDH of 1:30 (w/w). The arrows indicate complete retardation.

Zhang and co-workers (2003) have reported a reduction in the number of water molecules in a lipoplex after complexation of liposomes with nucleic acids, resulting in a closer and more harmonious interaction between the two components. It is possible that a similar reaction occurs during complex formation between the DNA and LDHs, where loss of water molecules from the interlayer could lead to a slight decrease in interlayer spacing consequently “trapping” the DNA or at least part of the DNA within the interlayer region and enhancing complex formation.

Lu and co-workers (2016) have recently hypothesized a new, more likely mechanism of DNA interaction with LDHs. They have suggested that LDHs are electrostatically attracted to and bind to the LDH surfaces via the phosphate backbone of the DNA molecules. The phosphate oxygen thus forms co-ordination metal-oxygen-phosphate bonds resulting in the adsorption of DNA onto

the outer surface of the LDH (Figure 4.5). The binding of DNA to the external surface of the LDH nanoparticles was also previously observed by Ladewig[1] *et al* (2010) and Dong *et al* (2015). The negative zeta potentials of most of the DNA:LDH complexes (Table 4.2), also reflects that the DNA was adsorbed onto the surfaces of the LDH rather than intercalated within the interlayer. Surface adsorption appears to be the most likely mechanism of DNA binding to the LDH in this study.

It was found that optimal binding occurred at a DNA:LDH ratio of 1:30 (w/w) for all the LDH samples (Figure 4.4).

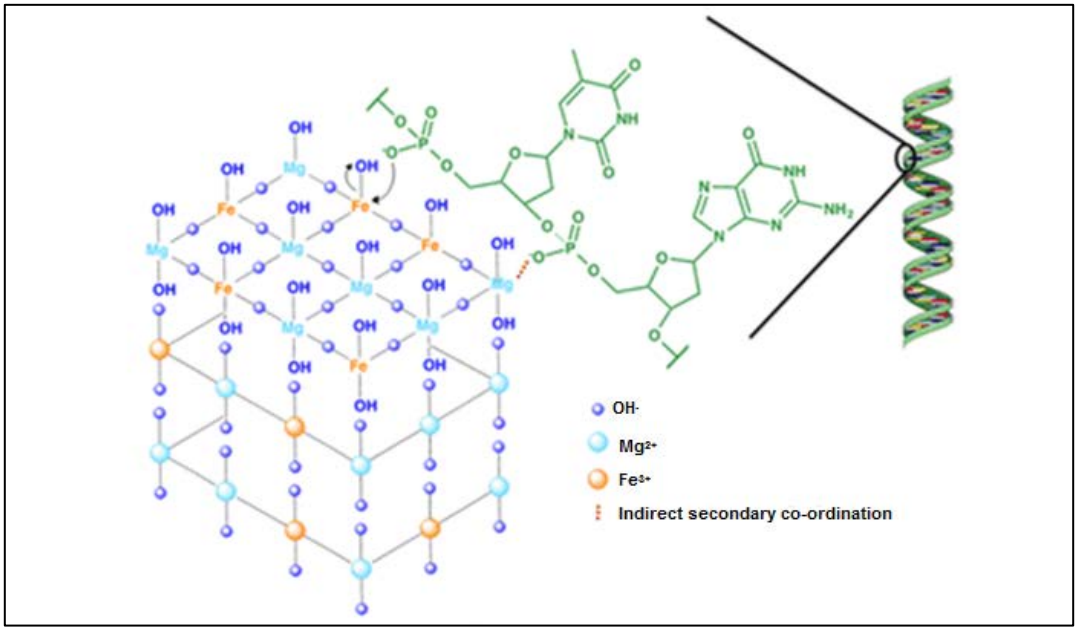

Figure 4.5 Co-ordination between DNA phosphate backbone and LDH outer surface (adapted from Lu *et al*., 2016).

TEM analysis of the DNA:LDH complexes revealed compact complexes with lateral lengths ranging from 10-250 nm. This was confirmed by NTA analysis of the DNA:LDH complexes which showed that the complexes ranged in modal size from 20 to 180 nm (Table 4.2).

Table 4.2 Size and zeta potential of DNA:LDH complexes.

LDH	PARENT LDH		DNA:LDH COMPLEXES	
	SIZE (nm)	ZETA POTENTIAL (mV)	SIZE (nm)	ZETA POTENTIAL (mV)
MgAl 0.25	148.4	-11.6	180.1	-9.8
MgAl 0.33	72.4	15.0	25.1	-21.3
MgFe 0.25	307.4	1.2	20.3	-29.3
MgFe 0.33	27.9	-12.8	25.8	9.7
ZnAl 0.25	30.0	-7.2	44.4	-20.0
ZnAl 0.33	67.9	29.7	61.2	-30.9
MgAlArg 0.25	193.1	-19.8	26.9	-11.8
MgAlArg 0.33	123.7	6.7	30.8	-27.3
MgAlHist 0.25	60.8	-24.6	34.6	-28.0
MgAlHist 0.33	44.5	22.7	53.9	-23.5

In general the sizes of the DNA:LDH complexes were smaller than that of the parent LDHs, with a few exceptions. It is possible that the large particle size observed for MgAl 0.25 could be due to aggregation of the nanoparticles in solution. It is also possible that one DNA strand combined or interlinked with several LDH nanoparticles resulting in such aggregations [Xu *et al*., 2006]. The higher the absolute zeta potential value, the greater the colloidal stability of a solution [Ostolska and Wiśniewska, 2014]. The zeta potentials obtained for both the parent LDHs as well as the DNA:LDH complexes were lower than absolute 30 indicating the strong possibility of aggregation. Zeta potential values of lower than absolute 5 corresponds to rapid coagulation or aggregation leading to the formation of larger particles, as was observed with MgFe 0.25. The negative zeta potential values of the complexes also suggest that the DNA binds to the outer surfaces of the LDH rather than being incorporated within the interlayer. This negative surface charge would be expected to impede internalization into the cell, but Desigaux and co-workers (2006) have indicated that the negative zeta potential of the complex is not an impediment to cellular uptake. It was interesting to note that some of the DNA:LDH complexes displayed an almost 'square' or "cube" shaped morphology, whilst some appeared hexagonal in shape (Figures 4.6 and 4.7).

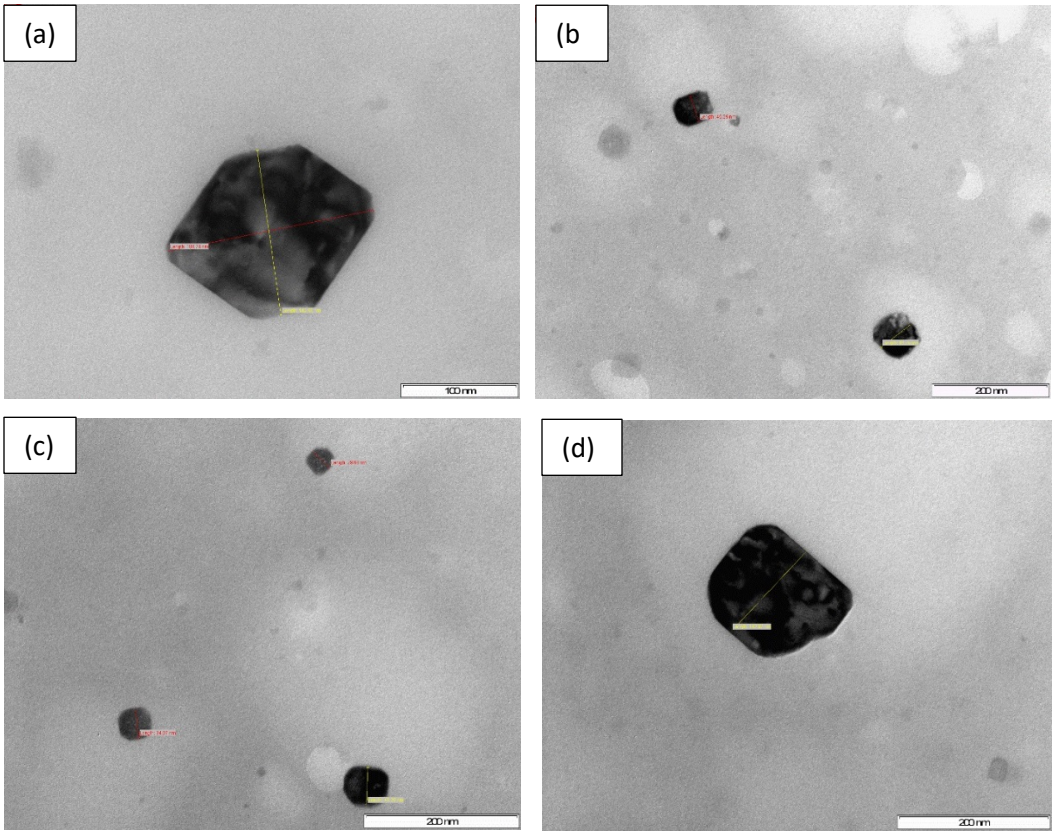

Figure 4.6 TEM images of DNA:LDH complexes (a) DNA-MgFe 0.25 at 300K magnification, (b) DNA-MgFe 0.33 at 150K magnification, (c) DNA-ZnAl 0.25 at 200 K magnification and (d) DNA-ZnAl 0.33 at 200K magnification. The bar represents 100 nm in (a) and 200 nm in (b), (c) and (d) respectively.

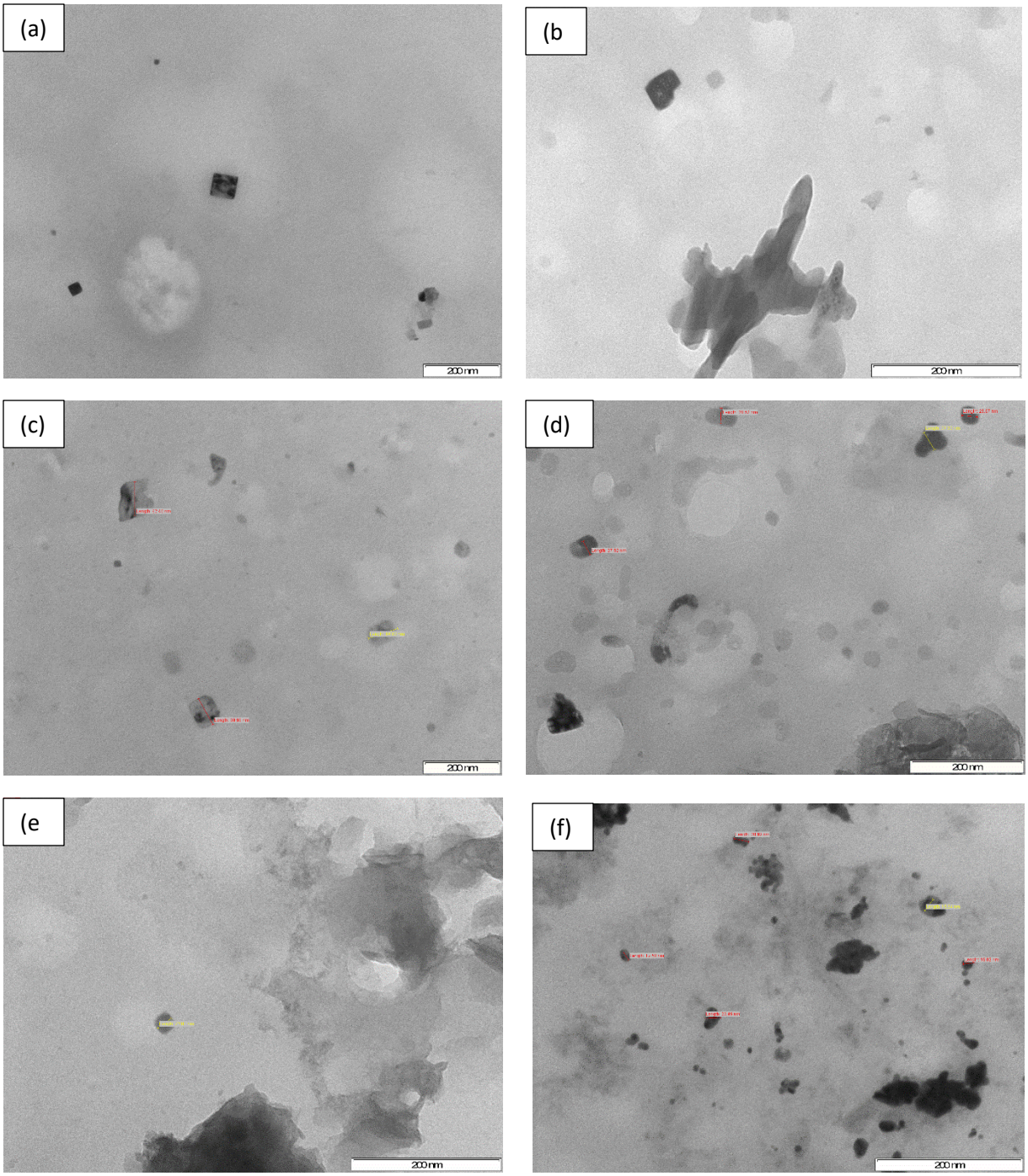

Figure 4.7 TEM images of DNA:LDH complexes (a) DNA-MgAl 0.25 at 60K magnification, (b) DNA-MgAl 0.33 at 200K magnification , (c) DNA-MgAlArg 0.25 at 100K magnification, (d) DNA-MgAlArg 0.33 at 150K magnification, (e) DNA-MgAlHist 0.25 at 200K magnification and (f) DNA-MgAlHist 0.33 at 200K magnification. The bar represents 200 nm in (a) – (f).

A large degree of compaction occurs during the formation of the complex, when one compares the size of naked DNA as well as the native LDH nanoparticles. This compaction occurs due to the electrostatic interaction between the cations present on the LDH surface and the phosphate backbone of the DNA molecules [Matulis *et al*., 2000]. The phosphate groups of the DNA are electrostatically neutralized by associating with the cations on the LDH molecules, leading to a condensed, more stable complex structure, the shape of which depends on the extent of condensation [Smith *et al*., 1997].

There have been many studies reporting that nucleic acid binding occurs due to ion exchange with interlayer anions [Xu and Lu, 2006; Ladewig *et al*., 2009], whilst recent reports suggest that the binding actually occurs between the phosphate backbone of the nucleic acid and the external surfaces of the LDH [Lu *et al*., 2016; Dong *et al*., 2015]. The actual mode of binding in this study was investigated using XRD analysis. The d-spacing values of the parent MgAl 0.33 LDH as well as the DNA:MgAl 0.33 complex are identical (Figure 4.8), indicating that the DNA does not intercalate within the LDH interlayer. DNA intercalation within the interlayer would have resulted in an increase in d_{003} to 23.7 Å, which is the diameter of DNA [Berg *et al*., 2006]. The unchanged d_{003} value in the DNA:MgAl 0.33 complex, confirms that DNA binds to the outer surfaces of the LDH. The slight shift to the right of the diffraction peaks of the MgAl 0.33:DNA complex, most probably occurs as a result of the DNA binding to the outer surface of the LDH.

The LDHs prepared for this study were made using nitrate precursors, but it is very possible that the interlayer anions in the prepared LDHs were replaced by carbonate instead of nitrate, due to the higher selectivity for carbonate anions [Costantino *et al*., 2008], and the fact that the LDHs were not prepared under nitrogen. This could contribute to poorer ion exchange of DNA with the interlayer anions

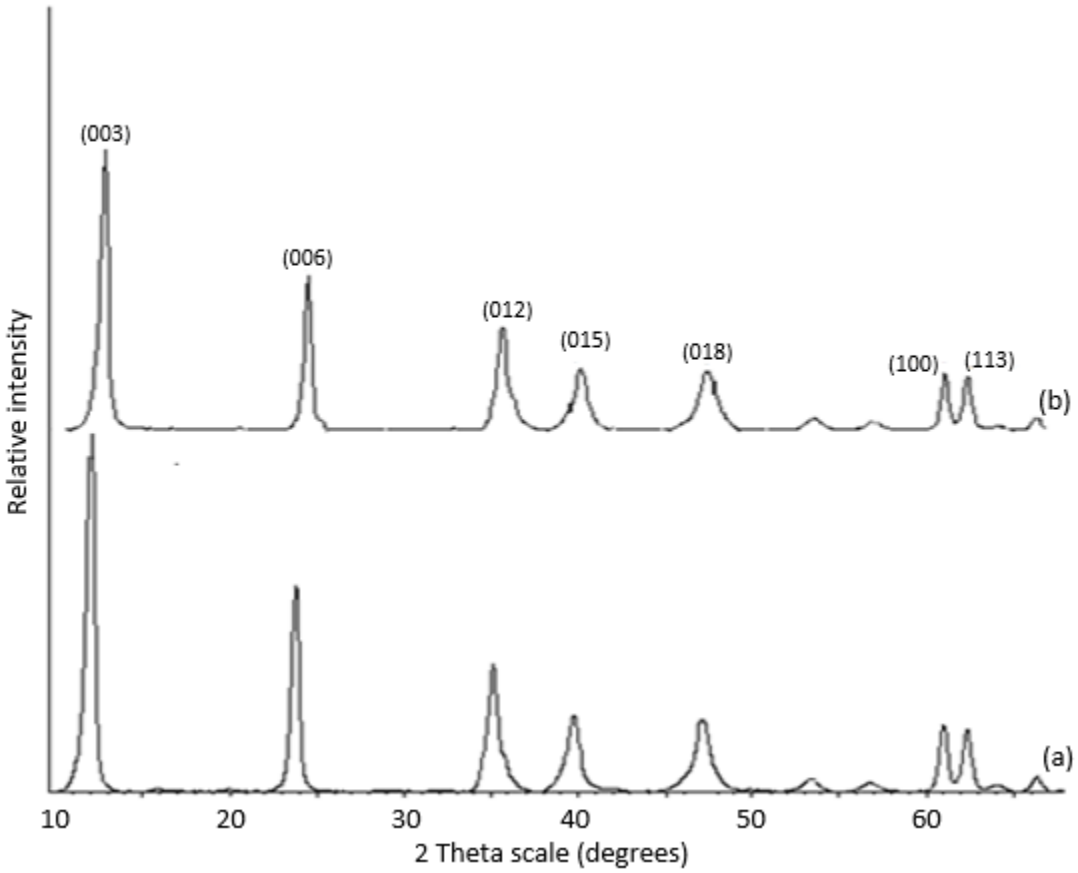

Figure 4.8 XRD pattern of (a) MgAl 0.33 (b) DNA:MgAl 0.33 complex.

An attempt was made to prepare the siRNA:LDH complexes in the same way that the DNA:LDH complexes were prepared, by vigorously vortexing for 10 minutes, but this proved unsuccessful. Complete binding of the siRNA to the LDH samples was only obtained after incubation overnight at 60 °C. Chen *et al* (2013) have suggested that a temperature of 60 °C would be inappropriate for intercalation of siRNA due to its susceptibility to higher temperatures, but Hickerson and co-workers (2008) have reported that the integrity of siRNA is not affected by incubation at temperatures up to 95 °C. The gel retardation results (Figure 4.9), confirmed that the siRNA remains in its integral form even after an overnight incubation at 60 °C. Upon overnight incubation at 60 °C the siRNA bound completely with the various LDH samples, albeit at different ratios (Figure 4.9). The MgAl 0.25 and MgAlHist 0.33 samples bound completely at a siRNA:LDH ratio of 1:30, the MgAlArg 0.25 and MgAlHist 0.25 exhibited complete binding at a siRNA:LDH

ratio of 1:20, whilst the MgAl 0.33 and MgAlArg 0.33 bound optimally at a siRNA:LDH ratio of 1:10. The MgFe 0.25, MgFe 0.33, ZnAl 0.25 and ZnAl 0.33 LDH samples bound completely with the siRNA at a ratio of 1:40. Previous studies have shown that some of the siRNA intercalates into the interlayers of the LDH, while some is actually adsorbed onto the LDH surface [Chen *et al*., 2013]. It was interesting to observe that unlike the DNA-LDH complexes which remained clearly visible in the wells of the gel, the siRNA-LDH complexes were not visible in some of the wells, even though no 'free' siRNA was visible on the gels. It is presumed that this occurs because siRNA units enter the LDH interlayer where they are electrostatically bound. Since the siRNA are now 'shielded' within the interlayer, the fluorescence, (due to the presence of ethidium bromide in the gel interacting with the nucleic acid), is not clearly visible.

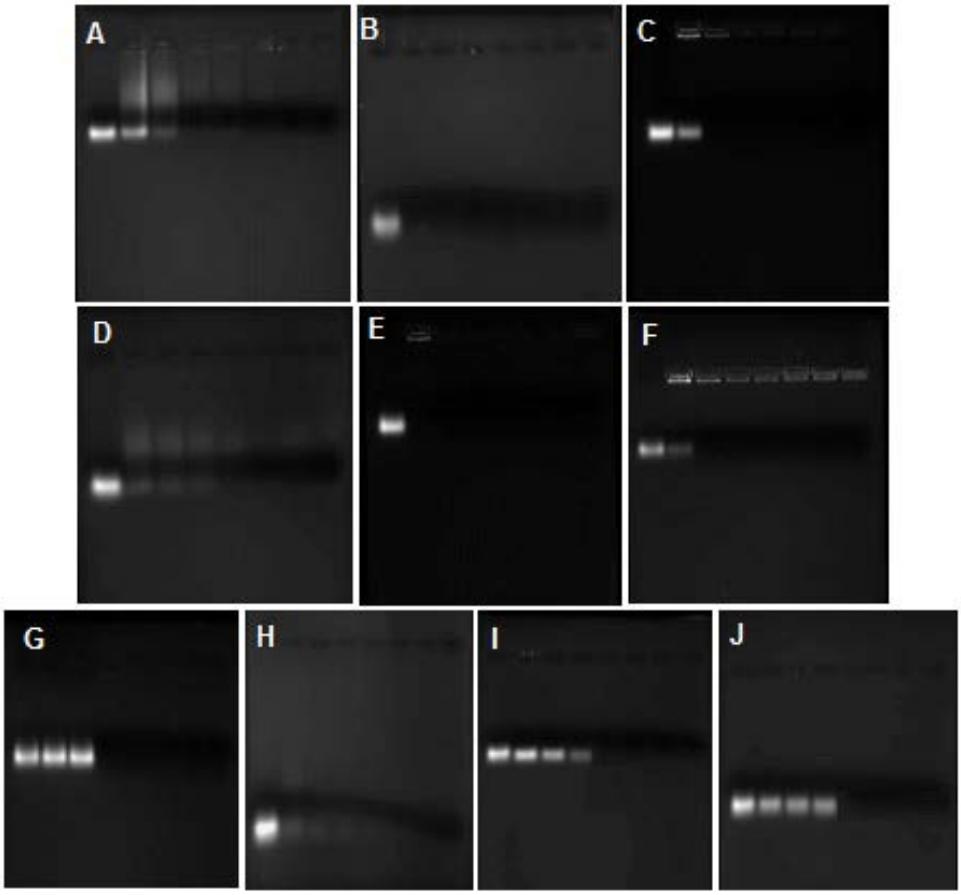

Figure 4.9 Gel retardation patterns of (A) MgAl 0.25, (B) MgAlArg 0.25, (C) MgAlHist 0.25, (D) MgAl 0.33, (E) MgAlArg 0.33, (F) MgAlHist 0.33 (G) MgFe 0.25, (H) MgFe 0.33, (I) ZnAl 0.25, (J) ZnAl 0.33 after incubation with siRNA at 60 °C overnight.

TEM analysis of the siRNA:hydrotalcite complexes shows a large degree of condensation of the LDH structure upon binding with siRNA. The nanoparticles, which before binding ranged in size from 20-200 nm, condensed down to a size range of 4-50 nm in lateral diameter. The complexes appear somewhat spherical but not quite uniform in size or morphology (Figure 4.10).

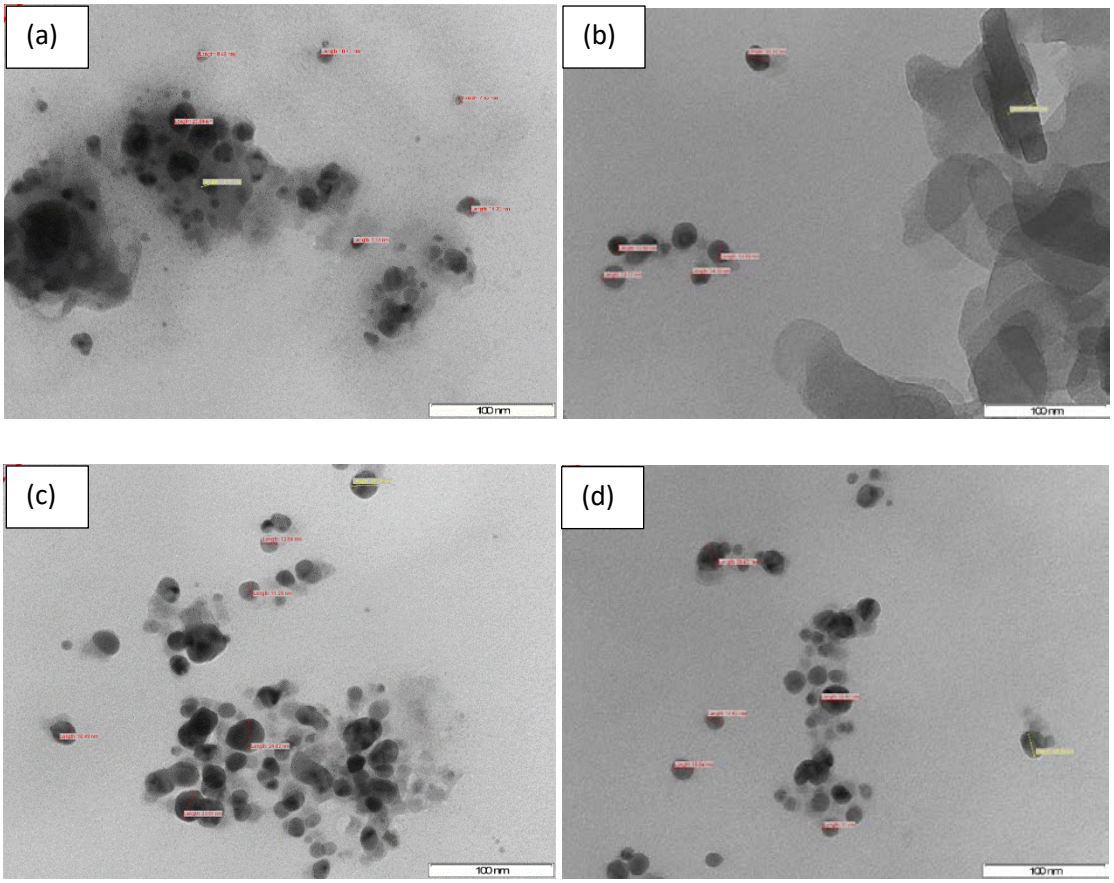

Figure 4.10 TEM images of complexes (a) siRNA-MgAl 0.25, (b) siRNA-MgAl 0.33, (c) siRNA-MgAlArg 0.33 and (d) siRNA-MgAlHist 0.33 at 300 K magnification. The bar represents 100 nm in (a) – (d).

The HT-like compounds complexed with siRNA showed a similar condensation formation to those observed for the siRNA-MgAl 0.25, siRNA-MgAl 0.33, siRNA-MgAlArg 0.33 and siRNA-MgAlHist 0.33 (Figure 4.11). Lateral sizes of the complexes ranged between 5 and 30 nm.

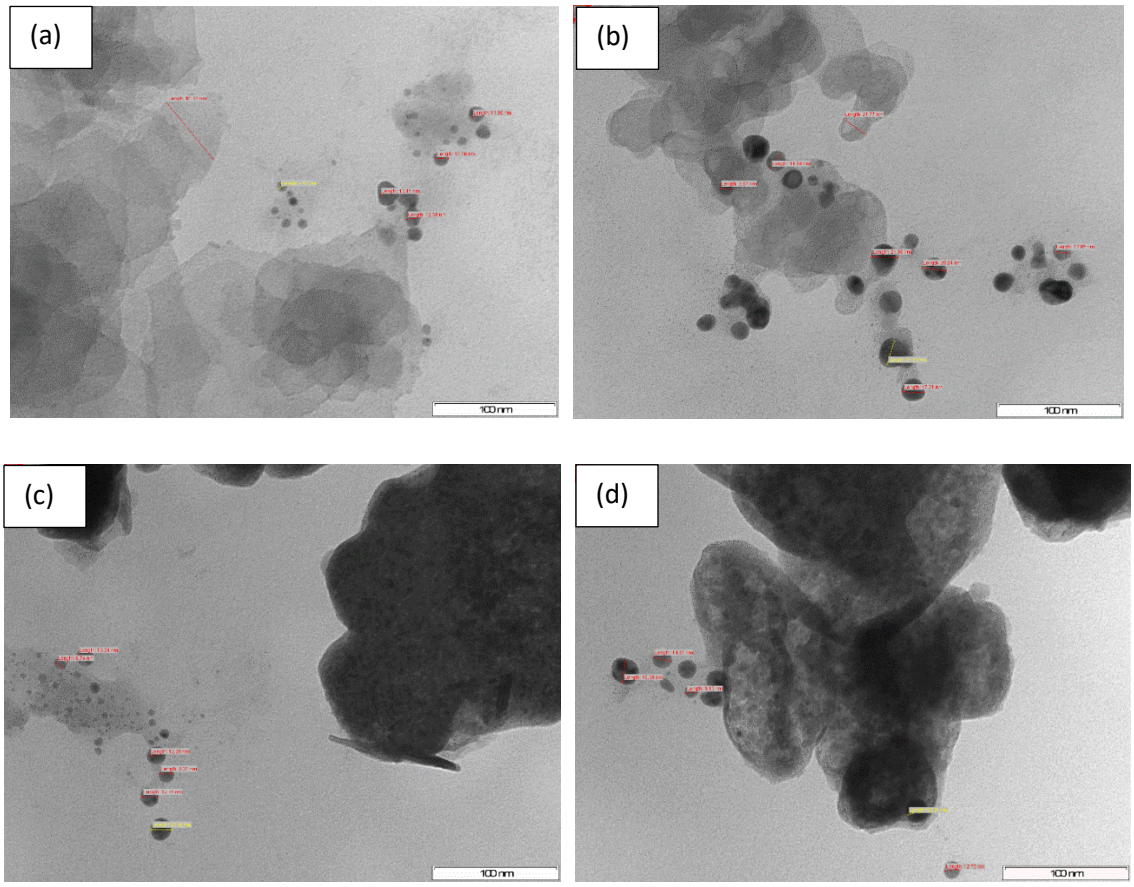

Figure 4.11 TEM images of complexes (a) siRNA-MgFe 0.25, (b) siRNA-MgFe 0.33, (c) siRNA-ZnAl 0.25 and (d) siRNA-ZnAl 0.33 at 300K magnification. The bar represents 100 nm in (a) – (d).

The condensation in structure seen for all the other LDH-siRNA complexes is different from that observed for the siRNA-MgAlArg 0.25 and siRNA-MgAlHist 0.25 complexes. Instead of the compact 'spherical shaped' complexes, nanoflakes were observed (Figure 4.12). It appears as if the amino acid functionalized hydrotalcites prepared in the ratio of Mg:Al:aa of 3:1:1 have a more rigid structure, that is unable to condense down completely upon complexation with the siRNA, and the nanoparticles merely folds over around the siRNA.

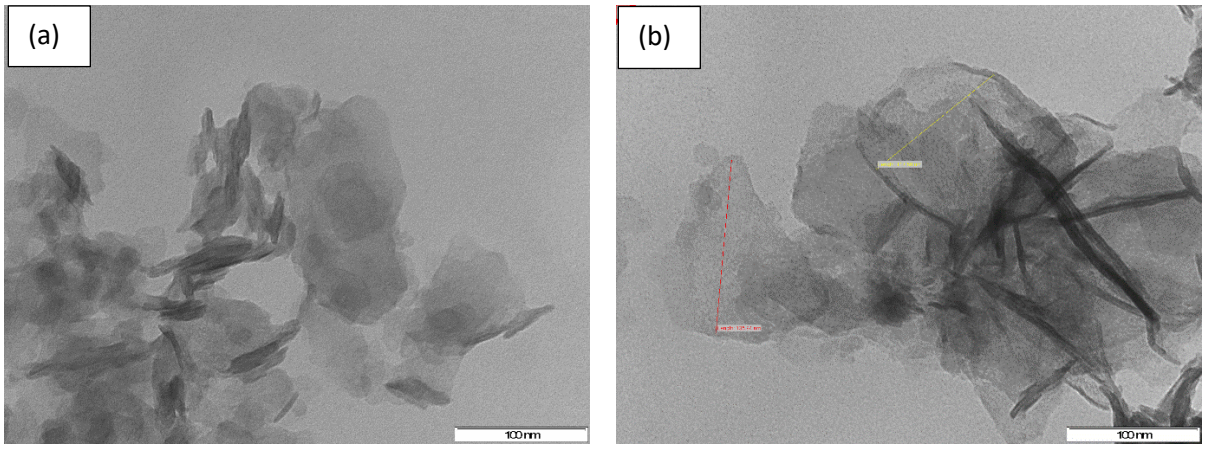

Figure 4.12 TEM images of complexes (a) siRNA-MgAlArg 0.25 and (b) siRNA-MgAlHist 0.25 at 300K magnification. The bar represents 100 nm in (a) and (b).

Unlike the DNA:LDH complexes which have an almost 'square/cube' shape, the siRNA:LDH complexes are more spherical in shape. The difference in shape suggests that the mechanism of structural condensation of the siRNA:LDH complexes is most probably quite different from the mechanism involved in DNA:LDH structural condensation. siRNAs are much smaller molecules than DNA, and are thus probably easily intercalated within the interlayer region of the LDHs. Unlike the electrostatic attraction occurring between the cations on the outer surface of the LDH molecules and DNA, the electrostatic attraction most probably occurs between the cations on the inner surfaces of the LDH molecules and siRNA, resulting in the distinct difference in shape of the DNA:LDH complexes compared to the siRNA:LDH complexes.

Computational simulation studies by Zhang *et al* (2012) suggest that RNA molecules intercalate within the LDH interlayers, where the RNA molecule is oriented parallel to the hydroxide layers. The strong electrostatic interactions between the siRNA molecules and the positively charged LDH sheets keep the siRNA molecules 'bound' within the interlayer.

The small sizes of the siRNA:LDH complexes was confirmed by NTA analysis (Table 4.3). The zeta potential values obtained for the siRNA:LDH complexes suggest greater colloidal stability than the DNA:LDH complexes, which could be a contributing factor to the generally smaller size of particles observed. The small siRNA:LDH complex size could also be attributed to the initial high speed vortexing during complex preparation, which is reported to result in better interaction

between the siRNA and the carrier vector [Barichello *et al*., 2012]. There is also a greater change in zeta potential of the siRNA:LDH complexes compared to the parent LDHs, which shows that the LDHs have a high affinity for siRNA [Rojas *et al*., 2015]. The negative charge of the siRNA:LDH complexes indicates that siRNA similar to the DNA binds predominantly to the outer surfaces of the LDH [Wong *et al*., 2010; Chen *et al*., 2013].

Table 4.3 Size and zeta potential of siRNA:LDH complexes.

LDH	PARENT LDH		siRNA:LDH COMPLEXES	
	SIZE (nm)	ZETA POTENTIAL (mV)	SIZE (nm)	ZETA POTENTIAL (mV)
MgAl 0.25	148.4	-11.6	28.4	-34.7
MgAl 0.33	72.4	15.0	47.0	-30.3
MgFe 0.25	307.4	1.2	45.1	-28.2
MgFe 0.33	27.9	-12.8	55.4	-21.8
ZnAl 0.25	30.0	-7.2	27.0	-29.7
ZnAl 0.33	67.9	29.7	25.7	-46.1
MgAlArg 0.25	193.1	-19.8	34.3	-28.1
MgAlArg 0.33	123.7	6.7	36.0	-13.5
MgAlHist 0.25	60.8	-24.6	41.0	-22.6
MgAlHist 0.33	44.5	22.7	48.8	-24.0

4.3.2 NUCLEASE DIGESTION AND NUCLEIC ACID RELEASE ASSAY

The ultimate role of a gene delivery vector is to eventually deliver its load into the cell *in vivo*. Here the complexes would be exposed to degradative enzymes such as nucleases. It is therefore essential to investigate whether the vector is able to transport the nucleic acids into the cell in its integral form. This may be determined by performing a nuclease digestion assay, where the nucleic acid-vector complex is exposed to serum nucleases in an environment mimicking *in vivo* conditions. The intercalation reaction between DNA and LDH is reversible and the DNA may be released either by addition of K_2CO_3 [Wu *et al*., 2014] or by dropping the pH of the solution. In

this study, the nucleic acid was released from the vector by dropping the pH. An acidic pH disrupts and dissolves the hydroxide layers of the LDH, resulting in release of the nucleic acid [Zhang *et al*., 2012]. The sample is then exposed to gel electrophoresis to visualize the integrity of the nucleic acid and/or extent of nuclease digestion. Integral DNA would appear as three distinct bands (depending on the forms of DNA initially present in the sample) and integral siRNA would appear as a single band. Nucleic acid that had been degraded by the serum enzymes would appear as smears on the gel. If the nucleic acid remains in its integral form after exposure to the nuclease digestion assay, then this suggests that the vector would be suitable for *in vivo* applications.

From the results obtained (Figure 4.13), it can be clearly seen that the DNA:LDH complex does offer some degree of protection to the DNA from serum nucleases. The naked, unprotected DNA (lane 2) was disintegrated after exposure to serum nucleases as the DNA appeared as a smudged band on the gel. For the DNA:LDH complexes, the DNA retained its integrity with the bands of the linear, circular and supercoiled forms of the DNA still being quite clearly visible (lane 4). Some of the DNA:LDH complex still remained in the well, as was also reported by Kriven *et al* (2004) who suggested that DNA can only be completely released from the complex at a pH of 2 or less. The mechanism of release of the DNA from the DNA:LDH complex has been proposed to be via a dissolution process that occurs in the endosome due to low pH [Ladewig *et al*., 2009; Choy *et al*., 2000]. LDHs begin to dissolve in a pH range of 4-5, resulting in the release of their cargo in a pH-dependent manner [Wong *et al*., 2010].

The buffering capacity of LDHs have been well documented and this property has been exploited in the production of antacids from LDHs for many years [Cunha *et al*., 2010]. Bejoy (2001) reported that hydrotalcites are capable of buffering the contents of the stomach at pH 4 for extended periods of time. It is this property that has also made LDHs increasingly attractive for medical applications, where it can be used for controlled release of medicines. Thus the incomplete degradation of the complex, indicated by the presence of some of the complexes remaining in the well, as can be seen in lane 4 (Figure 4.13), was as expected after an overnight

incubation period. The slow dissolution process of the DNA:LDH complex indicates that the DNA transfection rate via LDH nanoparticles would be a slow process. This is the reason for the extended incubation period of 72 hours for the transfection studies (Chapter 6).

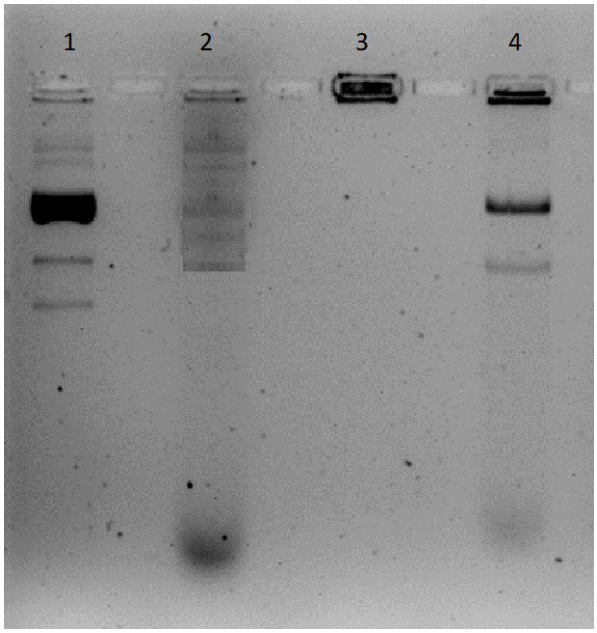

Figure 4.13 Results of nuclease digestion assay of DNA:MgAl 0.33. Lane 1 : naked DNA, Lane 2: DNA exposed to nuclease digestion, Lane 3 :MgAl 0.25 DNA-LDH complex, and Lane 4: MgAl 0.25 DNA-LDH complex exposed to nuclease digestion.

There does appear to be a small amount of degradation of the DNA from the DNA:LDH complex. This confirms reports by Xu *et al* (2007), Ladewig[1] *et al* (2010) and Lu *et al* (2016) that some of the DNA is bound to the surface of the LDH, leaving the DNA partially exposed to nuclease digestion. Similar results were obtained for the siRNA:LDH complex (Figure 4.14). The naked siRNA is almost totally digested by the nuclease present in the serum (lane 2), whilst there appears to be minimal degradation of the siRNA:LDH complex after exposure to nuclease digestion. Most of the siRNA from the siRNA:LDH complex exposed to nuclease digestion still appears to be present in the well of the gel (lane 4), indicating that the siRNA is still bound to the LDH. This implies that some degree of protection has been afforded to the siRNA by the LDHs.

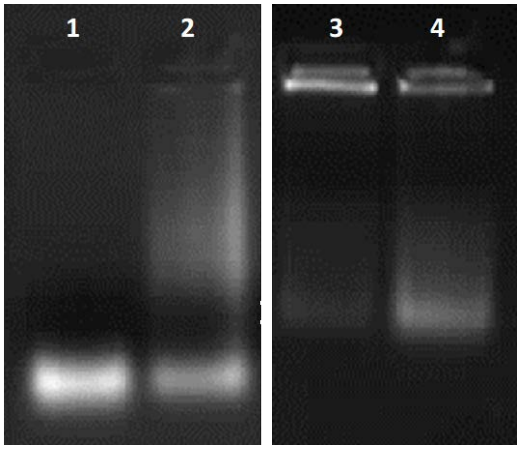

Figure 4.14 Results of nuclease digestion assay of siRNA:MgAl 0.25. Well 1 was loaded with naked siRNA, well 2 contained siRNA exposed to nuclease digestion, well 3 was loaded with the MgAl 0.25 siRNA-LDH complex, and well 4 contained the MgAl 0.25 siRNA-LDH complex exposed to nuclease digestion.

4.4 CONCLUSION

The optimal binding ratio of DNA:LDH was found to be 1:30 (w/w). The optimal binding ratios of siRNA:LDH complexes varied between 1:10 to 1:40 (w/w) depending on the LDH used. The MgAl 0.25 and MgAlHist 0.33 samples bound completely at a siRNA:LDH ratio of 1:30 (w/w), the MgAlArg 0.25 and MgAlHist 0.25 exhibited complete binding at a siRNA:LDH ratio of 1:20 (w/w), whilst the MgAl 0.33 and MgAlArg 0.33 bound optimally at a siRNA:LDH ratio of 1:10 (w/w). The MgFe 0.25, MgFe 0.33, ZnAl 0.25 and ZnAl 0.33 LDH samples bound completely with the siRNA at a ratio of 1:40 (w/w).

Results of the nuclease digestion assay show that most of the nucleic acid (DNA/RNA), appear to retain its integrity after being exposed to the serum nucleases, and afforded reasonable protection to the respective nucleic acid cargo. Hence, these LDHs show potential as suitable gene carriers for further transfection studies.

CHAPTER 5

5. *IN VITRO* ASSAYS: CYTOTOXICITY, GENE EXPRESSION AND GENE SILENCING STUDIES

5.1. INTRODUCTION

The use of cell-based assays is important for testing the various parameters with regards to their physiological processes and their response to external factors and compounds. Hence, they have become useful tools to predict the possible outcome of *in vivo* studies. Their use in preclinical applications of gene and drug therapy is without doubt. The cell viability, MTT assay and luciferase gene expression studies were conducted on the human cell lines: embryonic kidney (HEK293), hepatocellular carcinoma (HepG2), and colon adenocarcinoma (Caco-2). The human cervical carcinoma cells stably transformed with the luciferase gene (Hela-*tat-luc)*, was also used in the MTT assay, but solely employed in the gene silencing assay. A brief description of the cell lines is provided below.

HEK293

In 1973, Frank Graham in the Netherlands, transformed cultures of normal human embryonic kidney cells (from an apparently healthy, legally aborted fetus) with sheared adenovirus 5 DNA to form HEK293 cells. The cell line was so named because it was Grahams 293rd experiment [www.hek293.com (Date accessed: 15th September 2017)]. The transformation was due to the incorporation of a 4.5 kb insert from the viral genome into human chromosome 19 [https://en.wikipedia.org/wiki/HEK_293_cells (Date accessed: 15th September 2017)]. The exact cell type of HEK293 is unknown as adenovirus 5 significantly changes cell morphology and expression post-transformation, but it is speculated to be neuronal in origin.

HEK293 cells have a modal chromosome number of 64, and are referred to as being hypotriploid, because they contain less than three times the number of chromosomes of a normal diploid human cell. HEK293 expresses the corticotrophin releasing factor type 1 receptor, sphingosine-1-phosphate receptors EDG1, EDG3 and EDG5, muscarinic acetylcholine receptor M3 and the

transient receptor potential TRPC1, TRPC3, TRPC4, TRPC6 [www.hek293.com (Date accessed: 15th September 2017)]. HEK293 cells (Figure 5.1) are extremely popular in cell culture due to their ease of growth and transfectibility, which makes them ideal for gene expression studies.

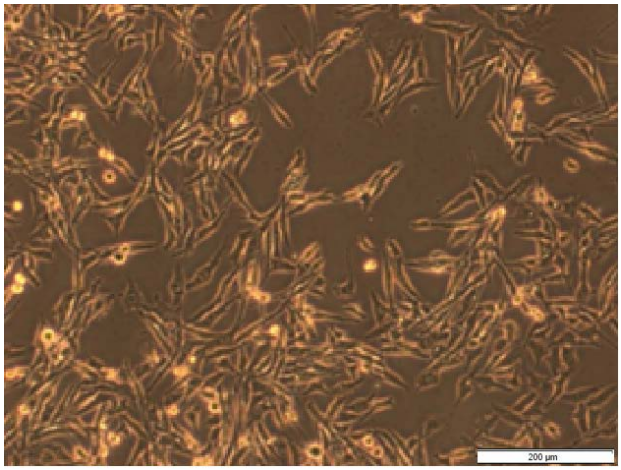

Figure 5.1 Image of HEK293 cells (x100) captured using an *Olympus* inverted microscope.

HepG2

The HepG2 cell line (Figure 5.2) was derived from a well differentiated liver hepatocellular carcinoma of a 15-year old Caucasian male [www.hepG2.com (Date accessed: 15th September 2017)]. The cells have a modal chromosome number of 55. HepG2 cells are relatively easy to culture and grow as adherent monolayers and/or small aggregates with an epithelial morphology. When properly cultured, HepG2 cells differentiate to form apical and basolateral cell surfaces, which bear resemblance to liver structures *in vivo*. This makes HepG2 cells useful in the study of intracellular transport between different liver cell types. The high degree of morphological and functional differentiation of HepG2 cells *in vitro*, as well as the absence of viral infection (no hepatitis B surface antigens), makes them ideal models for hepatocellular carcinoma studies [Costantini *et al*., 2013]. HepG2 cells are regularly used when examining toxicity of substances to the liver, liver metabolism and drug metabolism studies.

HepG2 cells contain unique asialoglycoprotein receptors that bind and internalize galactose terminal asialoglycoproteins [Wu and Wu, 1987; Wu and Wu, 1988], making HepG2 a useful cell

line for receptor mediated endocytosis studies. These cells have even been used in trials with bio-artificial liver devices [www.hepG2.com (Date accessed: 15th September 2017)].

HepG2 cells secrete a number of plasma proteins such as albumin, transferrin, fibrinogen, alpha-2-macroglobulin, alpha-1-antitrypsin, alpha-1-antichymotrypsin, plasminogen, haptoglobulin, ceruloplasmin, alpha-1-acid glycoprotein, alpha-2-HS-glycoprotein, beta-lipoprotein and retinol binding protein [https://en.wikipedia.org/wiki/Hep_G2 (Date accessed: 15th September 2017)], and has 3-hydroxy-3-methylglutaryl-CoA reductase and hepatic triglyceride lipase activities.

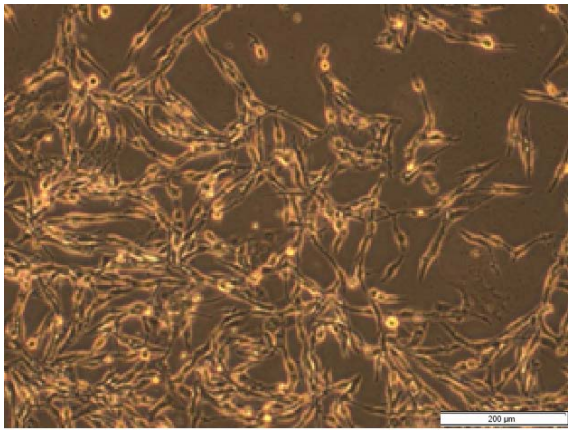

Figure 5.2 Image of HepG2 cells (x100) captured using an *Olympus* inverted microscope.

Caco-2

Caco-2 cells (Figure 5.3) have a modal chromosome number of 96, and were first isolated from a primary colonic tumour, from a 72 year old Caucasian male in the 1970s. It is a continuous, heterogeneous cell line that undergoes spontaneous differentiation and expresses the morphological and biochemical characteristics of intestinal enterocytes, making them ideal models of the intestinal barrier for *in vitro* cytotoxicity studies [Natoli *et al*., 2012; Sambuy *et al.,* 2005]. Caco-2 cells are adherent cells that display an epithelial morphology and grow in a monolayer. Caco-2 cells express a number of enzymes such as sucrase-isomaltase, peptidases and esterases, and nutrient transporters of sugars, amino acids, bile acids, carboxylic acids, as well as transporters of micronutrients such as heavy metals and nucleosides [Sambuy *et al.,* 2005; https://en.wikipedia.org/wiki/Caco-2 (Date accessed: 15th September 2017)].

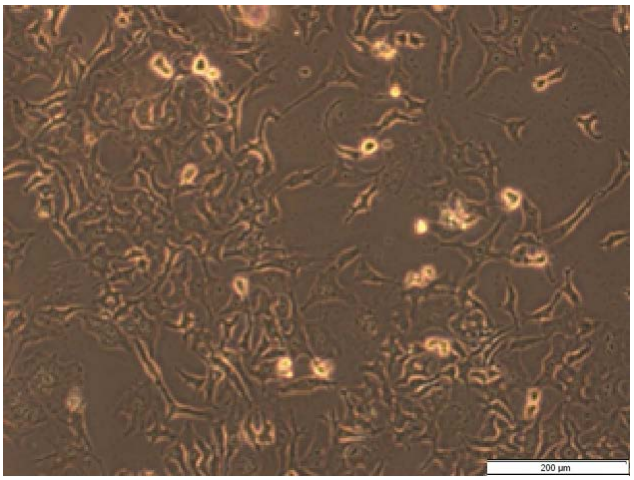

Figure 5.3 Image of Caco-2 cells (x100) captured using an Olympus inverted microscope.

Hela-*tat-luc*

The original Hela cell line was derived from a cervical carcinoma of a 31-year old African American female in 1951 [https://en.wikipedia.org/wiki/HeLa (Date accessed: 15th September 2017)]. These were the first human immortal cell line used for medical research. The Hela-*tat-luc* cells (Figure 5.4) used in this study have been transfected with the Tat protein from the human immunodeficiency type 1 virus (HIV-1), and also stably transformed using the firefly luciferase gene.

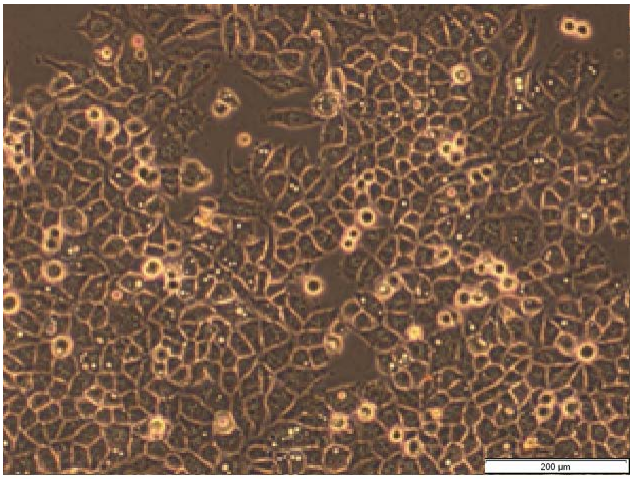

Figure 5.4 Image of HeLa-*tat-luc* cells (x100) captured using an *Olympus* inverted microscope.

5.1.1 CYTOTOXICITY STUDIES

Before undertaking gene expression and silencing studies, it is essential to determine the cytotoxicity of the LDHs in cell culture, since high levels of toxicity, even in the presence of good transfection, would render the nanoparticles unsuitable for *in vivo* applications. There are currently many convenient and cost-effective colorimetric and fluorometric based cytotoxicity assays available, where the samples can be assessed directly on the culture plate using a plate reader [Weyermann *et al*., 2005]. These methods include lactate dehydrogenase release, neutral red uptake, crystal violet staining, ATP and the 3-(4,5-dimethylthiazol-2-yl)-2,5-diphenyltetrazolium (MTT) assays [Fotakis and Timbrell, 2006; Weyermann *et al*., 2005], among others.

For this study, the MTT assay was used to assess cell viability after exposure to the nucleic acid:LDH complexes. The MTT assay was first proposed by Mosmann (1983) and has been extensively used despite disadvantages such as decreased formazan production due to the actions of reducing agents and respiratory chain inhibitors of mitochondrial MTT reduction. It has also been reported that the MTT assay could be influenced by factors such as medium pH, D-glucose concentration of the growth medium and cellular concentration of pyridine nucleotides [Chiba *et al*., 1998]. Advantages of the MTT assay include the simplicity of the method, high sensitivity and the use of equipment easily found in most laboratories.

MTT is a water-soluble salt containing a tetrazolium ring, which can be cleaved by mitochondrial succinate dehydrogenases, leading to the formation of an insoluble, purple-colored formazan product which is impermeable to the cell membrane and therefore accumulates within healthy cells [Fotakis and Timbrell, 2006]. The amount of formazan produced is proportional to the number of viable cells present in the culture. Hence, the ability of the cells to reduce MTT correlates to the cells viability, since only viable cells will have an active mitochondrion [Chiba *et al*., 1998]. There have been many modifications to Mosmann's method over the years [Tada *et al*., 1986; Denizot and Lang, 1986; Carmichael *et al*., 1987; Twentyman and Luscombe, 1987], and the method employed for this study is similar to that reported by Carmicheal and co-workers (1987), with DMSO being used to solubilize the formazan instead of mineral oil. This is because

DMSO does not cause precipitation of proteins and results in a clearer formazan solution, with stable optical density [Twentyman and Luscombe, 1987].

5.1.2 GENE EXPRESSION AND SILENCING STUDIES

A transfection study is carried out to determine whether a vector is able to efficiently deliver the nucleic acid into a cell resulting in either sustained expression of the transgene (DNA) or silencing of the target gene (siRNA).

The plasmid DNA utilised in this study is the pCMV-*luc DNA*, described previously in chapter 4 (section 4.1). The luciferase assay is based on the fact that mammalian cells do not naturally express the luciferase gene, which is only expressed upon successful transfection of the pCMV-*luc* DNA into eukaryotic cells. This reaction requires the addition of the substrates luciferin, ATP and oxygen, to catalyze the production of light or luminescence, which can be measured using a luminometer. The luciferase gene isolated from the firefly *P. pyralis* is composed of seven exons separated by six very short introns, all less than 60 bases in length [de Wet *et al*., 1987].

The reactions catalyzed by firefly luciferase are:

$$\text{Luciferase + luciferin + ATP} \xleftrightarrow{Mg^{2+}} \text{luciferase.luciferyl AMP + PPi}$$

$$\text{luciferase.luciferyl AMP + } O_2 \rightarrow \text{luciferase + oxyluciferin + AMP + } CO_2 + h\nu \text{ (light)}$$

The amount of light produced is directly proportional to the quantity of luciferase present in the reaction mixture.

The luciferase enzyme activity can also be used as an indicator of gene silencing. The Hela *tat-luc* cell line stably expresses the luciferase gene and the anti-*luc*-siRNA specifically targets the luciferase gene. Efficient delivery of the anti-*luc*-siRNA results in a decrease in luciferase activity, which can be similarly measured using a luminometer.

5.2. MATERIALS AND METHODS

5.2.1 MATERIALS

Eagle's Minimum Essential Medium (EMEM) containing Earle's salts and L-glutamine, trypsin-versene and penicillin-streptomycin mixtures was purchased from *Lonza BioWhittaker* (Walkersville, USA). Foetal bovine serum (FBS) was purchased from *Hyclone GE Healthcare* (Utah, USA). Phosphate-buffered saline (PBS) tablets were purchased from *Calbiochem* (Canada). The MTT salt (3-(4,5-dimethylthiazol-2-yl)- 2,5-diphenyltetrazolium bromide) was purchased from *Merck* (Darmstadt, Germany). All sterile tissue culture plastic ware obtained from *Corning Inc.* (NY, USA). HepG2 and Caco-2 cells were sourced from *Highveld Biologicals (PTY) LTD* (Lyndhurst, South Africa). HEK293 (human embryonic kidney) cells were supplied by the University of Witwatersrand, Medical School, South Africa. HeLa *tat luc* cell line was provided by the Department of Physiology, University of KwaZulu-Natal, Westville Campus. The pCMV-*luc* DNA was purchased from *Plasmid Factory* (Bielefeld, Germany), while the anti-luc-siRNA was obtained from *Thermo-Scientific Dharmacon Products* (Lafayette, CO). The Luciferase Assay kit was purchased from the *Promega Corporation*, Madison, USA. The bicinchoninic acid (BCA) assay reagents were purchased from the *Sigma-Aldrich Co*., St. Louis, USA. All other reagents were of analytical grade.

5.2.2 MTT ASSAY

Cells were maintained in EMEM supplemented with 10 % (v/v) gamma-irradiated FBS and 1 % antibiotics (100 U/mL penicillin, 100 µg/mL streptomycin) at 37 °C and 5% CO_2, in a HEPA Class 100 Steri-Cult CO_2 incubator (*Thermo-Electron Corporation,* Waltham, Massachusetts, USA). The MTT assay was carried out using Caco-2, HEK293 and HepG2 cells for the DNA:LDH complexes and using the HeLa- *tat-luc* cell line for the siRNA:LDH complexes.

For the MTT assay, cells were trypsinized and seeded into 48-well plates at a seeding density of approximately 3 X 10^4 cells/well, and incubated at 37 °C for 24 hours to allow for attachment. The medium was then replaced with fresh medium, and the respective DNA:LDH complexes were added to the wells and allowed to incubate for 48 hours at 37 °C. Complexes prepared were at

DNA:LDH ratios (sub-optimal, optimal and supra-optimal), as determined from the gel retardation assays (chapter 4, section 4.3). A positive control containing only cells was set as 100 % cell survival/viability. All assays were performed in triplicate. After the 48-hour incubation period the spent medium was removed and 200 µL fresh medium and 200 µL MTT reagent (5 mg/mL in PBS) was added to each well.

The cells were incubated at 37 °C for a further 4 hours, after which the MTT-medium solution was removed and 200 µL DMSO was added to solubilize the formazan crystals. Absorbance was read at 540 nm using a *Mindray* MR-96A microplate reader (*Vacutec*, Hamburg, Germany).

5.2.3 LUCIFERASE GENE EXPRESSION STUDIES

DNA transfection studies were carried out in the HEK293, HepG2 and Caco-2 cell lines, using the pCMV-*luc* plasmid DNA. The cells were seeded in 48 well plates at a cell density of 3.0×10^4 cells per well and incubated at 37 °C for 24 hours. The medium was then replaced with fresh medium and the respective DNA:LDH complexes were added to the wells and allowed to incubate for 72 hours at 37 °C. Complexes were prepared as in 5.2.2. Each assay was done in triplicate. Two controls were used, cells only and cells with naked plasmid DNA. After the 72-hour incubation period, the luciferase activity of the cells was determined using the Promega luciferase assay system.

The cells were prepared by removing the growth medium and washing twice with PBS. Thereafter, 80 µl of 1× cell lysis reagent (25 mM Tris-phosphate, pH 7.8; 2 mM dithiothreiotol, 2 mM 1,2- diaminocyclohexane – N, N, N'N'- tetra-acetic acid, 10 % (v/v) glycerol, 1 % (v/v) triton X-100) was added to the cells, which were then gently rocked on a Stuart Scientific Platform Shaker for 15 minutes at 30 rev/ min. The lysed cells were dislodged from the multiwell plates by gently scraping. The cell suspension was then pelleted by centrifugation at 12000 x g for 5 seconds. The cell free extract was retained for the determination of luciferase activity. A volume of 20 µl of each of the cell free extracts was transferred to a white multiwell plate and placed in a GloMax® Multi+ detection system (*Promega*). Luciferase assay reagent (100 µL; 20 mM Tricine, 1.1 mM Magnesium carbonate hydroxide pentahydrate, 2.7 mM Magnesium sulphate, 0.1 mM

EDTA, 33.3 mM dithiothreitol, 270 µM coenzyme A, 470 µM luciferin, 530 µM ATP) was then automatically injected into the samples and the luminescence was read immediately. The protein content of the cell free extracts was determined using the BCA assay, at 540 nm. All luminescence readings were normalized against the protein content and expressed as relative light units per milligram protein (RLU/mg protein). The results were presented as means ± SD.

5.2.4 LUCIFERASE GENE SILENCING STUDIES

The overall procedure for the gene silencing studies was similar to that for the DNA transfection studies (5.2.3). The Hela *tat-luc* cell line, stably expressing the luciferase gene was used and the complexes comprised of anti-*luc*-siRNA and LDH prepared at ratios as determined by the binding assays (chapter 4, section 4.3). The only difference in methodology for the knockdown studies was that the cells were allowed to incubate with the complexes for 48 hours instead of the 72-hour incubation period used for the DNA transfection studies. This was because previous reports have shown that optimal gene knockdown occurs between a 36 and 48-hour incubation period [Ladewig[2] *et al*., 2010]. Wong and co-workers (2010) have also reported effective gene silencing following a 24-hour incubation period. To validate transfection, the luciferase assay was carried out as described above (5.2.3).

5.3 STATISTICAL ANALYSIS

All graphs were plotted in Microsoft Excel™. All data are presented as mean ± standard deviation (± SD n=3). Graphpad Instat Prism 4.0.3 software was used for statistical analysis. Multi group comparisons of means were carried out using one-way analysis of variance (ANOVA) followed by the Tukey-Kramer *post hoc* test. Statistical significance for all tests was set at ***p<0.0005 (high significance), **p<0.005 (medium significance) and *p<0.05 (low significance). Each experimental value was compared to its corresponding control.

5.4 RESULTS AND DISCUSSION

5.4.1 CYTOTOXICITY STUDIES

5.4.1.1 MTT ASSAY OF DNA:LDH COMPLEXES

Cytotoxicity of nanoparticles is influenced by a number of factors such as the cell line used, cell culture conditions, nanoparticle size, nanoparticle concentration and duration of exposure [Choi and Wang, 2011]. The six DNA:hydrotalcite complexes were very well tolerated by the all cell lines at the ratios and conditions tested (Figure 5.5). The cell viabilities, after a 48 hour incubation period with complexes prepared at optimal ratio were, for Caco-2 cells -MgAl 0.25 (83.50 %), MgAl 0.33 (91.16 %), MgAlArg 0.25 (105.2 %), MgAl Arg 0.33 (102.9 %), MgAlHist 0.25 (103.3 %) and MgAlHist 0.33 (102.8 %); for the HEK293 cells -MgAl 0.25 (103.7 %), MgAl 0.33 (99.69 %), MgAlArg 0.25 (98.58 %), MgAl Arg 0.33 (102.1 %), MgAlHist 0.25 (105.3 %) and MgAlHist 0.33 (109.8 %); and for the HepG2 cells - MgAl 0.25 (97.57 %), MgAl 0.33 (101.5 %), MgAlArg 0.25 (108.3 %), MgAl Arg 0.33 (103.5 %), MgAlHist 0.25 (109.1 %) and MgAlHist 0.33 (106.3 %) respectively.

A similar trend was observed for all cell lines after exposure to the other DNA:LDH complexes as shown in Figure 5.6. The cell viabilities, after a 48-hour incubation period with complexes prepared at optimal ratio were, for Caco-2 cells -MgFe 0.25 (91.38 %), MgFe 0.33 (96.83 %), ZnAl 0.25 (95.90 %) and ZnAl 0.33 (94.16 %); for the HEK293 cells - MgFe 0.25 (106.8 %), MgFe 0.33 (100.5 %), ZnAl 0.25 (110.6 %) and ZnAl 0.33 (98.15 %); and for HepG2 cells - MgFe 0.25 (99.02 %), MgFe 0.33 (100.6 %), ZnAl 0.25 (109.3 %) and ZnAl 0.33 (108.9 %) respectively. The Tukeys comparison test revealed no statistical significance, except in the case of MgAl 0.25 at the supra-optimal binding ratios. Minimal cell death was observed with the Caco-2 cell line after treatment with all the complexes, but the presence of the complexes appeared to be growth-promoting in the case of the HEK293 and the HepG2 cell lines. The complexes appeared to 'shroud' the cells, protecting them, and also promoting growth of the cells. Balcomb *et al* (2015) reported similar results and suggested that the increased cell viabilities, especially with iron containing LDHs was on account of the increased redox potential and cell oxidative processes brought about within the cell due to the presence of increased intracellular iron.

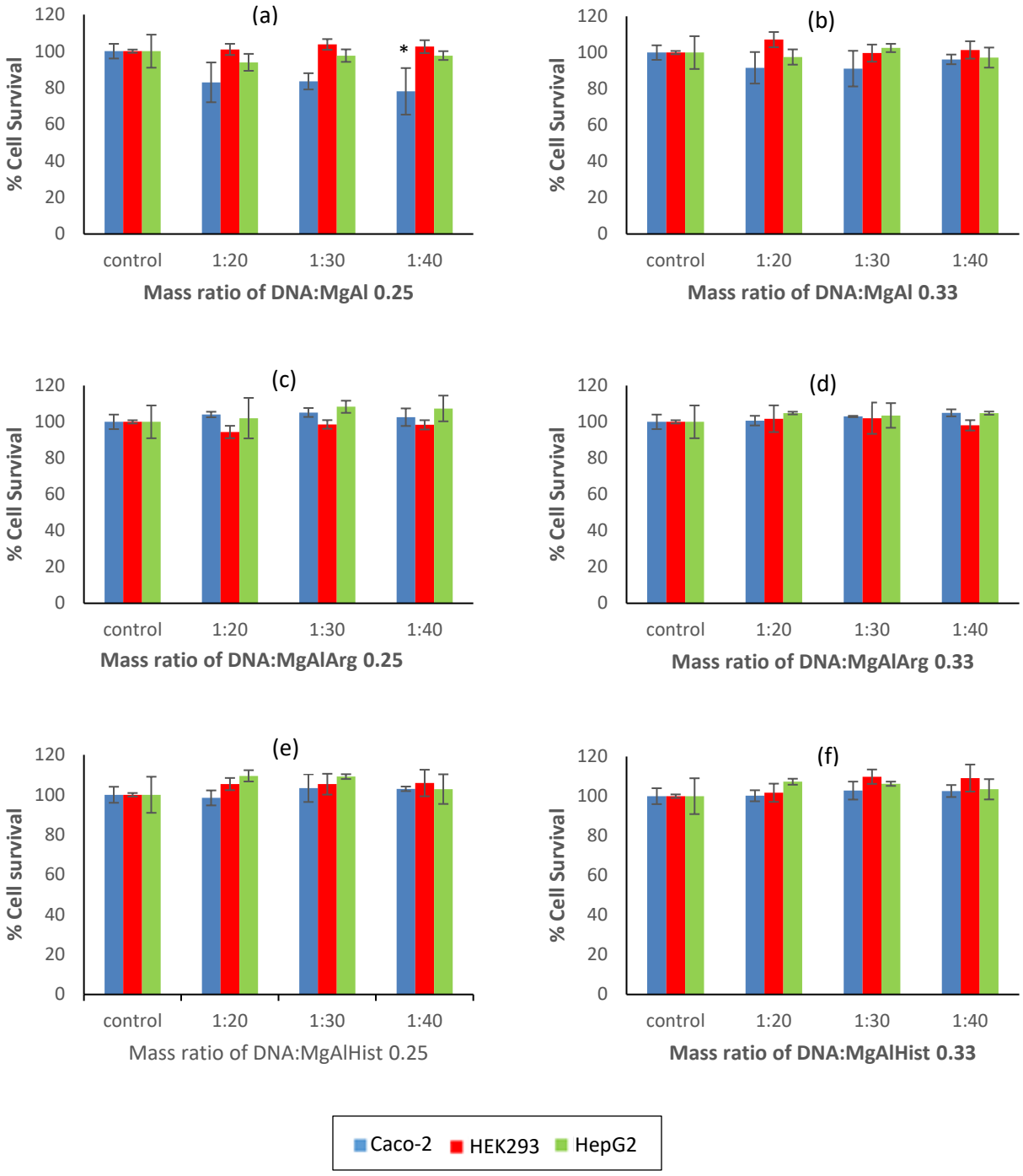

Figure 5.5 MTT assay of Caco-2, HEK293 and HepG2 cells exposed to (a) pCMV-*luc* DNA:MgAl 0.25 complexes, (b) pCMV-*luc* DNA:MgAl 0.33 complexes, (c) pCMV-*luc* DNA:MgAlArg 0.25 complexes,(d) pCMV-*luc* DNA:MgAlArg 0.33 complexes, (e) pCMV-*luc* DNA:MgAlHist 0.25 complexes and (f) pCMV-*luc* DNA:MgAlHist 0.33 complexes. Data is represented as means ±SD (*n*=3). *p<0.05 was considered statistically significant.

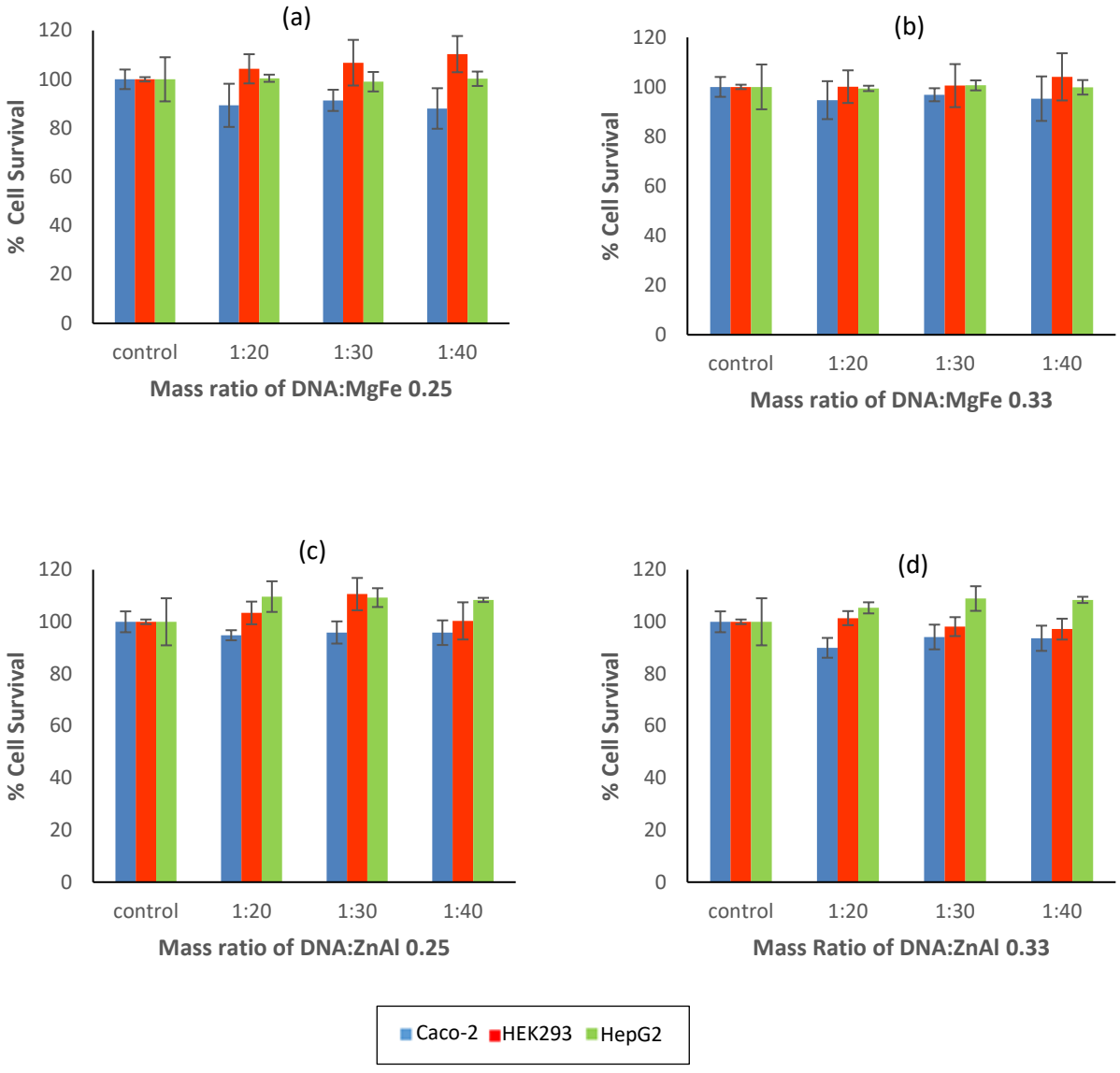

Figure 5.6 MTT assay of Caco-2, HEK293 and HepG2 cells exposed to (a) pCMV-*luc* DNA:MgFe 0.25 complexes, (b) pCMV-*luc* DNA:MgFe 0.33 complexes, (c) pCMV-*luc* DNA:ZnAl 0.25 complexes and (d) pCMV-*luc* DNA:ZnAl 0.33 complexes. Data is represented as means ±SD (*n*=3). No statistically significant change in percent cell survival was observed.

5.4.1.2 MTT ASSAY OF siRNA:LDH COMPLEXES

The Hela-*tat-luc* cells all displayed prolific growth in the presence of all the siRNA-LDH complexes as can be seen in Figures 5.7-5.9. The cell viabilities, at optimal binding ratio, in the presence of the hydrotalcites were MgAl 0.25 (117.6 %), MgAlArg 0.25 (103.5 %), MgAlHist 0.25 (110.7 %), MgAl 0.33(114.7 %), MgAlArg 0.33 (107.9 %) and MgAlHist 0.33 (107.8 %). The iron containing complexes showed higher cell viability than the other complexes, with cell viabilities in the presence of MgFe 0.25 being 136.7 % and MgFe 0.33 being 135.2 % respectively (Figure 5.9). The viabilities in the presence of ZnAl 0.25 and ZnAl 0.33, were 109.7 % and 112.5 % respectively. The high cell viabilities of the hydrotalcites were expected, as there have been previous reports of hydrotalcites exhibiting negligible cytotoxicity at biologically relevant concentrations [Chen *et al*., 2013].

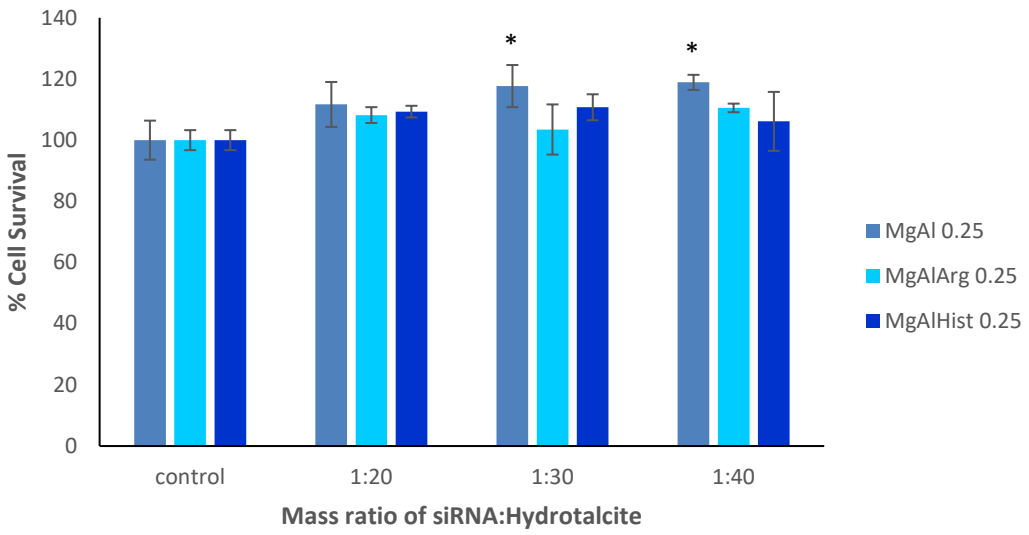

Figure 5.7 MTT assay of Hela-*tat-luc* cells exposed to anti-*luc* siRNA:MgAl 0.25 complexes, anti-*luc* siRNA:MgAlArg 0.25 complexes and anti-*luc* siRNA:MgAlHist 0.25 complexes. Data is represented as means ±SD (n=3). *p<0.05 was considered statistically significant.

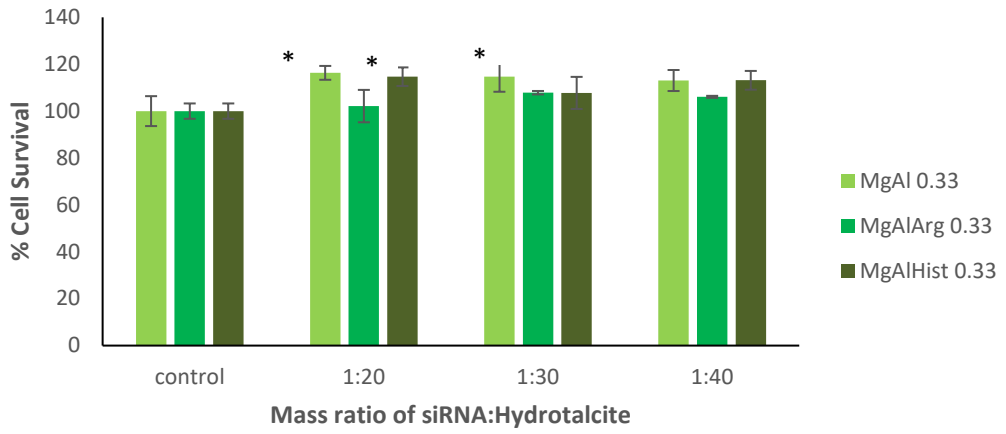

Figure 5.8 MTT assay of Hela-*tat*-*luc* cells exposed to anti-*luc* siRNA:MgAl 0.33, anti-*luc* siRNA:MgAlArg 0.33 complexes and anti-*luc* siRNA:MgAlHist 0.33 complexes. Data are represented as means ±SD (*n*=3). *p<0.05 was considered statistically significant.

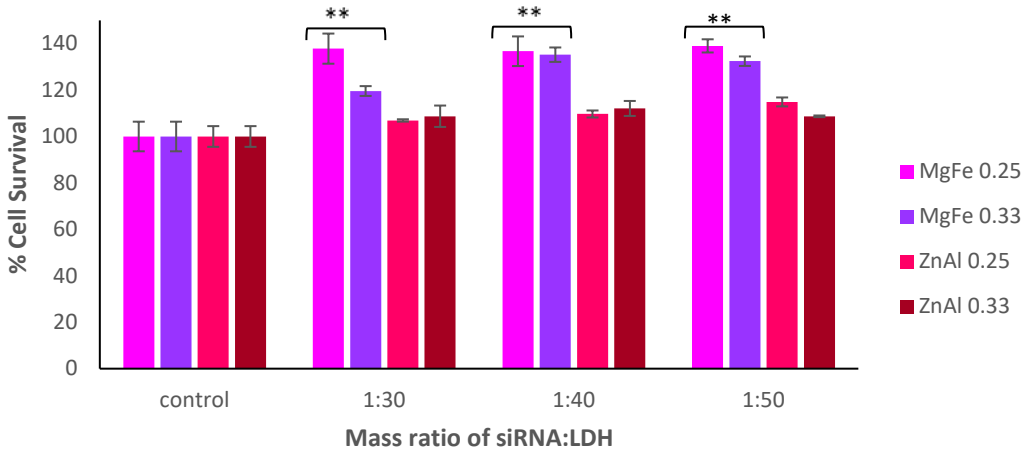

Figure 5.9 MTT assay of Hela-*tat*- *luc* cells exposed to anti-*luc* siRNA:MgFe 0.25 complexes, anti-*luc* siRNA:MgFe 0.33 complexes, anti-*luc* siRNA:ZnAl 0.25 complexes and anti-*luc* siRNA: ZnAl 0.33 complexes. Data are represented as means ±SD (*n*=3). **p<0.005 was considered statistically significant.

There have been many reports on the low toxicity of LDHs [Yan *et al*., 2014], with a drug delivery study showing that LDHs not only decreased the toxicity of the parent drug, but also increased the desired effect of the drug both *in vitro* and *in vivo* [Kura *et al*., 2014]. The results of this study confirm the low/almost negligible toxicity of LDHs. Results obtained in this study affirms reports by Xu and Lu (2006), that LDHs are about 10 times less cytotoxic than commonly used polymer transfection agents.

5.4.2 LUCIFERASE GENE EXPRESSION STUDIES

The level of transgene expression of the luciferase gene in all cell lines tested indicated successful transfection of the pCMV-*luc* DNA.

Results obtained indicate that the degree of transfection is largely cell line dependent. The HEK293 cell line displayed the highest luciferase gene expression, with the Caco-2 cell line showing lower but promising gene expression. The HepG2 cell line showed minimal gene expression, which was approximately 800 fold less than that displayed by the HEK293 and Caco-2 cell lines. Possible reasons for the difference in expression observed for the three cell lines investigated in this study, may be due to the different cell types having a preference for different endocytic pathways [Elouahabi and Ruysschaert, 2005], and also due to differences in cell membrane properties of the different cell lines [Spector and Yorek, 1985], that affect cellular uptake.

The level of luciferase activity of the non-functionalized LDHs (Figure 5.10), in the HEK293 was as follows: MgAl 0.25 < MgFe 0.25 < ZnAl 0.33 < ZnAl 0.25 < MgAl 0.33 < MgFe 0.33. MgFe 0.33 showed 15% greater transfection than MgAl 0.25. In the Caco-2 cell line, luciferase activity was as follows: MgFe 0.25 < ZnAl 0.25 < MgAl 0.25 < ZnAl 0.33 < MgAl 0.33 < MgFe 0.33. The HepG2 cell line showed a minimal but measurable degree of luciferase activity for all the non-functionalized LDHs. This was expected as HepG2 cells have a reputation of being a difficult to transfect cell line [Cemazar *et al.,* 2009]. Although MgAl 0.33 showed best transfection of all the LDHs tested, with the HepG2 cell line, the level of transfection observed was not as significant, as their functionalized counterparts.

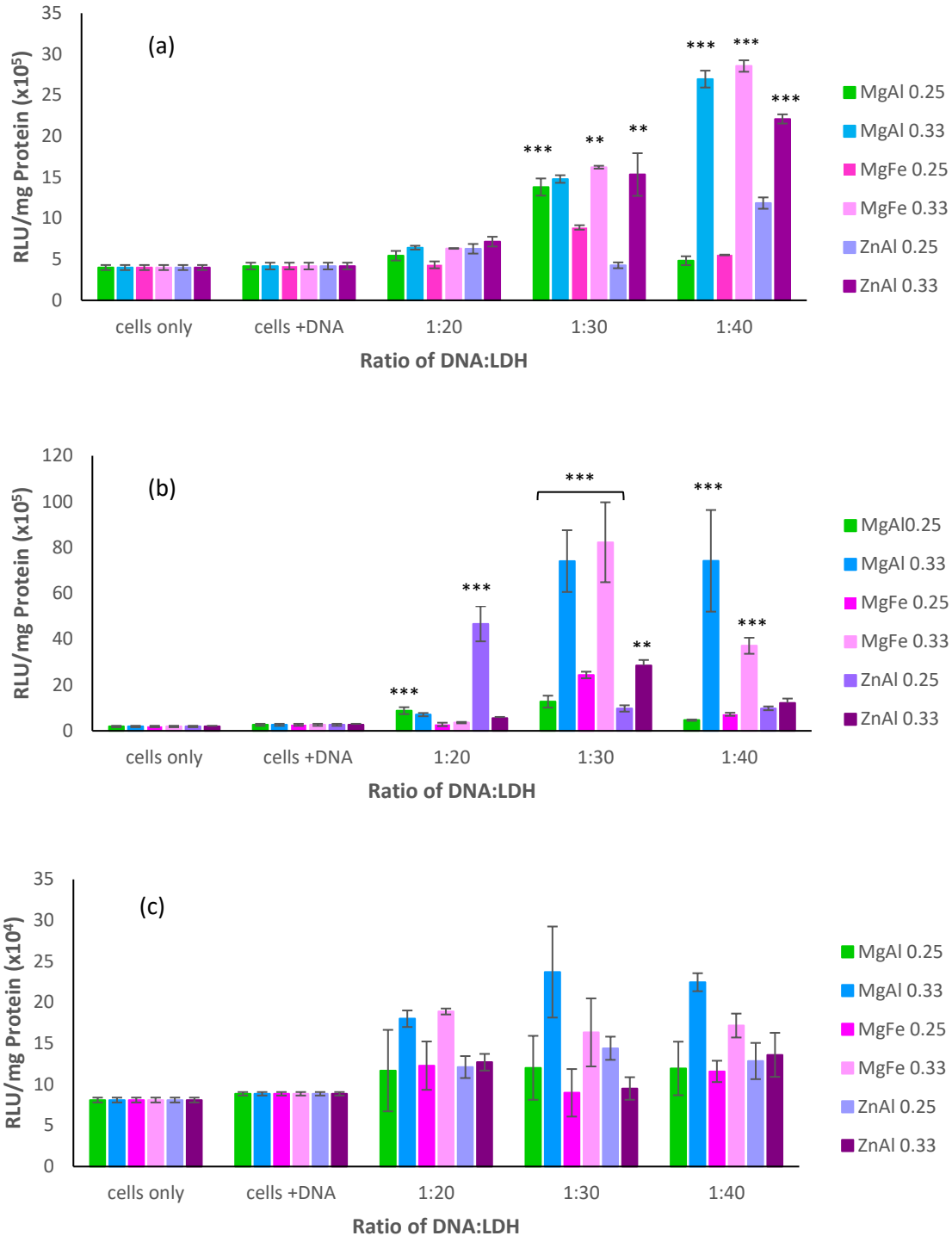

Figure 5.10 Luciferase Assay Results of non-functionalized LDHS in (a) Caco-2, (b) HEK293 and (c) HepG2 cell lines. Data is represented as means ±SD (*n*=3). **p<0.005, ***p<0.0005 was considered statistically significant.

A generally low level of transfection was observed with MgAl 0.25 in all cell lines tested, which was expected considering the large size of the DNA:MgAl 0.25 complex, probably due to aggregation caused by the DNA complexing to several LDH nanoparticles. This would have resulted in poor cellular uptake and internalization and consequently lower levels of transfection. Overall the non-functionalized LDHs prepared in the M^{2+}:M^{3+} ratio of 2:1 displayed significantly higher transfection than those prepared in the 3:1 ratio. The use of the MgAl 0.33 LDH carrier resulted in the highest level of transfection from all the HTs, in all cell lines tested. Li and co-workers (2014) have reported that LDHs prepared at M^{2+}:M^{3+} ratio of 2:1 show better adsorption of nucleic acids than those prepared in a 3:1 ratio. It seems that this increased adsorption of nucleic acid corresponded to increased transfection.

The zeta potential and size of a nanoparticle plays a key role in the cellular uptake of the particles [Nagaraj *et al*., 2015; Dong *et al*., 2015]. It also provides a good indication of the colloidal stability of the nanoparticles for *in vivo* application. Negative zeta potentials are expected to lead to poor cellular uptake and consequently poor transfection. Zeta potential is not necessarily an indication of the actual surface charge of the nanoparticle, but rather it is a measure of the potential difference between the particle surface and the solvent, and is dependent on other factors such as the pH of the solvent [Honary and Zahir, 2013]. Desigaux and coworkers (2006) have previously hypothesized that a negative zeta potential would not impede cellular internalization. Thus, even though the nanocomplexes displayed a negative zeta potential at pH 7, the zeta potential may be altered at physiological pH resulting in reduced effects on the transfection efficacy.

Positively charged nanoparticles are usually associated with enhanced cellular uptake (Kim *et al* 2014). This was exemplified by MgFe 0.33 (the only DNA:LDH complex with a positive zeta potential), which showed the greatest transfection of all the samples investigated. Rojas and co-workers (2015), have reported that transfection efficiency decreases as particle size increases beyond 200 nm, and that smaller particles (< 100 nm) may release their load faster, but may lead to toxicity, suggesting an ideal size range of 100-200 nm. On the contrary, the cytotoxicity assay results discussed earlier in this chapter show that although most of the complexes ranged in size from 20 to 60 nm, they do not exhibit much cytotoxicity.

Targeted drug delivery studies by Nagaraj and co-workers (2015) suggest that ZnAl LDHs may be better nano-carriers than MgAl LDHs. Here again, the current results contradict this, as MgAl 0.33 clearly displays significantly better transfection than the ZnAl 0.33 LDHs as shown in Figure 5.10.

The transfection results of the amino acid functionalized HTs in the Caco-2, HEK293 and HepG2 cell lines are shown in Figures 5.11, 5.12 and 5.13 respectively. In the Caco-2 cell line the luciferase activity was as follows: MgAlArg 0.25 < MgAlHist 0.25 < MgAlArg 0.33 < MgAl 0.25 < MgAlHist 0.33 < MgAl 0.33 (Figure 5.11).

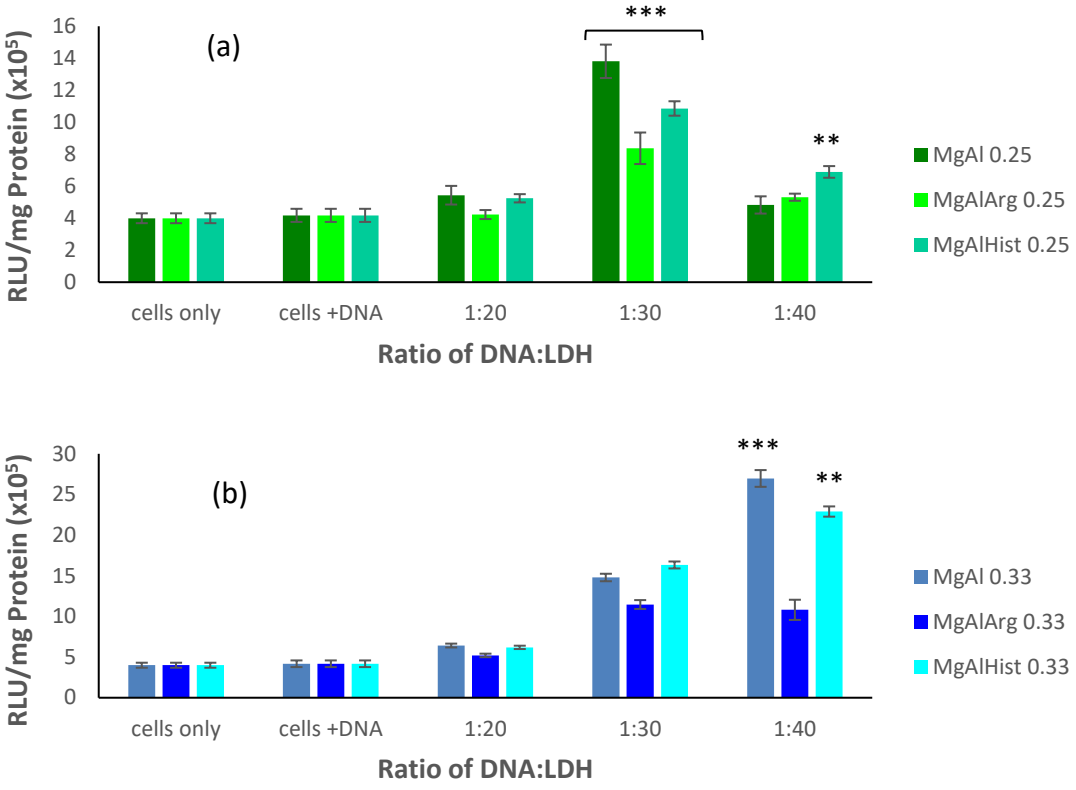

Figure 5.11 Luciferase gene expression using (a) MgAl 0.25, MgAlArg 0.25 and MgAlHist 0.25 and (b) MgAl 0.33, MgAlArg 0.33 and MgAlHist 0.33 in Caco-2 cells with 2 sets of controls, one containing only Caco2 cells and the second control containing cells with pCMV-*luc* DNA. Data is represented as means ±SD (*n*=3). **p<0.005, ***p<0.0005 was considered statistically significant.

In the HEK293 cell line the luciferase activity was as follows: MgAlArg 0.25 < MgAl 0.25 < MgAlArg 0.33 < MgAlHist 0.25 < MgAlHist 0.33 < MgAl 0.33 (Figure 5.12).

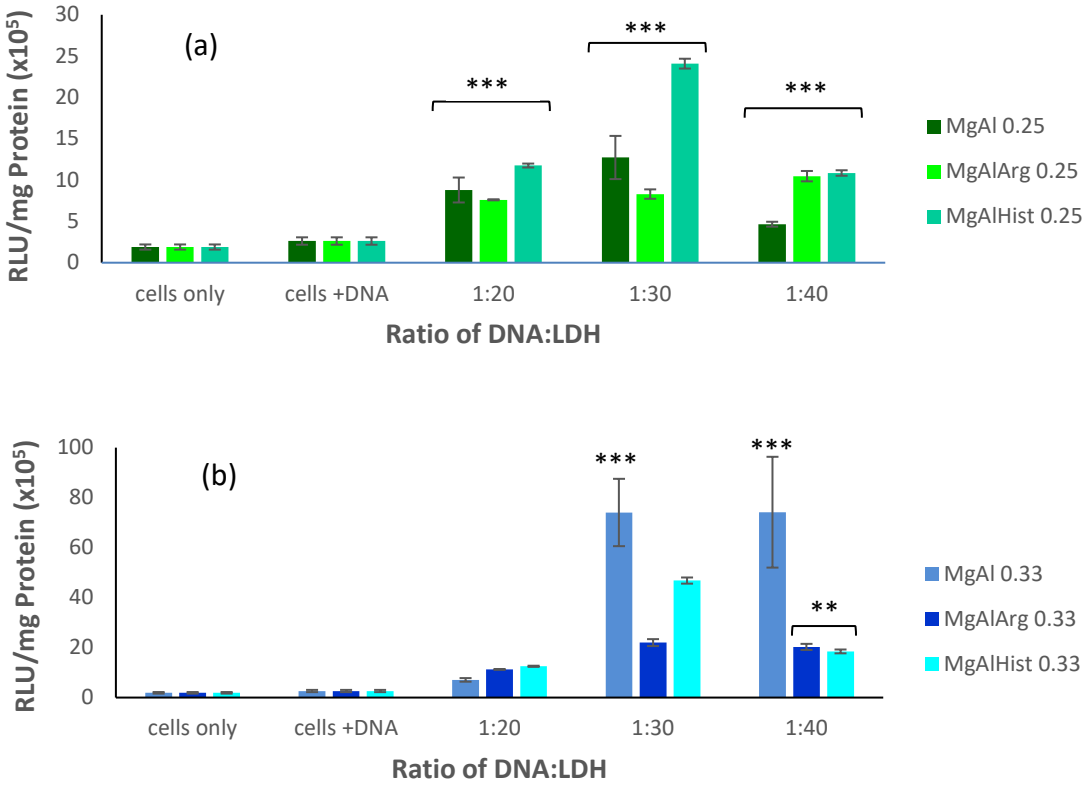

Figure 5.12 Luciferase assay using (a) MgAl 0.25, MgAlArg 0.25 and MgAlHist 0.25 and (b) MgAl 0.33, MgAlArg 0.33 and MgAlHist 0.33 in HEK293 cells with 2 sets of controls, one containing only HEK293 cells and the second control containing cells with pCMV-*luc* DNA. Data is represented as means ±SD (*n*=3). **p<0.005, ***p<0.0005 was considered statistically significant.

Transfection of HTs in HepG2 (Figure 5.13), as with the non-functionalized LDHs, both resulted in minimal DNA uptake.

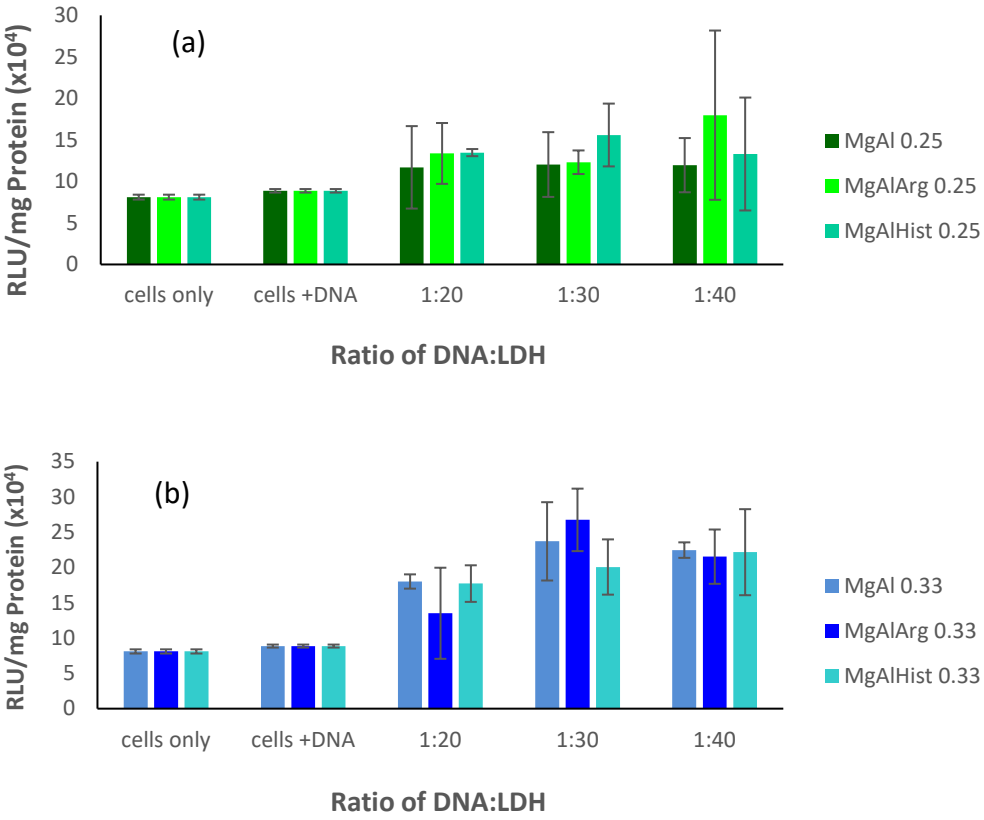

Figure 5.13 Luciferase assay using (a) MgAl 0.25, MgAlArg 0.25 and MgAlHist 0.25 and (b) MgAl 0.33, MgAlArg 0.33 and MgAlHist 0.33 in HepG2 cells with 2 sets of controls, one containing only HepG2 cells and the second control containing cells with pCMV-*luc* DNA. Data is represented as means ±SD (*n*=3). No significant transfection was observed.

Similar to the non-functionalized LDHs, aa-HTs prepared in the M^{2+}:M^{3+} ratio of 2:1 showed higher transfection than those prepared in the 3:1 ratio. Characterization of the aa-HTs indicated a higher degree of incorporation of the amino acid in MgAlArg 0.33 (2.62%, ζ-potential +6.7) and MgAlHist 0.33 (1.89%, ζ-potential +22.7) when compared to MgAlArg 0.25 1.27%, ζ-potential -19.8) and MgAlHist 0.25 (0.90%, ζ-potential -24.6), as indicated by the quantitative assays in chapter 3, and confirmed by the zeta potentials of the aa-functionalized HTs (chapter 4, section 4.3). The higher degree of incorporation of amino acid in the aa-HTs prepared in the M^{2+}:M^{3+} ratio of 2:1, appears to have resulted in higher transfection efficiency. Histidine functionalized HTs displayed better transfection efficiency than arginine functionalized HTs in the Caco-2 and HepG2 cells lines, as shown in Figures 5.11 and 5.13. There have been reports indicating that the

incorporation of histidine into gene delivery vehicles does improve cellular uptake, as well as enhance endosomal escape through the proton sponge effect [Shi *et al*., 2013; Meng *et al*., 2017], as does the incorporation of arginine [Gao *et al*., 2008; Wang *et al*., 2015]. The results of this study suggest that histidine functionalization of the gene delivery vehicle results in better transfection than arginine functionalization.

5.4.3 LUCIFERASE GENE SILENCING STUDIES

The results of the gene silencing studies are shown in Figures 5.14-5.16. Control 1 was untreated Hela *tat-luc* cells, and this was represented as 100%, as luciferase activity can be assumed to be highest in this control. Control 2 comprised of Hela *tat-luc* cells treated with naked anti-*luc*-siRNA, which produced gene silencing of less than 4%. This can be expected, as naked RNA can be easily degraded by nucleases before it reaches the cell, as was seen in the nuclease protection assay (Chapter 4, Section 4.2.4). The much greater percentage of gene silencing observed with the siRNA:LDH complexes confirms the requirement and significance of a gene delivery vehicle for efficient delivery and gene silencing. The siRNA:LDH complexes, all had negative zeta potentials (Chapter 4, Section 4.3) which was probably due to the siRNA binding to the outer surfaces of the LDHs, but this did not appear to be a hindrance to cellular uptake, internalization and the subsequent gene silencing.

The HT complexes prepared in a MgAl ratio of 3:1 ie. MgAl 0.25 showed a higher percentage of gene silencing than the HTs prepared in a MgAl ratio of 2:1 ie. MgAl 0.33. The highest degree of silencing for the non-functionalized HTs was 44.63%, which was observed for the siRNA:MgAl 0.25 complex prepared at the supra-optimal binding ratio. The amino acid functionalized HTs showed a higher degree of gene silencing (Figures 5.14 and 5.15), than the non-functionalized HTs. The arginine functionalized HTs (MgAlArg 0.25 and MgAlArg 0.33) showed almost identical gene silencing profiles, with the sub-optimal binding ratios of siRNA:HT exhibiting the greatest degree of silencing (approximately 56.9% gene silencing). The histidine functionalized HTs (MgAlHist 0.25 and MgAlHist 0.33) showed slightly improved gene silencing on average when

compared to the arginine functionalized HTs. This was a similar trend to the gene expression observed using the pCMV-*luc* DNA.

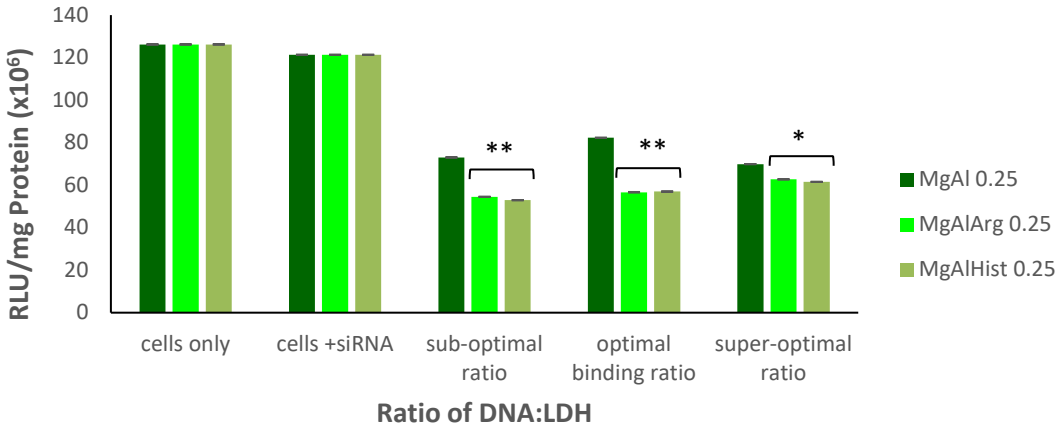

Figure 5.14 Luciferase gene silencing using MgAl 0.25, MgAlArg 0.25 and MgAlHist 0.25 in Hela *tat luc* cells with 2 sets of controls, one containing only Hela *tat-luc* cells and the second control containing Hela *tat luc* cells with anti-*luc* siRNA. Data is represented as means ±SD (*n*=3). *p<0.05, **p<0.005 was considered statistically significant.

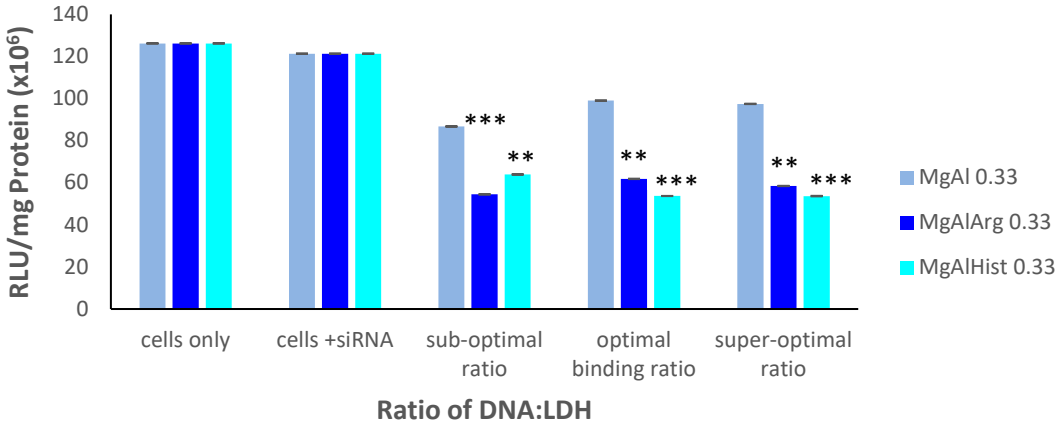

Figure 5.15 Luciferase gene silencing using MgAl 0.33, MgAlArg 0.33 and MgAlHist 0.33 in Hela *tat luc* cells with 2 sets of controls, one containing only Hela *tat-luc* cells and the second control containing Hela *tat luc* cells with anti-*luc* siRNA. Data is represented as means ±SD (*n*=3). **p<0.005, ***p<0.0005 was considered statistically significant.

A comparatively high percentage of gene silencing (58.07 %) was observed for the sub-optimal binding ratio for MgAlHist 0.25. The other histidine functionalized HT (MgAlHist 0.33) displayed silencing levels of 57.5 % each, for both the optimal and super-optimal binding ratios. Arginine and histidine are both amino acids with positively charged side chains at physiological pH. This overall positive charge possibly enhances the proton sponge effect leading to faster endosomal release of the complex, consequently resulting in more effective gene silencing.

It was also interesting to note that both siRNA-MgAlArg 0.25 and siRNA-MgAlHist 0.25 complexes brought about significantly greater gene silencing (56.8 % and 58.0 % respectively) than non-functionalized MgAl 0.25 (34.8 %). Both siRNA-MgAlArg 0.25 and siRNA-MgAlHist 0.25 complexes appeared as nanoflakes that were folded over, whereas siRNA-MgAl 0.25 complexes were spherical in shape (Chapter 4, Figures 4.10 and 4.12). Previous reports state that rod-shaped nanoparticles are more likely to pass through the nuclear pores and deliver the siRNA within the nucleus, whereas the load of spherical/hexagonal/square shaped complexes are generally released in the perinuclear region [Ladewig[2] *et al*., 2010; Rojas *et al*., 2015]. Interestingly the "folded-over" nanoflake structured siRNA-MgAlArg 0.25 and siRNA-MgAlHist 0.25 complexes) displayed better gene silencing than non-functionalized MgAl 0.25. It is possible that functionalization of MgAl 0.25 with the amino acids did actually enhance the proton-sponge effect resulting in release of the siRNA from these complexes in the perinuclear area of the cytosol, before they could actually enter the nucleus. Since the perinuclear area is the site of function of the siRNA, this increased the gene silencing efficiency of siRNA-MgAlArg 0.25 and siRNA-MgAlHist 0.25 complexes.

On average, considering all ratios investigated, the MgFe 0.25:siRNA complexes showed better gene silencing than the MgFe 0.33:siRNA complexes (Figure 5.16). In contrast to this, MgFe 0.33:siRNA complexes at optimal binding ratio displayed the highest degree of gene silencing (54.77 %), from all the samples tested. The MgFe 0.33:siRNA complexes have a modal size of 55.4 nm (Chapter 4, Section 4.3), and smaller LDHs have been reported to be better siRNA delivery vehicles than LHDs larger than 100 nm in diameter [Chen *et al*., 2013]. In this complex the ratio of Mg:Fe was 2:1 and this result once again confirmed that LDHs prepared in M^{2+}:M^{3+} ratio of 2:1 are better transfection vectors than those prepared in the ratio of 3:1.

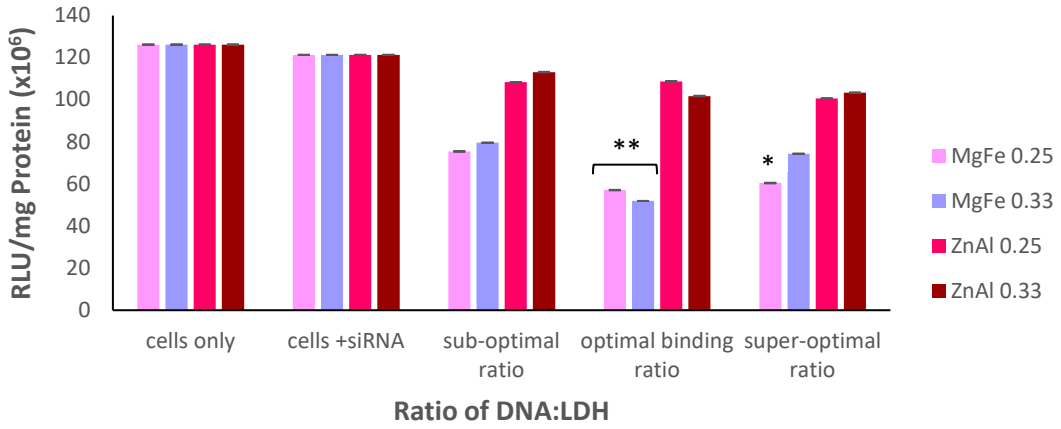

Figure 5.16 Luciferase gene silencing using MgFe 0.25, MgFe 0.33, ZnAl 0.25 and ZnAl 0.33 in Hela *tat luc* cells with 2 sets of controls, one containing only Hela *tat-luc* cells and the second control containing Hela *tat luc* cells with anti-*luc* siRNA. Data is represented as means ±SD (*n*=3). *p<0.05, **p<0.005 was considered statistically significant.

The lowest levels of gene silencing were observed with the complexes of siRNA and ZnAl LDHs (Figure 5.16). The percentage silencing for ZnAl 0.25 complexes and ZnAl 0.33 complexes was 16.11 and 15.93 % respectively. Posati and co-workers (2012) have previously reported significant uptake of ZnAl LDH nanoparticles in Hela cells, but the reasons for the low level of gene silencing observed in this study remains unclear. The Hela-*tat-luc* cells have displayed prolific growth in the presence of the siRNA:ZnAl complexes (Section 5.4.1.2), but unfortunately, this has not significantly affected gene silencing.

All the nanocomplexes prepared for this study showed some degree of gene silencing despite them all having a negative surface charge which was most probably as a result of the siRNA binding to the outer surfaces of the LDH. This negative zeta potential has not appeared to hinder cellular internalization, and may have actually resulted in a faster silencing owing to the quick release of siRNA from the surface of the LDH, when the LDH nanocomplexes start to dissolve in the endosome.

5.5 CONCLUSION

The results of the cytotoxicity assay indicate that all the LDHs prepared are non-toxic to the cell lines (at the concentrations tested) making them suitable candidates for future *in vivo* studies.

Gene expression studies revealed that HTs prepared in the M^{2+}:M^{3+} ratio of 2:1 (w/w) (both functionalized and non-functionalized) are better transfection agents than those prepared in the 3:1 (w/w) ratio. The results also indicate that functionalizing HTs with positively charged amino acids does not necessarily improve DNA transfection efficiency, since the non-functionalized LDHs MgAl 0.33 and MgFe 0.25 displayed the highest levels of transfection of all the samples investigated.

Results of the gene silencing studies clearly indicate that the complexes prepared from amino acid functionalized HTs exhibit greater gene silencing than the non-functionalized HTs. The presence of the positively charged amino acids probably resulted in exploitation of the proton sponge effect for quicker endosomal escape and subsequently increased levels of gene silencing.

CHAPTER SIX

6. CONCLUSION

LDHs have recently garnered much attention in the quest for safer and more effective gene delivery systems. Recent studies suggest that functionalization of inorganic gene delivery vehicles leads to enhanced transfection. In this study, the effect of functionalizing HTs with positively charged amino acids as compared to non-functionalized LDHs, with respect to gene delivery, was investigated.

LDHs and aa-functionalized HTs were successfully synthesized using the co-precipitation method, as confirmed by various analytical techniques. Characteristic XRD patterns with sharp, symmetrical, intense peaks at the lower 2θ values; broader, asymmetric, less intense peaks at the higher 2θ values, and the distinctive doublet peak at 2θ value of around 60 were observed for all prepared HTs/LDHs. The nanoparticles, which displayed flat, plate-like morphology, varied in size between 30 nm and 200 nm, with zeta potentials ranging from -24.7 to 29.7. The degree of incorporation of amino acid in the aa-functionalized HTs were found to be 0.90 % in MgAlHist 0.25, 1.89 % in MgAlHist 0.33, 1.20 % in MgAlArg 0.25 and 2.62 % in MgAlArg 0.33.

All the synthesized HTs and LDHs bound both DNA and siRNA, producing stable complexes and concurrently providing adequate protection against serum nuclease digestion. Vigorous agitation of DNA:HT/LDH complexes at room temperature resulted in complete binding within 10 minutes, without the need for overnight incubation at higher temperatures, as reported in other studies. The negative zeta potentials of most of the nucleic acid: LDH nanocomplexes combined with results of the XRD analysis of the DNA:MgAl 0.33 complex suggests that the nucleic acids bound to the outer surfaces of the LDHs, and does not actually intercalate within the interlayers.

Results of the MTT assays indicate that the nucleic acid:LDH nanocomplexes were well tolerated by all the cell lines tested. Minimal cell death was observed in the Caco-2 cell line whilst the presence of the nucleic acid:LDH nanocomplexes actually had a growth promoting effect on the HEK 293, HepG2 and Hela-*tat*-*luc* cell lines.

Transfection levels of the pCMV-luc plasmid as measured by the luciferase reporter gene assay was found to be cell line dependent. Minimal transfection was observed in the HepG2 cell line, while transgene expression in the HEK293 and Caco-2 cell lines was up to 800-fold higher than that measured in the HepG2 cell line. The highest levels of transgene expression were obtained with the non-functionalized LDHs MgAl 0.33 and MgFe 0.25. It can therefore be concluded that functionalization of LDHs with positively charged amino acids does not lead to enhanced transfection of plasmid DNA. This was in stark contrast to results obtained for the gene silencing studies, which revealed that the employment of aa-functionalized HTs as siRNA vectors lead to higher levels of gene knockdown when compared to the non-functionalized LDHs. Amino acid functionalized LDHs appear to be able to bypass one of the major hurdles faced in the formulation of a successful siRNA vector, which is the release of uncomplexed siRNA from the endocytic pathway before it reaches the lysosome. This has been achieved in the current study by exploitation of the proton-sponge effect, which is enhanced by the presence of the positively charged amino acids, arginine and histidine.

Results from this study suggests that aa-functionalized HTs are more effective siRNA vectors than pDNA carriers and would therefore be more applicable to gene silencing strategies. Possible future endeavors include the study of aa-functionalized HTs in *in vivo* gene silencing strategies using a suitable mouse model, as well as further modification of the vectors for targeted delivery.

REFERENCES

- Abderrazek K, Najoua FS, Srasra E, *Synthesis and characterization of [Zn–Al] LDH: Study of the effect of calcination on the photocatalytic activity*, Applied Clay Science **119** (2016) 229-235.
- Ahmed M, Jiang X, Deng Z and Narain R, *Cationic Glyco-Functionalized Single-walled carbon nanotubes as efficient gene delivery vehicles*, Bioconjugate Chemistry **20** (2009) 2017-2022.
- Ahmed[1] M, Deng Z, Liu S, Lafrenie R, Kumar A and Narain R, *Cationic Glyconanoparticles: Their complexation with DNA, Cellular uptake and transfection efficiencies*, Bioconjugate Chemistry **20** (2009) 2169-2176.
- Aisawa S, Takahashi S, Ogasawara W, Umetsu Y, Narita E, *Coprecipitation behaviour of amino acids with Zn-Al layered double hydroxide precipitates,* Clay Science **11** (2000) 317-328.
- Aisawa S, Takahashi S, Ogasawara W, Umetsu Y, Narita E, *Direct intercalation of amino acids into layered double hydroxides by coprecipitation,* Journal of Solid State Chemistry **162** (2001) 52-62.
- Aisawa S, Sasaki S, Takahashi S, Hirahara H, Nakayama H, Narita E, I*ntercalation of amino acids and oligopeptide into Zn-Al layered double hydroxide by coprecipitation reaction,* Journal of Physics and Chemistry of solids **67** (2006) 920-925.
- Alexandrica C, Silion M, Hritcu D, Popa MI, *Layered double hydroxides as adsorbents for anionic dye removal from aqueous solutions,* Environmental Engineering and Management Journal **14** (2) (2015) 381-388.
- Anbarasan R, Lee WD, Im SS, *Adsorption and intercalation of anionic surfactants onto layered double hydroxides - XRD study*. Bulletin of Materials Science **28**(2) (2005) 145–149.
- Auerbach SM, Carrado *KA and* Dutta PK, *Handbook* of *Layered Materials*, Marcel Dekker Inc., (*2004)* New York.
- Balcomb B, Singh M, Singh S, *Synthesis and characterization of layered double hydroxides and their potential as nonviral gene delivery vehicles*, Chemistry Open **4** (2015) 137-145.
- Barichello JM, Kizuki S, Tagami T, Soares LAL, Ishida T, Kikuchi H, Kiwada H, *Agitation during lipoplex formation harmonizes the interaction of siRNA to cationic liposomes,* International Journal of Pharmaceutics **430** (2012) 359-365.

- Barth A, *The infrared absorption of amino acid side chains*, Progress in Biophysics & Molecular Biology **74** (2000) 141–173.
- Beavers K (1999) *A crystal chemical study on Layered Double Hydroxides (LDHs): An approach to develop an anion exchanger*, Ph.D. Thesis, (1999) University of Hanover, Germany.
- Bejoy N, Hydrotalcite: The clay that cures, *Resonance* (2001) 57-61.
- Bellotto M, Rebours B, Clause O and Lynch J, *A re-examination of hydrotalcite crystal chemistry*, Journal of Physical Chemistry **100** (1996) 8527-8534.
- Benício LPF, Silva RA, Lopes JA, Eulálio D, dos Santos RMM, de Aquino LA, Vergütz L, Novais RF, da Costa LM, Pinto FG, Tronto J, *Layered double hydroxides: Nanomaterials for applications in agriculture,* Revista Brasileira de Ciêcia do Solo **39** (1) (2015) 1-13.
- Benito P, Herrero M, Labajos FM, Rives V, *Effect of post-synthesis microwave hydrothermal treatment on the properties of layered double hydroxides and related materials*, Applied Clay Science **48** (2010) 218-227.
- Berg JM, Tymoczko JL, Stryer L, *Biochemistry*, Sixth Edition, WH Freeman and Company, New York (2006) pp 787.
- Bi X, Zhang H, Dou L, *Layered double hydroxide based nanocarriers for drug delivery,* Pharmaceutics **6** (2014) 298-332.
- Bish DL, *Anion exchange in Takovite: Application to other hydroxide minerals,* Bulletin de Mineralogie **103** (1980) 170-175.
- Bookin AS, Drits VA, *Polytype diversity of the hydrotalcite-like minerals I. Possible polytypes and their diffraction features,* Clays and Clay Minerals **41** (5) (1993) 551-557.
- Bontchev RP, Liu S, Krumhansl JL, Voigt J, Nenoff TM, *Synthesis, characterization, and ion exchange properties of hydrotalcite* $Mg_6Al_2(OH)_{16}(A)_x(A')_{2-x}\ 4H_2O$ *(A, A' =* Cl^-, Br^-, I^-, *and* NO_3^-, $2 \geq x \geq 0$*) derivatives*, Chemistry of Materials **15**(19) (2003) 3669-3675.
- Boulet P, Greenwell, HC, Stackhouse S, Coveney PV, *Recent advances in understanding the structure and reactivity of clays using electronic structure calculations*, Journal of Molecular Structure THEOCHEM **762** (2006) 33-48.
- Bravo-Suarez, *Review of the Synthesis of Layered Double Hydroxides: A Thermodynamic Approach,* Quim. Nova, **27** (4) (2004) 601-614.

- Brindley WG and Kikkawa S, *Thermal behavior of hydrotalcite and of anion-exchanged forms of hydrotalcite,* Clays and Clay Minerals **28** (2) (1980) 87-91.
- Brindley WG and Kikkawa S, *A crystal chemical study of Mg,Al and Ni,Al hydroxyl-perchlorates and hydroxyl-carbonates,* American Mineralogist **64** (1979) 836-843.
- Brown G and Gastuche MC, *Mixed Magnesium-Aluminium Hydroxides II. Structure and Structural Chemistry of Synthetic Hydroxycarbonates and Related Mineral Compounds,* Clay Minerals **7** (1967) 193-201.
- Butenko E, Malyshev A, Kapustin A, *Influence of Hydrocarbon Radicals on the Structure of Layered Double Hydroxides*, American Journal of Materials Science and Engineering **2**(1) (2014) 1-6.
- Cardoso LP, Celis R, Cornejo J, Valim JB, *Layered double hydroxides as supports for the slow release of acid herbicides*, Journal of Agricultural and Food Chemistry **54** (16) (2006) 5968-5975.
- Carja G, Ciobanu G, Toyota M, *The role of the organic solvent in obtaining hydrotalcite-like anionic clay nanopowders with specific textural and porous properties,* Scientific Study and Research **VII** (1) (2006) 157-162.
- Carlino S, *The intercalation of carboxylic acids into layered double hydroxides: A critical evaluation and review of different methods*, Solid State Ionics **98**(1) (1997) 73-84.
- Carmichael, J DeGraff WG, Gazdar AF, Minna JD, Mitchell JB, *Evaluation of a tetrazolium-based semiautomated colorimetric assay. Assessment of chemosensitivity testing,* Cancer Research **47** (1987) 936-946.
- Cavani F, Trifiro F, Vaccari A, *Hydrotalcite type Anionic Clays: Preparation, Properties and Applications*, Catalysis Today **11** (1991) 173-301.
- Cemazar M, Hreljac I, Sersa G, Filipic M, *Construction of EGFP expressing HepG2 cell line using electroporation,* World Congress on Medical Physics and Biomedical Engineering (2009) 128-131.
- Chen M, Cooper HM, Zhou JZ, Bartlett PF, Xu ZP, *Reduction in the size of layered double hydroxide nanoparticles enhances the efficiency of siRNA delivery,* Journal of Colloid and Interface Science **390** (2013) 275-281.

- Chiba K, Kawakami K, Tohyama K, *Simultaneous evaluation of cell viability by neutral red, MTT and crystal violet staining assays of the same cells,* Toxicology in Vitro **12** (1998) 251-258.
- Choi J and Wang NS, *Nanoparticles in Biomedical Applications and Their Safety Concerns*, (2011) Reza Fazel-Rezai (Ed.), ISBN: 978-953-307-637-9, InTech, Available from: http://www.intechopen.com/articles/show/title/nanoparticles-in-biomedical-applications-and-their-safety-concerns.
- Choi S-J, Oh J-M, Choy J-H, *Safety aspect of layered nanoparticles: size dependency in vitro and in vivo,* Journal of Nanoscience and Nanotechnology **8** (2008) 5297-5301.
- Choi G, Yang J-H, Park G-Y, Vinu A, Elzatahry A, Yo CH, Choy J-H, *Intercalative ion-exchange route to amino acid layered double hydroxide nanohybrids and their sorption properties*, European Journal of Inorganic Chemistry (2015) 925-930 DOI:10.1002/ejic.201403115.
- Choy J-H, Kwak S-Y, Jeong Y-J, Park J-S, *Inorganic layered double hydroxides as nonviral vectors*, Angewandte Chemie International Edition **39**(22) (2000) 4042-4045.
- Choy J-H, Kwak S-Y, Park J-S, Jeong Y-J, *Cellular uptake behavior of [γ-32P] labeled ATP-LDH nanohybrids*, Journal of Materials Chemistry **11** (2001) 1671-1674.
- Choy J-H, Jung J-S, Oh J-M, Park M, Jeong J, Kang Y-K, Han O-J*, Layered double hydroxide as an efficient reservoir for folate derivatives*, Biomaterials **25** (2004) 3059-3064.
- Choy J-H, Choi S-J, Oh J-M, Park T, *Clay minerals and layered double hydroxides for novel biological applications,* Applied Clay Science **36** (2007) 122-132.
- Chung H-E, Park D-H, Choy J-H, Choi S-J, *Intracellular trafficking pathway of layered double hydroxide nanoparticles in human cells: Size-dependent cellular delivery*, Applied Clay Science 65-66 (2012) 24-30.
- Cocheci L, Barvinschi P, Pode R, Popovici E, Seftel EM, *Structural characterization of some Mg/Zn-Al type hydrotalcites prepared for chromate sorption from wastewater,* Chemical Bulletin of "Politehnica" University of Timisoara, Romania **55** (69) (2010) 40-45.
- Coelhoe C, Stimpfling T, Leroux F, Verney V, *Inorganic-Organic hybrid materials based on amino acid modified hyrotalcites used as UV-absorber fillers for polybutylene succinate,* European Journal of Inorganic Chemistry (2012) 5252-5258.

- Costa FR, Leuteritz A, Wagenknecht U, Jehnichen D, Häußler L, Heinrich G, *Intercalation of Mg–Al layered double hydroxide by anionic surfactants: Preparation and characterization*, Applied Clay Science **38** (2008) 153-164.
- Costantini S, Di Bernado G, Cammorata M, Castello G, Colonna G, *Gene expression signature of human HepG2 cell line,* Gene **518** (2) (2013) 335-345.
- Costantino U, Ambrogi V, Nocchetti M, Perioli L, *Hydrotalcite-like compounds: Versatile layered hosts of molecular anions with biological activity*, Microporous and Mesoporous Materials **107** (2008) 149-160.
- Costantino U, Marmottini F, Nocchetti M, Vivani R, *New synthetic routes to hydrotalcite-like compounds – characterization and properties of the obtained materials*, European Journal of Inorganic Chemistry **10** (1998) 1439-1446.
- Crosby S, Tran D, Cocke D, Duraia EM, Beall GW, *Effect of isomorphous substitution on the thermal decomposition mechanism of hydrotalcites,* Materials **7** (2014) 7048-7058.
- Cullity BD, Stock SR, *Elements of X-Ray Diffraction,* 3rd edition, Prentice Hall: Upper Saddle River, NJ, (2001).
- Cunha VRR, Ferreira AMC, Constantino VRL, Tronto J, Valim JB, *Layered double hydroxides: inorganic nanoparticles for storage and release of species of biological and therapeutic interest*, Quimica Nova **33** (1) (2010) 159-171.
- Daniels A, Singh M, Ariatti M, *Pegylated and non-pegylated siRNA lipoplexes formulated with cholesteryl cytofectins promote efficient luciferase knockdown in Hela tat luc cells*, Nucleosides Nucleotides Nucleic Acids **32** (4) (2013) 206-220.
- de Roy A, Forano C, Besse JP, *Layered double hydroxides: Synthesis and post-synthesis Modification,* In: Layered Double Hydroxides: Present and Future, Edited by Vincente Rives (2006) 1-39.
- Del Arco M, Fernández A, Martín C, Rives V, *Release studies of different NSAIDs encapsulated in Mg,Al,Fe-hydrotalcites*, Applied Clay Science **42** (2009) 538-544.
- Del Arco[1] M, Gutiérrez S, Martín C, Rives V, Rocha J, *Synthesis and characterization of* layered *double hydroxides (LDH) intercalated with non-steroidal anti-inflammatory drugs (NSAID),* Journal of Solid State Chemistry **177** (2004) 3954-3962.

- Del Arco[2] M, Cebadera E, Gutiérrez S, Martín C, Montero MJ, Rives V, Rocha J and Sevilla MA, *Mg, Al layered double hydroxides with interalated indomethacin: Synthesis, characterization, and pharmacological study*, Journal of Pharmaceutical Sciences **93** (6) (2004) 1649-1658.
- Del Hoyo C, *Layered double hydroxides and human health: an overview,* Applied Clay Science **36** (2007) 103-121.
- Denizot F, Lang R, Rapid colorimetric assay for cell growth and survival: Modifications to the tetrazolium dye procedure giving improved sensitivity and reliability, Journal of Immunological Methods **89** (1986) 271-277.
- Desigaux L, Belkacem BM, Richard P, Cellier J, Leone P, Cario L, Leroux F, Taviot-Guého C, Pitard B, Self-assembly and characterization of layered double hydroxide/LDH hybrids, Nano Letters **6** (2) (2006) 199-204.
- de Wet JR, Wood KV, DeLuca M, Helinski DR, Subramani S*, Firefly luciferase gene: Structure and expression in mammalian cells*, Molecular and Cellular Biology **7** (2) (1987) 725-737.
- Dinnebier RE, Billenge SJL, *Powder Diffraction, Theory and Practice,* RSC Publishing, Cambridge, UK (2008).
- Dong H, Chen M, Rahman S, Parekh HS, Cooper HM, Xu ZP, *Engineering small MgAl-layered double hydroxide nanoparticles for enhanced gene delivery,* Applied Clay Science **100** (2014) 66-75.
- Dong H, Parekh HS, Xu ZP, *Particle size and number-dependent delivery to cells by layered double hydroxide nanoparticles,* Journal of Colloid and Interface Science **431** (2015) 10-16.
- Dong L, Gou G, Huang J, Sun Y, Xue B, *A review on gene delivery system of layered double hydroxide,* Applied Mechanics and Materials **320** (2013) 533-539.
- Elsaesser A, Howard CV, *Toxicology of nanoparticles*, Advanced drug delivery reviews **64** (2012) 129-137.
- Elouahabi A, Thiry M, Pector V, Fuks R, Ruysschaert JM, Vandenbranden M, *The role of endosome destabilizing activity in the gene transfer process mediated by cationic lipids,* FEBS letters **414** (2) (1997) 187-192.
- Elouahabi A, Ruysschaert JM, *Formation and intracellular trafficking of lipoplexes and polyplexes*, Molecular Therapy **11** (3) (2005) 336-347.

- Ennadi A, Legrouri A, De Roy A, Besse JP, *X-Ray diffraction pattern simulation for thermally treated [An-Al-Cl] layered double hydroxide,* Journal of Solid State Chemistry **152** (2000) 568-572.
- Evans DG and Duan X, *Preparation of layered double hydroxides and their applications as additives in polymers, as precursors to magnetic materials and in biology and medicine*, Chemical Communications **5** (2006) 485-496.
- Evans DG and Slade RCT, *Structural Aspects of Layered Double Hydroxides*, Structure and Bonding **119** (2006) 1-87.
- Fan G, Li F, Evans DG, Duan X, *Catalytic applications of layered double hydroxides: recent advances and perspectives,* Chemical Society reviews **43** (2014) 7040-7066.
- Feng J, He Y, Liu Y, Du Y, Li D, *Supported catalysts based on layered double hydroxides for catalytic oxidation and hydrogenation: general functionality and promising application prospects,* Chemical Society Reviews **44** (2015) 5291-5319.
- Fong N, Guagliardo P, Williams J, Musemeci A, Martin D, Smith SV, *Clay particles – potential of positron annihilation lifetime spectroscopy (PALS) for studying interlayer spacing,* Journal of Physics: Conference Series **262** (2011) 012022.
- Forano C, Hibino T, Leroux F, Taviot-Gucho C, Layered Double Hydroxides, In: Handbook of Clay Science, Edited by F. Bergaya, BKG Thong and G Lagaly (2006) 1021-1096.
- Fortner JD, Solenthaler C, Hughes JB, Puzrin AM, Plötze M, *Interactions of clay minerals and a double layered hydroxide with water stable, nano scale fullerene aggregates (nC_{60})*, Applied Clay Science **55** (2012) 36-43.
- Fotakis G, Timbrell JA, *In vitro cytotoxicity assays: Comparison of LDH, neutral red, MTT and protein assay in hepatoma cell lines following exposure to cadmium chloride,* Toxicology Letters **160** (2006) 171-177.
- Fried M and Crothers DM, *Equilibria and kinetics of repressor-operator interactions by polyacrylamide gel electrophoresis,* Nucleic Acids Research **9** (23) (1981) 6505-6525.
- Frost RL, Weier ML, and Kloprogge JT, *Raman spectroscopy of some natural hydrotalcites with sulphate and carbonate in the interlayer*, Journal of Raman Spectroscopy **34** (10) (2003) 760-768.

- Frost[1] RL, Weier ML, Clissold ME, Williams PA, Infrared spectroscopic study of natural hydrotalcites carrboydite and hydrohonessite, Spectrochimica Acta Part A **59** (2003) 3313-3319.
- Gao L, Nie L, Wang T, Qin Y, Guo Z, Yang D, Yan X, *Carbon nanotube delivery of the GFP gene into mammalian cells*, ChemBiochem **7** (2006) 239-242.
- Gao Y, Xu Z, Chen S, Gu W, Chen L, Li Y, *Arginine-chitosan/DNA self-assemble nanoparticles for gene delivery: In vitro characteristics and transfection efficiency*, International Journal of Pharmaceutics **359** (1-2) (2008) 241-246.
- Garner MM and Revzin A, *A gel electrophoresis method for quantifying the binding of proteins to specific DNA regions: application to components of the Escherichia coli lactose operon regulatory system,* Nucleic Acids Research **9** (13) (1981) 3047-3059.
- Gasuche MC, Brown G, Moerland MM, *Mixed Magnesium-Aluminium Hydroxides I. Preparation and Characterization of Compunds formed in Dialysed Systems-,* Clay Minerals **7** (1967) 177-192.
- Gu Z, Thomas AC, Xu ZP, Campbell JH, Lu GQ, *In vitro sustained release of LMWH from MgAl-layered double hydroxide nanohybrids,* Chemistry of Materials **20** (11) (2008) 3715-3722.
- Guo X, Li S, Hou W, Han S, Hu J, Li D, *Layered double hydroxides with hydrotalcite type structure containing Fe^{3+}, Al^{3+} and Mg^{2+}*, Chemical Research in Chinese Universities **19** (2) (2003) 211-215.
- Ha JU and Xanthos M, *Drug release characteristics from nanoclay hybrids and their dispersions in organic polymers*, International Journal of Pharmaceutics **414** (2011) 321-331.
- Habib S, Singh M, Ariatti M, *Glycosylated liposomes with proton sponge capacity: Novel hepatocyte specific gene carriers*, Current Drug Delivery **10** (2013) 685-695
- He J, Wei M, Li B, Kang Y, Evans DG, Duan X*, Preparation of Layered Double Hydroxides*, Structure and Bonding **119** (2005) 89-119.
- Herrero M, Labajos FM, Rives V, *Size control and optimization of intercalated layered double hydroxides*, Applied Clay Science **42** (2009) 510-518.
- Hernandez-Moreno MJ, Ulibarri MA, Rendon JL, Serna CJ, *IR Characteristics of hydrotalcite-like compounds,* Physics and Chemistry of Minerals **12** (1985) 34-38.

- Hibino T, *Delamination of layered double hydroxides containing amino acids,* Chemistry of Materials **16** (2004) 5482-5488.
- Hickerson RP, Vlassov AV, Wang Q, Leak D, Ilves H, Gonzalez-Gonzalez E, Contag CH, Johnston BH, Kaspar RL, *Stability of unmodified siRNA and relevance to clinical use*, Oligonucleotides **18** (4) (2008) 345-354.
- Holden NS and Tacon CE, *Principles and problems of the electrophoretic mobility shift assay,* Journal of Pharmacological and Toxicological Methods **63** (2011) 7-14.
- Honary S, Zahir F, *Effect of zeta potential on the properties of nano-drug delivery systems – A Review (Part 2),* Tropical Journal of Pharmaceutical Research **12** (2) (2013) 265-273.
- Hou X, Bish D, Wang S, Johnstone T, Kirkpatrick R, *Hydration, expansion, structure and dynamics of layered double hydroxides,* American Mineralogist **88** (2003) 167-179.
- Hu H, Xiu KM, Xu SL, Yang WT, Xu FJ, *Functionalized layered double hydroxide nanoparticles conjugated with disulfide-linked polycation brushes for advanced gene delivery,* Bioconjugate Chemistry **24** (6) (2013) 968-978.
- Huang L, Hung M-C, Wagner E (Editors), *Nonviral vectors for gene therapy,* Academic Press. San Diego, California, USA (1999).
- Ikeda T, Amoh H, Yasunaga T, *Stereoselective exchange kinetics of L- and D-Histidines for Cl^- in the interlayer of a hydrotalcite-like compound by chemical relaxation method,* Journal of the American Chemical Society **106** (1984) 5772-5775.
- Imani R, Emami SH, Faghihi S, *Synthesis and characterization of an octaarginine functionalized graphed oxide nanocarrier for gene delivery applications,* Physical Chemistry Chemical Physics **17** (2015) 6328-6339.
- Ingram L and Taylor HFW, *The Crystal Structures of Sjögrenite and Pyroaurite,* Mineralogical Magazine **36** (280) (1967) 465-479.
- Intissar M, Jumas J-C, Besse J-P, Leroux F, *Reinvestigation of the layered double hydroxide containing tetravalent cations: Unambiguous response provided by XAS and Mössbauer spectoscopies*, Chemistry of Materials **15** (24) (2003) 4625-4632.
- Jabłońska M, Chmielarz L, Węgrzyn A, *Hydrotalcite-like materials containing manganese: A short review*, Copernican Letters **4** (2013) 59-65.

- Jaiswal A, Gautam RK, Chattopadhyaya MC, *Layered double hydroxides and the environment: An overview,* In: Advanced Materials for Agriculture, Food and Environmental Safety (Eds. A Tiwari and M Syväjärvi), (2014) John Wiley and Sons, Inc., Hoboken, NJ, USA.
- Jellicoe TC, Fogg AM, *Synthesis and characterization of layered double hydroxides intercalated with sugar phosphates*, Journal of Physics and Chemistry of Solids **73** (12) (2012) 1496-1499.
- Jiao FP, Chen XQ, Fu ZD, Hu YH, Wang YH, *Synthesis and structural characterization of L-(-)-malic acid pillared layered double hydroxides*, Latin American Applied Research **39** (2009) 127-130.
- Kagunya W, Baddour-Hadjean R, Kooli F, Jones W**,** *Vibrational* Modes *in layered double hydroxides and their calcined derivatives,* Chemical Physics **236** (1998) 225-234.
- Kameda T, Oba J, Yoshioka T, *Removal of boron and fluoride in wastewater using Mg-Al layered double hydroxide and Mg-Al oxide*, Journal of Environmental Management **188 (**2017) 58-63.
- Kandare E and Hossenlopp JM, *Thermal degradation of acetate-intercalated hydroxyl double and layered hydroxyl salts*, Inorganic Chemistry **45**(9) (2006) 3766-3773.
- Kelkar CP and Schutz AA, *Ni-, Mg- and Co-containing hydrotalcite-like materials with a sheet-like morphology: synthesis and characterization,* Microporous Materials **10** (1997) 163-172.
- Khan AI and O'Hare D, *Intercalation chemistry of layered double hydroxides: recent developments and applications,* Journal of Materials Chemistry **12** (2002) 3191-3198.
- Klemkaite K, Prosycevas I, Taraskevicius R, Khinsky A, Kareiva A, *Synthesis and Characterization of layered double hydroxides with different cations [Mg, Co, Ni, Al], decomposition and reformation of mixed metal oxides to layered structures,* Central European Journal of Chemistry **9**(2) (2011) 275-282.
- Kloprogge JT and Frost RL, *Fourier Transform Infrared and Raman Spectroscopic Study of the Local Structure of Mg-, Ni- and Co-Hydrotalcites,* Journal of Solid State Chemistry **146** (1999) 506-515.
- Kloprogge JT, Hickey L, Frost RL, *Heating stage Raman and Infrared emission spectroscopic study of the dehydroxylation of synthetic Mg-hydrotalcite,* Applied Clay Science **18** (2001) 37-49.

- Kloprogge JT, Wharton D, Hickey L, Frost RL, *Infrared and Raman study of the interlayer anions CO_3^{2-}, NO_3^-, SO_4^{2-} and ClO_4^{2-} in Mg/Al-hydrotalcite*, American Mineralogist **87** (2002) 623-629.
- Kloprogge JT, Hickey L, Frost RL, *The effects of Synthesis pH and Hydrothermal treatment on the Formation of Zinc Aluminum Hydrotalcites,* Journal of Solid State Chemistry **177** (2004) 4047-4057.
- Komarala EP, Doshi S, Mohammed A, Bahadur D, *Efficient antibacterial activity via protein degradation of a 3D layered double hydroxide-reduced graphene oxide nanohybrid,* Royal Society of Chemistry Advances **6** (2016) 40389-40398.
- Kooli F, Kosuge K, Tsunashima A, *Mg-Zn-Al-CO_3 and Zn-Cu-Al-CO_3 hydrotalcite-like compounds: preparation and characterization,* Journal of Materials Science **30** (1995) 4591-4597.
- Kooli F, Depége C, Ennaqadi A, de Roy A, Besse JP, *Rehydration of Zn-Al layered double hydroxides*, Clays and Clay Minerals **45** (1) (1997) 92-98.
- Kovanda F, Grygar T, Dorničák V, Rojka T, Bezdička P, Jirátová K, *Thermal behavior of Cu-Mg-Mn and Ni-Mg-Mn layered double hydroxides and characterization of formed oxides,* Applied Clay Science **28**(2005) 121-136.
- Kovanda F, Jindová E, Doušová B, Koloušek D, Pleštil J, Sedláková Z, *Layered double hydroxides intercalated with organic anions and their application in preparation of LDH/polymer nanocomposites,* Acta Geodynamica et Geomateriali **6** (153) (2009) 111-119.
- Kralj M and Pavelic K, *Medicine on a small scale*, EMBO reports **4** (11) (2003) 1008-1012.
- Kriven WM, Kwak S-Y, Wallig MA, Choy J-H, *Bio-resorbable nanoceramics for gene and drug delivery,* Materials Research Society Bulletin **29** (1) (2004) 33-37.
- Kuang Y, Zhao L, Zhang S, Zhang F, Dong M, Xu S, *Morphologies, preparations and applications of double layered hydroxide Micro-/Nanastructures*, Materials **3** (2010) 5220-5235.
- Kulyukhin SA, Krasavina EP, Rumer IA, Klimovich IV, *Sorption of Strontium and Yttrium radionuclides from aqueous solutions onto layered double hydroxides of various compositions,* Radiochemistry **56** (6) (2014) 593-606.
- Kumar PP, Kalinichev AG, Kirkpatrick RJ, *Hydration, swelling, interlayer structure, and hydrogen bonding in organolayered double hydroxides: Insights from molecular dynamics*

simulation of citrate-intercalated hydrotalcite, Journal of Physical Chemistry B **110** (9) (2006) 3841-3844.

- Kumar S and Rai SB, *Spectroscopic studies of L-arginine molecule,* Indian Journal of Pure and Applied Physics **48** (2010) 251-255.
- Kumar S, Rai AK, Rai SB, Rai DK, *Infrared and Raman spectra of Histidine: an ab initio DFT calculations of histidine molecule and its different protonated forms*, Indian Journal of Physics **84** (5) (2010) 563-573.
- Kuo Y, Kuthati Y, Kankala RK, Wei P, Wang C, Liu C, Sung P, Mou C, Lee C, *Layered double hydroxide nanoparticles to enhance organ-specific targeting and anti-proliferative effect of cisplatin*, Journal of Materials Chemistry B **3** (2015) 3447-3458.
- Kura AU, Hussein MZ, Fakurazi S, Arulselvan P, *Layered double hydroxide nanocomposite for drug delivery systems; bio-distribution, toxicity and drug activity enhancement,* Chemistry Central Journal **8** (47) (2014) 1-8.
- Kwak S-Y, Jeong Y-J, Park J-S, Choy J-H, *Bio-LDH nanohybrid for gene therapy*, Solid State Ionics **151** (2002) 229-234.
- Lacerda L, Raffa S, Prato M, Bianco A, Kostarelos K, *Cell penetrating CNTs for delivery of therapeutics*, Nanotoday **2** (6) (2007) 38-43.
- Ladewig K, Xu ZP, Lu GQ, *Layered double hydroxide nanoparticles in gene and drug delivery,* Expert Opinion Drug Delivery **6** (9) (2009) 907-922.
- Ladewig[1] K, Niebert M, Xu ZP, Gray PP, Lu GQ, *Controlled preparation of layered double hydroxide nanoparticles and their application as gene delivery vehicles,* Applied Clay Science **48** (2010) 280-289.
- Ladewig[2] K, Niebert M, Xu ZP, Gray PP, Lu GQM, *Efficient siRNA delivery to mammalian cells using layered double hydroxide nanoparticles,* Biomaterials **31** (2010) 1821-1829.
- Lee D-J, Kessel E, Lehto T, Liu X, Yoshinaga N, Padari K, Chen Y-C, Kempter S, Uchida S, Radler JO, Pooga M, Sheu M-T, Kataoka K, Wagner E, *Systemic delivery of folate-PEG siRNA lipoplexes with enhanced intracellular stability for in vivo gene silencing in leukemia,* Bioconjugate Chemistry **28**(9) (2017) 2393-2409, DOI: 10.1021/acs.bioconjchem.7b00383.

- Li[1] B, Wu P, Ruan B, Liu P, Zhu N, *Study on the adsorption of DNA on the layered double hydroxides*, Spectrochimica Acta Part 1: Molecular and Biomolecular Spectroscopy, **121**(2014) 387-393.
- Li C, Wei M, Evans DG, Duan X, *Recent advances for layered double hydroxides (LDHs) materials as catalysts applied in green aqueous media,* Catalysis Today **247** (2015) 163-169.
- Li L, Gu W, Chen W, Xu ZP, *Co-delivery of siRNAs and anti-cancer drugs using layered double hydroxide nanoparticles,* Biomaterials **35** (2014) 3331-3339.
- Li S, Li J, Wang CJ, Wang Q, Cader MZ, Lu J, Evans DG, Duan X, 'O Hare D, *Cellular uptake and gene delivery using layered double hydroxide nanoparticles,* Journal of Materials Chemistry B **1** (2013) 61-68.
- Liang W and Lam JKW, *Endosomal Escape Pathways for Non-Viral Nucleic Acid Delivery Systems, Molecular Regulation of Endocytosis*, Dr. Brian Ceresa (Ed.) (2012), InTech, DOI: 10.5772/46006. Available from: http://www.intechopen.com/books/molecular-regulation-of-endocytosis/endosomal-escape-pathways-for-non-viral-nucleic-acid-delivery-systems.
- Liu J, Harrison R, Zhou JZ, Liu TT, Yu C, Lu GQ, Qiao SZ, Xu ZP, *Synthesis of nanorattles with layered double hydroxide core and mesoporous silica shell as delivery vehicles*, Journal of Materials Chemistry **21** (2011) 10641-10644.
- Liu H-C, Yang X-Y, Ran G-P, Min E-Z, Liu J-K, Ying P-L, Xin Q, Li C, *Structure and base properties of calcined hydrotalcites,* Chinese Journal of Chemistry **17** (4) (1999) 319-330.
- Lu M, Shan Z, Andrea K, Macdonald B, Beale S, Curry DE, Wang L, Wang S, Oakes KD, Bennett C, Wu W, Zhang X, *Chemisorption mechanism of DNA on Mg/Fe layered double hydroxides nanoparticles: Insights into engineering effective siRNA delivery systems,* Langmuir **32** (11) (2016) 2659-2667.
- Luan L, Liu S, Sun D, *Dispersion control and nematic ordering of Ni/Al layered double hydroxide suspensions*, Journal of solid State Chemistry 182 (2009) 1462-1467.
- Lv H, Zhang S, Wang B, Cui S, Yan J, *Toxicity of cationic lipids and cationic polymers in gene delivery,* Journal of Controlled Release **114** (2006) 100-109.

- Lv W, Du M, Ye W, Zheng Q, *The formation mechanism of layered double hydroxide nanoscrolls by facile trinal-phase hydrothermal treatment and their adsorption properties,* Journal of Materials Chemistry A **3** (2015) 23395-23402.
- Malherbe F, Besse J-P, *Investigating the effects of guest-host interactions on the properties of anion-exchanged Mg-Al hydrotalcites*, Journal of Solid State Chemistry **155** (2) (2000) 332-341.
- Mallakpour S and Dinari M, *Using Mg-Al-Layered double hydroxide intercalated with chiral dicarboxylic acid for the reinforcement of isoleucine amino acid containing poly(amide-imide),* Polymer Composites **37** (11) (2016) 3288-3295.
- Matranga C, Tomari Y, Shin C, Bartel DP, Zamore PD, *Passenger-Strand Cleavage Facilitates Assembly of siRNA into Ago2-Containing RNAi Enzyme Complexes*, Cell **123** (4) (2005) 607-620.
- Matulis D, Rouzina I, Bloomfield VA, *Thermodynamics of DNA binding and condensation: isothermal titration calorimetry and electrostatic mechanism*, Journal of Molecular Biology **296** (2000) 1053-1063.
- Medina-Juárez O, García-Sánchez MA, Arellano-Sánchez U, Kornhauser-Straus I and Rojas-González F, *Optimal surface amino-functionalization following thermo-alkaline treatment of nanostructured silica adsorbents for enhanced CO_2 adsorption,* Materials **9** (11) (2016) 898 doi:10.3390/ma9110898.
- Meng Z, Luan L, Kang Z, Feng S, Meng Q, Liu K, *Histidine-enriched multifunctional peptide vectors with enhanced cellular uptake and endosomal escape for gene delivery,* Journal of Materials Chemistry B **5** (2017) 74-84.
- Meyn M, Beneke K, Lagaly G, *Anion exchange reactions of layered double hydroxides*, Inorganic Chemistry **29** (1990) 5201-5207.
- Meyn M, Beneke K, Lagaly G, *Anion exchange reactions of hydroxyl double salts,* Inorganic Chemistry **32** (1993) 1209-1215.
- Millange F, Walton RI, O' Hare D, *Time resolved in situ X-Ray diffraction study of the liquid-phase reconstruction of Mg-Al-carbonate hydrotalcite-like compounds,* Journal of Materials Chemistry **10** (2000) 1713-1720.

- Mills SJ, Christy AG, Genin JMR, Kameda T, Colombo F, *Nomenclature of the hydrotalcite supergroup: natural layered double hydroxides*, Mineralogical Magazine **76** (2012) 1289-1336.
- Misra C and Perrotta AJ, *Composition and properties of synthetic hydrotalcites,* Clays and Clay Minerals **40** (2) (1992) 145-150.
- Miyata S and Kumura T, *Synthesis of new hydrotalcite-like compounds and their physio-chemical properties,* Chemistry Letters (1973) 843-848.
- Miyata S, *Synthesis of hydrotalcite-like compounds and their structures and physico-chemical properties - The systems* Mg^{2+} *-*Al^{3+} *-*NO_3^- and Mg^{2+} *-*Al^{3+} *-*Cl^-, Mg^{2+} *-*Al^{3+} *-*ClO_4^-, Ni^{2+} *-*Al^{3+} *-*Cl^- *and* Zn^{2+} *-*Al^{3+} *-*Cl^-, Clays and Clay Minerals **23** (1975) 369-375.
- Miyata S and Okada A, *Synthesis of hydrotalcite-like compounds and their physico-chemical properties - The systems* Mg^{2+}*-*Al^{3+} *-*SO_4^{2-} *and* Mg^{2+} *-*Al^{3+} *-*CrO_4^{2-}, Clays and Clay Minerals **25** (1977) 14-18.
- Miyata S, *Anion exchange properties of Hydrotalcite-like compounds*, Clay and Clay Minerals **31** (4) (1983) 305-311.
- Mohanambe L and Vasudevan S, *Inclusion of poly-aromatic hydrocarbon (PAH) molecules in a functionalized layered double hydroxide,* Journal of Chemical Sciences **118** (1) (2006) 105-115.
- Mondal S, Dasgupta S, Maji K, *MgAl- Layered double hydroxide nanoparticles for controlled release of salicyclate,* Materials Science and Engineering C **68** (2016) 557-564.
- Mora M, Jiménez-Sanchidrián C, Ruiz JR, *Raman Spectroscopy study of Layered-double hydroxides containing magnesium and trivalent metals,* Materials Letters **120** (2014) 193-195
- Morachis JM, Mahmoud EA, Sankaranarayanan J, Almutairi A, *Triggered Rapid Degradation of Nanoparticles for gene delivery,* Journal of Drug Delivery (2012) doi: 10.1155/2012/291219.
- Mosmann T, *Rapid colorimetric assay for cellular growth and survivals: application to proliferation and cytotoxicity assays,* Journal of Immunological Methods **65** (1983) 55-63.
- Mout R, Moyano DF, Rana S, Rotello VM, *Surface functionalization of nanoparticles for nanomedicine*, Chemical Society Reviews **41** (2012) 2539-2544.

- Mulens V, Morales MP, Barber DF, *Development of magnetic nanoparticles for cancer gene therapy: A comprehensive review,* ISRN Nanomaterials (2013) 1-14.
- Musumeci AW, Mortimer GM, Butler MK, Xu ZP, Minchin RF, Martin DJ, *Fluorescent layered double hydroxide nanoparticles for biological studies*, Applied Clay Science **48** (2010) 271-279.
- Nagaraj VJ, Sun X, Mehta J, Martin M, Ngo T, Dey SK, *Synthesis, characterization and in vitro drug delivery capabilities of (Zn, Al)-based layered double hydroxide nanoparticles,* Journal of Nanotechnology (2015) Article ID 350370, 10 pages.
- Naicker K, Ariatti M, Singh M, *PEGylated galactosylated cationic liposomes for hepatocytic gene delivery,* Colloids and Surfaces B: Biointerfaces **122** (2014) 482-490.
- Nakayama H, Wada N, Tsuhako M, *Intercalation of amino acids and peptides into MG-Al layered double hydroxide by re-construction method,* International Journal of Pharmaceutics **269** (2004) 469-478.
- Nalawade P, Aware B, Kadam VJ, Hirlekar RS, *Layered double hydroxides: A review,* Journal of Scientific and Industrial Research **68 (**2009) 267-272.
- Natoli M, Leoni BD, D'Agnano I, Zucco F, Felsani A, *Good CACO-2 cell culture practices*, Toxicology in Vitro **26** (2012) 1243-1246.
- Newman SP and Jones W, *Synthesis, characterization and applications of layered double hydroxides containing organic guests*, New Journal of Chemistry (1998) 105-115.
- Newman SP and Jones W, *Comparative study of some layered hydroxide salts containing exchangeable interlayer anions,* Journal of Solid State Chemistry **148** (1999) 26-40.
- Newman SP, Jones W, O' Conner P, Stamires DM, *Synthesis of the $3R_2$ polytypeof a hydrotalcite-like mineral*, Journal of Materials Chemistry **12** (2002) 153-155.
- Nimesh S, Kumar R, Chandra R, *Novel polyallylamine-dextran sulfate-DNA nanoplexes: Highly efficient non-viral vector for gene delivery,* International Journal of Pharmaceutics **320** (2006) 143-149.
- Nguyen J, Steele TWJ, Merkel O, Reul R, Kissel T, *Fast degrading polyesters as siRNA nano-carriers for pulmonary gene therapy,* Journal of Controlled Release **132** (2008) 243-251.
- Oh JM, Hwang SH, Choy JH, *The effect of synthetic conditions on tailoring the size of hydrotalcite particles*, Solid State Ionics **151** (2006) 285-291.

- Ostolska I, Wiśniewska M*, Application of the zeta potential measurements to explanation of colloidal Cr_2O_3 stability mechanism in the presence of the ionic polyamino acids*, Colloid and Polymer Science **292**(10) (2014) 2453-2464 doi:10.1007/s00396-014-3276-y.
- Palmer SJ, Frost RL, Spratt HJ, *Synthesis and Raman spectroscopic study of Mg/Al, Fe hydrotalcites with variable cationic ratios,* Journal of Raman Spectroscopy **40** (9) (2009) 1138-1143.
- Pan B, Cui D, Xu P, Chen H, Liu F, Li Q, Huang T, You X, Shao J, Bao C, Gao F, He R, Shu M, Ma Y, *Design of dendrimer modified carbon nanotubes for gene delivery*, Chinese Journal of Cancer Research **19**(1) (2007) 1-6.
- Pan B, Cui D, Xu P, Ozkan C, Feng G, Ozkan M, Huang T, Che B, Li Q, He R, Hu G, *Synthesis and characterization of polyamidoamine dendrimer-coated multi-walled carbon nanotubes and their application in gene delivery systems*, Nanotechnology **20** (2009) 1-9.
- Park D-H, Jaeyong C, Kwon O-J, Yun C-O, Choy J-H, *Biodegradable inorganic nanovector: passive versus active tumor targeting,* Angewandte Chemie International Edition **55** (14) (2016) 4582-4586.
- Patel VB, Patel KN, Shah MM, Mayank B, *Spectrophotometric determination of histidine hydrochloride monohydrate in pharmaceutical formulations,* International Journal of PharmTech Research **1** (3) (2009) 852-856.
- Perera J, Weerasekera M, Kottegoda N, *Slow release anti-fungal skin formulations based on citric acid intercalated layered double hydroxides nanohybrids,* Chemistry Central Journal **9**:27 (2015) doi:10.1186/s13065-015-0106-3.
- Perez C, Sanchez A, Putnam D, Ting D, Langer R, Alonso MJ, *Poly (lactic acid)-poly (ethylene glycol) nanoparticles as new carriers for the delivery of plasmid DNA,* Journal of Controlled Release **75** (2001) 211-224.
- Pérez-Bernal ME, Ruano-Casero RJ, Benito F, Rives V, *Nickel-Aluminium layered double hydroxides prepared via inverse micelles formation,* Journal of Solid State Chemistry **182** (2009) 1593-1601.

- Perioli[1] L, Posati T, Noccetti M, Bellezza F, Costantino U, Cipiciani A*, Intercalation and release of anti-inflammatory drug diclofenac into nanosized ZnAl hydrotalcite-like compound*, Applied Clay Science **53** (2011) 374-378.
- Perioli[2] L, Ambrogi V, di Nauta L, Noccetti M and Rossi C, *Effects of hydrotalcite-like nanostructured compounds on biopharmaceutical properties and release of BCS class II drugs: The case of flurbiprofen*, Applied Clay Science **51** (2011) 407-413.
- Posati T, Bellezza F, Tarpani L, Perni S, Latterini L, Marsili V, Cipiciani A, *Selective internalization of ZnAl-HTlc nanoparticles in normal and tumor cells. A study of their potential use in cellular delivery*, Applied Clay Science **55** (2012) 62-69.
- Prevot V, Forano C, Besse JP, *Synthesis and thermal and chemical behaviors of tartrate and succinate intercalated Zn_3Al and Zn_2Cr layered double hydroxides*, Inorganic Chemistry **37**(17) (1998) 4293-4301.
- Prevot V, Forano C, Besse JP, *Reactivity of oxalate with ZnAl layered double hydroxides through new materials*, Journal of Materials Chemistry **9** (1999) 155-160.
- Qian L, Lu Z, Xu T, Wu X, Tian Y, Li Y, Huo Z, Sun X, Duan X, *Trinary Layered Double Hydroxides as High-Performance Bifunctional Materials for Oxygen Electrocatalysis*, Advanced Energy Materials **5** (2015) 1500245. doi: 10.1002/aenm.201500245.
- Qiu T, Li H, Cao Y, *Pre-staining thin layer chromatography method for amino acid detection,* African Journal of Biotechnology **9** (50) (2010) 8679-8681.
- Qu J, Zhang Q, Li X, He X, Song S, *Mechanochemical approaches to synthesize layered double hydroxides: a review, Applied Clay Science* **19** (2016)185-192.
- Ragusa A, Garcia I, Penades S, *Nanoparticles as nonviral gene delivery vectors,* IEEE Transactions on Nanobioscience **6**(4) (2007) 319-330.
- Rajamathi M, Thomas GS, Kamath PV, *The many ways of making anionic clays,* Proceedings of the Indian Academy of Science **13** (5-6) (2001) 671-680.
- Ren L, Hu J-S, Wan L-J, Bai C-L, *A simple method to synthesize double hydroxide nanoscrolls*, Materials Research Bulletin **42** (2007) 571-575.
- Richardson MS, *Layered Double Hydroxides as Anion and Cation Exchanging Materials*, Ph.D. Thesis (2007) University of North Texas, USA.

- Riley MK and Vermerris W, *Recent advances in nanomaterials for gene delivery – A Review*, Nanomaterials **7** (94) (2017) doi:10.3390/nano7050094.
- Rives V and Ulibarri MA, *Layered double hydroxides (LDH) intercalated with metal coordination compounds and oxometalates*, Coordination Chemistry Reviews **181** (1999) 61-120.
- Rojas R, Bedoya DA, Vasti C, Giacomelli CE, *LDH nanoparticles: synthesis, size control and applications in nanomedicine,* in Layered Double Hydroxides (LDHs) Synthesis, Characterization and Application, Edited by Sherman IT (2015) ISBN:978-1-63482-040-0.
- Rossi C, Schoubben A, Ricci M, Perioli L, Ambrogi V, Latterini L, Aloisi GG, Rossi A, *Intercalation of the radical scavenger ferulic acid in hydrotalcite-like anionic clays,* International Journal of Pharmaceutics **295** (2005) 47-55.
- Ruiz-Hitzky E, Aranda P, Darder M, Rytwo G, *Hybrid materials based on clays for environmental and biomedical applications,* Journal of Materials Chemistry **20** (2010) 9306-9321.
- Saber O and Tagaya[1] H, *New layered double hydroxide, Zn-Ti LDH: Preparation and Intercalation Reactions*, Journal of Inclusion Phenomena and Macrocyclic Chemistry **45** (2003) 109-116.
- Saber O and Tagaya[2] H, *Preparation and intercalation reactions of Zn-Sn LDH and Zn-Al-Sn LDH*, Journal of Porous Materials **10** (2003) 83-91.
- Sajid M and Basheer C, *Layered double hydroxides: Emerging sorbent materials for analytical extractions,* Trends in Analytical Chemistry **75** (2016) 174-182.
- Salak AN, Tedim J, Kuznetsova AI, Ribeiro JL, Vieira LG, Zheudkevich ML, Ferreira MGS, *Comparative X-ray Diffraction and infrared spectroscopy study of Zn-Al layered double hydroxides: Vanadate vs nitrate*, Chemical Physics **397** (2012) 102-108.
- Sambuy Y, De Angelis I, Ranaldi G, Scarino ML, Stammati A, Zucco F, *The CACO-2 cell line as a model of the intestinal barrier: influence of cell culture-related factors on CACO-2 cell functional characteristics,* Cell Biology and Toxicology **21** (2005) 1-26.

- Sarijo SH, Jadam ML, Saleh FM, *Intercalation of Fenoprofen into Layered Double Hydroxide for the Formation of Controlled Release Anti-Inflammatory Drug*, Advanced Materials Research **1142** (2017) 230-233.
- Seftel EM, Popovici E, Mertens M, De Witte K, Van Tendeloo G, Cool P, Vansant EF, *Zn-Al layered double hydroxides: Synthesis, characterization and photocatalytic application*, Microporous and Mesoporous Materials **113** (2008) 296-304.
- Senapati S, Thakur R, Verma SP, Duggal S, Mishra DP, Das P, Shripati T, Kumar M, Rana D, Maiti P, *Layered double hydroxides as effective anticancer drugs and tailoring release rate through interlayer anions,* Journal of Controlled Release **224** (2016) 186-198.
- Senra JD, Silva AC, Santos RV, Malta LFB, and Simas ABC, *Palladium on Layered Double Hydroxide: A Heterogeneous System for the Enol Phosphate Carbon-Oxygen Bond Activation in Aqueous Media*, Journal of Chemistry, vol. 2017 (2017) Article ID 8418939, 10 pages, doi:10.1155/2017/8418939.
- Sertsova AA, Subcheva EN, Yurtov EV, *Synthesis and study of structure formation of layered double hydroxides based on Mg, Zn, Cu and Al,* Russian Journal of Inorganic Chemistry **60** (1) (2015) 23-32.
- Shafiei S, Birgani ZT, Darvish A, Azimi MS, Solati-Hashjin M, *Layered double hydroxides for diagnostic applications,* International Congress of Medical Diagnosis Modern Technologies (2008) 1-16.
- Shang L, Nienhaus K, Nienhaus GU, *Engineered nanoparticles interacting with cells: size matters,* Journal of Nanobiotechnology **12** (5) (2014) doi: 10.1186/1477-3155-12-5.
- Shi J, Schellinger JG, Johnson RN, Choi JL, Chou B, Anghel El, Pun SH, *Influence of histidine incorporation on buffer capacity and gene transfection efficiency of HPMA-co-oligolysine brush polymers,* Biomacromolecules **14** (6) (2013) 1961-1970.
- Si J, Ping P, Xie H, Yang W and Lu H, *The influence of multiwalled carbon nanotubes-NiCoAl layered double hydroxide hybrids on fire safety performance of poly (ethylene-co-vinyl acetate) composites*, Polymer Composites (2017) doi:10.1002/pc.24281.
- Singh R, Pantarotto D, McCarthy D, Chaloin O, Hoebeke J, Partidos CD, Briand JP, Prato M, Bianco A, Kostarelos K, *Binding and condensation of plasmid DNA onto functionalized carbon*

nanotubes: toward the construction of nanotube-based gene delivery vectors, Journal of the American Chemical Society **127** (12) (2005) 4388-4396.

- Smith J, Zhang Y, Niven R, *Toward development of a non-viral gene therapeutic*, Advanced Drug Delivery Reviews **26** (1997) 135-150.
- Soenen SJ, Rivera-Gil P, Montenegro J-M, Parak WJ, De Smedt SC, Braeckmans K, *Cellular toxicity of inorganic nanoparticles: Common aspects and guidelines for improved nanotoxicity evaluation*, Nano Today **6** (2011) 446-465.
- Spector AA, Yorek MA, *Membrane lipid composition and cellular function,* The Journal of Lipid Research **26** (1985) 1015-1035.
- Stimpfling T, Vialat P, Hintze-Bruening H, Keil P, Shkirskiy V, Volovitch P, Ogle K, Leroux F, *Amino acid interleaved layered double hydroxides as promising hybrid materials for AA2024 corrosion inhibition,* European Journal of Inorganic Chemistry (2016) 2006-2016.
- Suzuki E, Idemura S, Ono Y, *Properties of hexacyanocobaltate(III)-exchanged hydrotalcite-like minerals,* Clays and Clay Minerals **37**(2) (1989) 173-178.
- Tada H, Shiho O, Kuroshima K-I, Koyama M, Tsukamoto K, *An improved colorimetric assay for interleukin 2*, Journal of Immunological Methods **93**(2) (1986) 157-165.
- Takagi K, Shichi T, Usami H, Sawaki Y, *Controlled photocycloaddition of unsaturated carboxylates intercalated in hydrotalcite clay interlayers,* Journal of the American Chemical Society **115** (1993) 4339-4344.
- Tao Q, Zhang Y, Zhang X, Yuan P, He H, *Synthesis and Characterization of Layered Double Hydroxides with a High Aspect Ratio*, Journal of Solid State Chemistry 179 (2006) 708-715
- Taylor HFW, *Segregation and Cation-Ordering in Sjögrenite and Pyroaurite*, Mineralogical Magazine **37** (287) (1969) 338-342.
- Templeton NS, *Cationic liposome-mediated gene delivery in vivo*, Bioscience Reports **22** (2002) 283-295.
- Tronto J, Bordonal AC, Naal Z, Valim JB, *Conducting Polymers / Layered Double Hydroxides Intercalated Nanocomposites*, In: Materials Science - Advanced Topics, Y. Mastai, (Ed.), InTech, (2013), 2-30.

- Trujillano R, Holgado MJ, Pigazo F, Rives V, *Preparation, physicochemical characterisation and magnetic properties of Cu–Al layered double hydroxides with CO_3^{2-} and anionic surfactants with different alkyl chains in the interlayer*, Physica B **373** (2006) 267–273.
- Twentyman PR, Luscombe M, *A study of some variables in a tetrazolium dye (MTT) based assay for cell growth and chemosensitivity*, British Journal of Cancer **56** (3) (1987) 279-285.
- Tyner KM, Schiffman SR, Giannelis EP, *Nanobiohybrids as delivery vehicles for camptothecin,* Journal of Controlled Release **95** (2004) 501-514.
- Vacarri A, *Preparation and catalytic properties of cationic and anionic clays*, Catalysis Today **41** (1998) 53-71.
- Valente JS, Hernandez-Cortez J, Cantu MS, Ferrat G, López-Salinas E, *Calcined layered double hydroxides Mg-Me-Al (Me: Cu, Fe, Ni, Zn) as bifunctional catalysts,* Catalysis Today **150** (2010) 340-345.
- Valencia-Sanchez MA, Liu J, Hannon GJ, Parker R, *Control of translation and mRNA degradation by miRNAs and siRNAs*, Genes & Development **20** (2006) 515-524.
- Velu S and Swamy CS, *Synthesis and physicochemical properties of new copper-manganese-aluminium ternary hydrotalcite-like compound,* Journal of Materials Science Letters **15** (19) (1996) 1674-1677.
- Vucelic M, Jones W, Moggridge GD, *Cation ordering in synthetic layered double hydroxides,* Clays and Clay Minerals **45** (6) (1997) 803-813.
- Wang G-H, Zhao YZ, Tan J, Zhu S-H, Zhou K-C, *Arginine functionalized hydroxyapatite nanoparticles and its bioactivity for gene delivery*, Transactions of Nonferrous Metals Society of China **25** (2015) 490-496.
- Wang G, Rao D, Li K, Lin Y, *UV Blocking by Mg-Zn-Al layered double hydroxides for the protection of asphalt road surfaces,* Industrial and Engineering Chemistry Research **53** (11) (2014) 4165-4172.
- Wang[1] L, Wang F, Xu L, *Layered double hydroxides based on different cations as catalysts for synthesis of poly(1,5-pentadiol) carbonate diols,* Indian Journal of Chemistry **54A** (2015) 607-612.

- Wang H, Liang X-H, Zhao R-X, Feng L-D, Li H, *Spectrophotometric determination of arginine in grape juice using 8-hydroxyquinoline*, Agricultural Sciences in China **7** (10) (2008) 1210-1215.
- Wang Q, Tang SVT, Lester E, O'Hare D, *Synthesis of ultrafine layered double hydroxide (LDHs) nanoplates using continuous-flow hydrothermal reactor*, Nanoscale **5** (2013) 114-117.
- Wang S, Huang J, Chen F, *Study on Mg-Al hydrotalcites in flame-retardant paper preparation,* Bioresources **7** (1) (2012) 997-1007.
- Wang Z, Wang E, Gao L, Xu L, *Synthesis and properties of Mg_2Al layered double hydroxides containing 5-fluorouracil*, Journal of Solid State Chemistry **178** (2005) 736-741.
- Wei P-R, Kuthati Y, Kankala RK, Lee C-H, *Synthesis and Characterization of Chitosan-Coated Near-Infrared (NIR) Layered Double Hydroxide-Indocyanine Green Nanocomposites for Potential Applications in Photodynamic Therapy*, International Journal of Molecular Science **16** (2015) 20943-20968.
- Weyermann J, Lochmann D, Zimmer A, *A practical note on the use of cytotoxicity assays,* International Journal of Pharmaceutics **288** (2005) 369-376.
- Wilson, AJC, *X-ray diffraction index for the identification of materials: an appeal for new data*, Journal of Scientific Instruments, **24**(4) *(*1947) 110.
- Wong Y, Markham K, Xu ZP, Chen M, Lu GQ, Bartlett PF, Cooper HM, *Efficient delivery of siRNA to cortical neurons using layered double hydroxide nanoparticles,* Biomaterials **31** (2010) 8770-8779.
- Wu GY, Wu CH, *Receptor-mediated in vitro gene transformation by a soluble DNA carrier system,* The Journal of Biological Chemistry **262** (10) (1987) 4429-4432.
- Wu GY, Wu CH, *Receptor-mediated gene delivery and expression in vivo,* The Journal of Biological Chemistry **263** (29) (1988) 14621-14624.
- Wu P, Li W, Zhu Y, Tang Y, Zhu N, Guo C, *The protective effect of layered double hydroxide against damage to DNA induced by heavy metals,* Applied Clay Science **100** (2014) 76-83.
- Wypych F, Chemical Modifications of Clay Surfaces, In: Clay Surfaces, Fundamentals and Applications, Edited by F. Wypych and KG Satyanarayana, (2004) Elsevier Academic Press, London.

- Xu X, Li D, Song J, Lin Y, Lv Z, Wei M, Duan X, *Synthesis of Mg-Al-carbonate layered double hydroxide by an atom-economic reaction*, Particuology 8 (3) (2010) 198–201.
- Xu ZP, Zhang J, Adebajo MO, Zhang H, Zhou C, *Catalytic applications of layered double hydroxides and derivatives,* Applied Clay Science **53** (2011) 139-150.
- Xu ZP, Niebert M, Porazik K, Walker TL, Cooper HM, Middelberg APJ, Gray PP, Bartlett PF, Lu GQ, *Subcellular compartment targeting of layered double hydroxide nanoparticles*, Journal of Controlled Release **130** (2008) 86-94.
- Xu R, *Progress in nanoparticle characterization: sizing and zeta potential measurement,* Particuology **6** (2008) 112-115.
- Xu ZP and Lu GQ, *Layered double hydroxide nanomaterials as potential cellular drug delivery agents*, Pure Applied Chemistry **78** (9) (2006) 1771-1779.
- Xu ZP, Zeng QH, Lu GQ, Yu AB, *Inorganic nanoparticles as carriers for efficient cellular delivery*, Chemical Engineering Science **61** (2006) 1027-1040.
- Xu ZP, Walker TL, Liu KL, Cooper HM, Lu GQ, Bartlett PF, *Layered double hydroxide nanoparticles as cellular delivery vectors of supercoiled plasmid DNA*, International Journal of Nanomedicine, **2** (2) (2007) 163-174.
- Yan M, Zhang Z, Cui S, Lei M, Zeng K, Liao Y, Chu W, Deng Y, Zhao C, *Improvement of pharmacokinetic and antitumor activity of layered double hydroxide nanoparticles by coating with PEGylated phospholipid membrane,* International Journal of Nanomedicine **9** (1) (2014) 4867-4878.
- Zhang S, Zhao B, Jiang H, Wang B and Ma B, *Cationic lipids and polymers mediated vectors for delivery of siRNA,* Journal of Controlled Release **123** (2007) 1-10.
- Zhang Y, Garzon-Rodriguez W, Manning MC, Anchordoquy TJ, *The use of fluorescence resonance energy transfer to monitor dynamic changes of lipid-DNA interactions during lipoplex formation,* Biochimica et Biophysica Acta **1614** (2003) 182-192.
- Zhang H, Ouyang D, Murthy V, Wong Y, Xu Z, Smith SC, *Hydrotalcite intercalated siRNA: Computational characterization of the interlayer environment,* Pharmaceutics **4** (2012) 296-313.

- Zhang K, Xu ZP, Lu J, Tang ZY, Zhao HJ, Good DA, Wein MQ, *Potential for layered double hydroxide-based, innovative drug delivery systems,* International Journal of Molecular Sciences **15** (2014) 7409-7428.
- Zhao Y, Li F, Zhang R, Evans DG, Duan X, *Preparation of layered double hydroxide nanomaterials with a uniform crystallite size using a new method involving separate nucleation and aging steps,* Chemistry of Materials **14** (2002) 4286-4291.
- Zheng H, Tang C, Yin C, *Exploring advantages/disadvantages and improvements in overcoming gene delivery barriers of amino acid modified trimethylated chitosan,* Pharmaceutical Research **32** (6) (2015) 2038-2050.
- Zümreoglu-Karan B and Ay AN, *Layered double hydroxides – multifunctional nanomaterials*, Chemical Papers **66**(1) (2012) 1-10.
- https://en.wikipedia.org/wiki/HEK_293_cells (Date accessed: 15th September 2017).
- https://en.wikipedia.org/wiki/Hep_G2 (Date accessed: 15th September 2017).
- https://en.wikipedia.org/wiki/Caco-2 (Date accessed: 15th September 2017).
- https://en.wikipedia.org/wiki/HeLa (Date accessed: 15th September 2017).
- http://www.pharmainfo.net/book/emerging-trends-nanotechnology-pharmacy-physicochemical-characterization-nanoparticles/zeta (Date accessed: 31st August 2017).
- www.hepG2.com (Date accessed: 15th September 2017).
- www.hek293.com (Date accessed: 15th September 2017).

APPENDIX

Table A1: Masses of cationic nitrates used to prepare samples.

		Mass (g) of precursor salt	
Compound	**Ratio M^{2+}:M^{3+}**	**M^{2+}**	**M^{3+}**
MgAl 0.25	3:1	25.6	18.75
MgAl 0.33	2:1	25.6	12.38
MgFe 0.25	3:1	25.6	20.02
MgFe 0.33	2:1	25.6	13.33
ZnAl 0.25	3:1	29.75	18.75
ZnAl 0.33	2:1	29.75	12.38

Table A2: Masses of cationic nitrates and amino acids used to prepare amino acid functionalized hydrotalcites.

		Mass (g)		
Compound	**Ratio M^{2+}:M^{3+}:amino acid**	**M^{2+}**	**M^{3+}**	**Amino Acid**
MgAlArg 0.25	3:1:1	5.12	3.76	2.11 (L-arginine hydrochloride)
MgAlArg 0.33	2:1:1	5.12	2.46	1.38 (L-arginine hydrochloride)
MgAlHist 0.25	3:1:1	5.12	3.76	1.92 (L-histidine hydrochloride)
MgAlHist 0.33	2:1:1	5.12	2.46	1.26 (L-histidine hydrochloride)

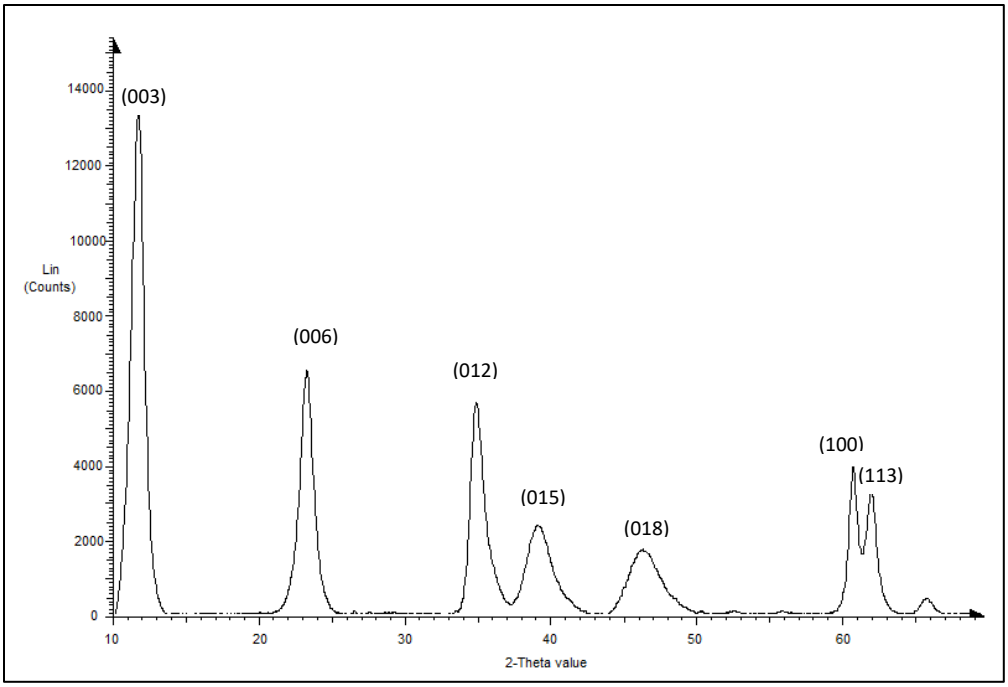

Figure A1 XRD diffractogram of MgAl 0.25.

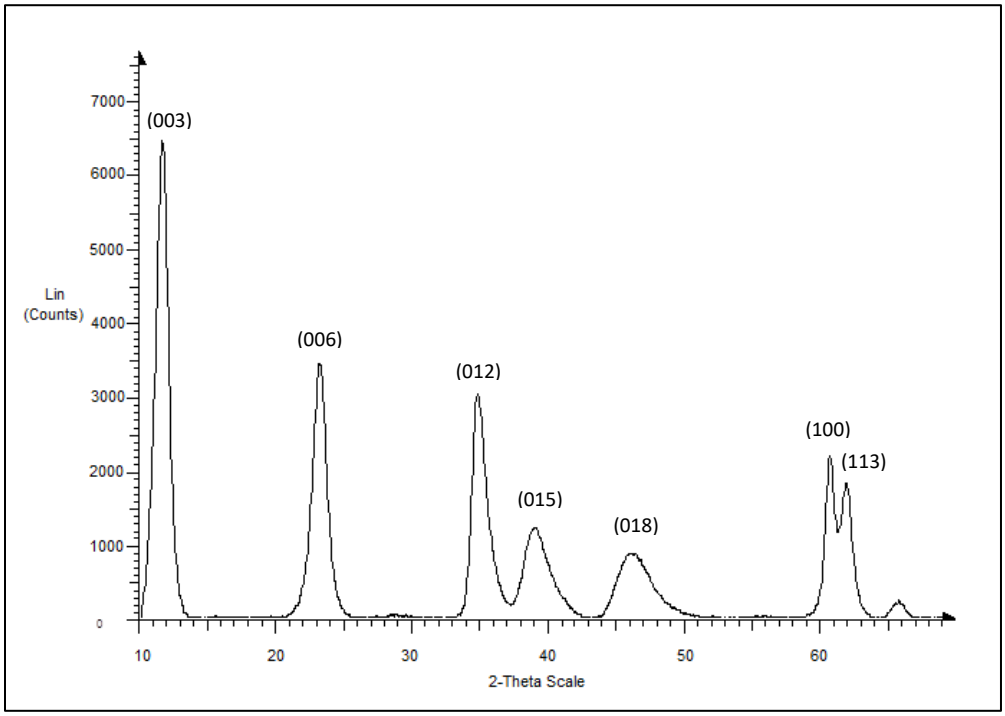

Figure A2 XRD diffractogram of MgAlArg 0.25.

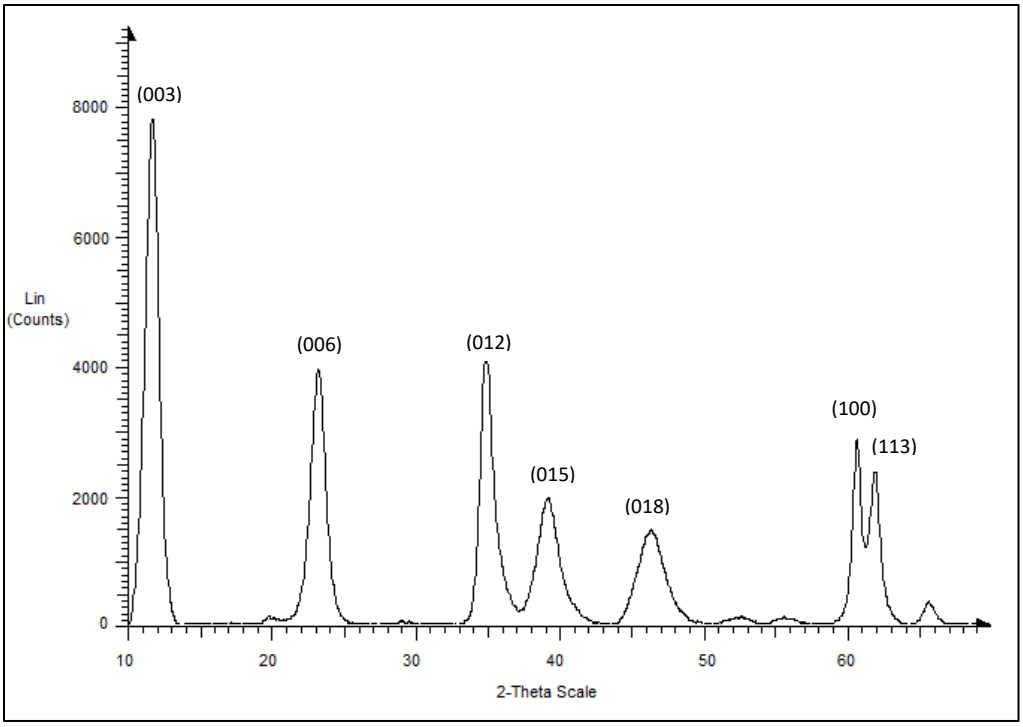

Figure A3 XRD diffractogram of MgAlHist 0.25.

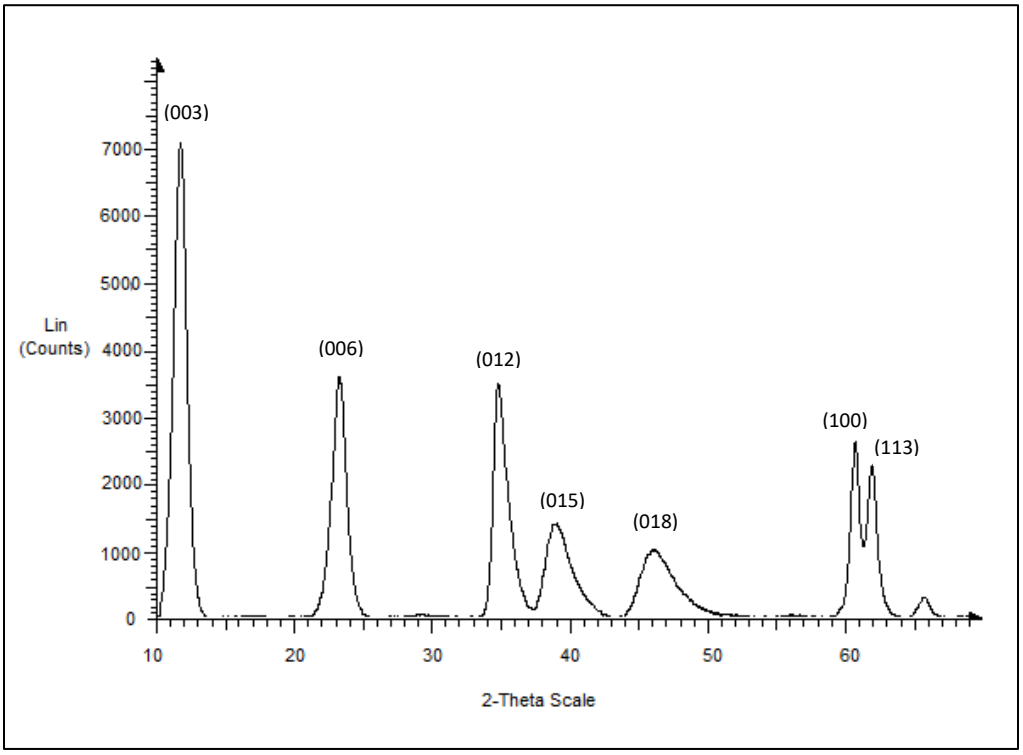

Figure A4 XRD diffractogram of MgAlArg 0.33.

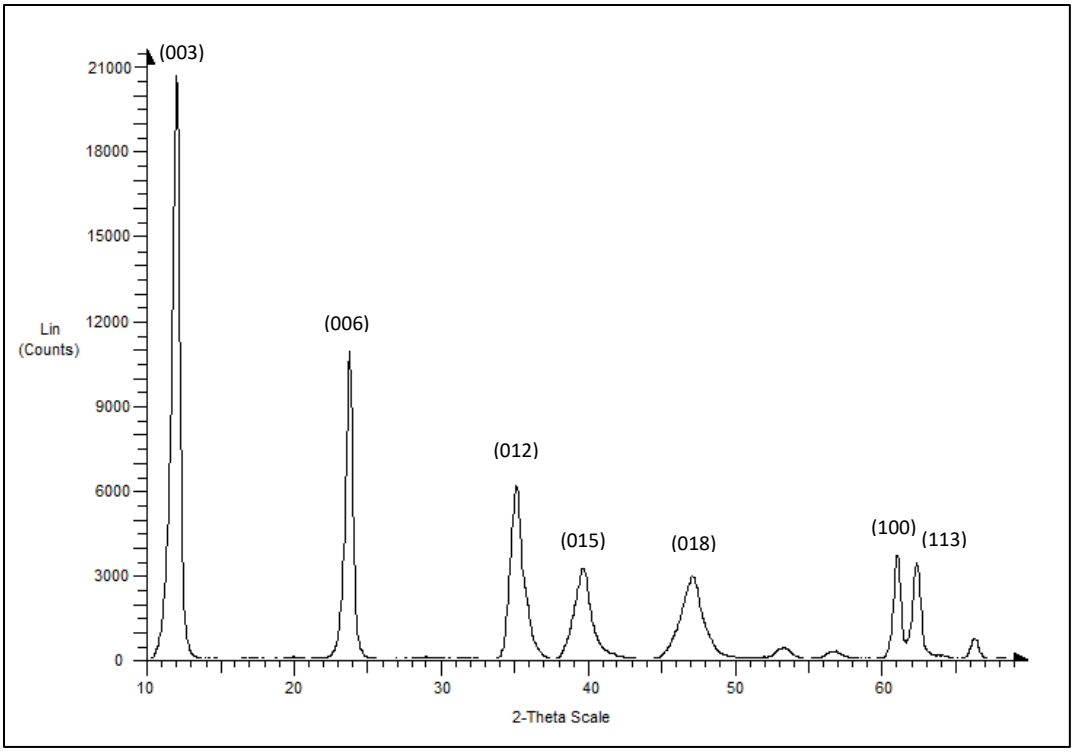

Figure A5 XRD diffractogram of MgAlHist 0.33.

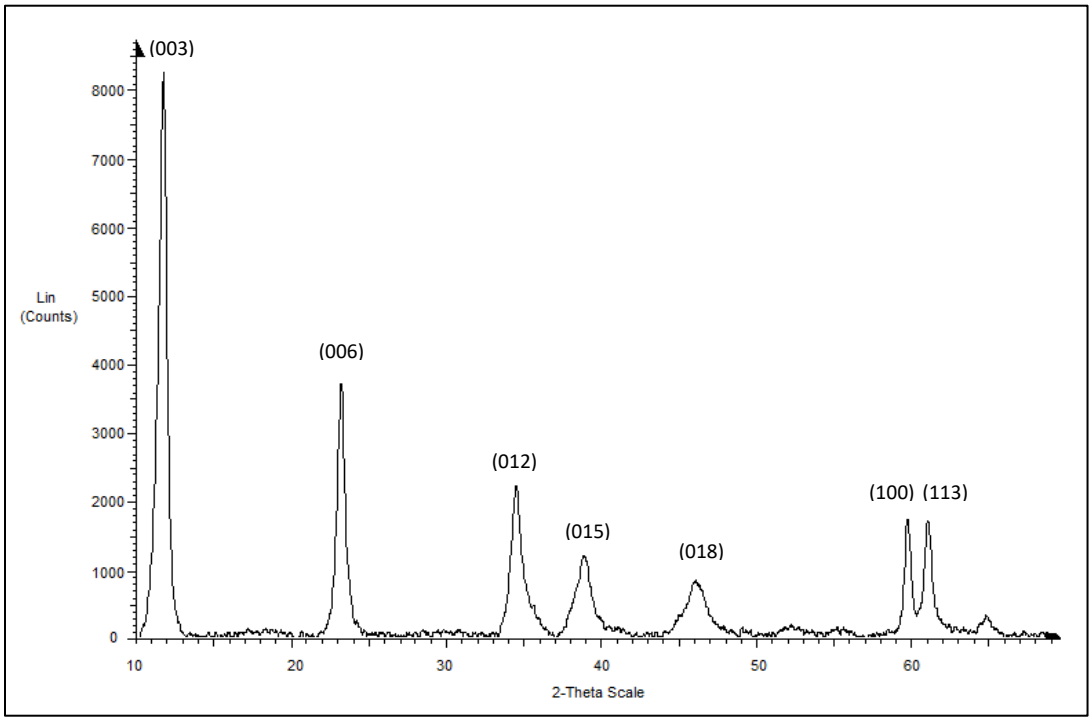

Figure A6 XRD diffractogram of MgFe 0.25.

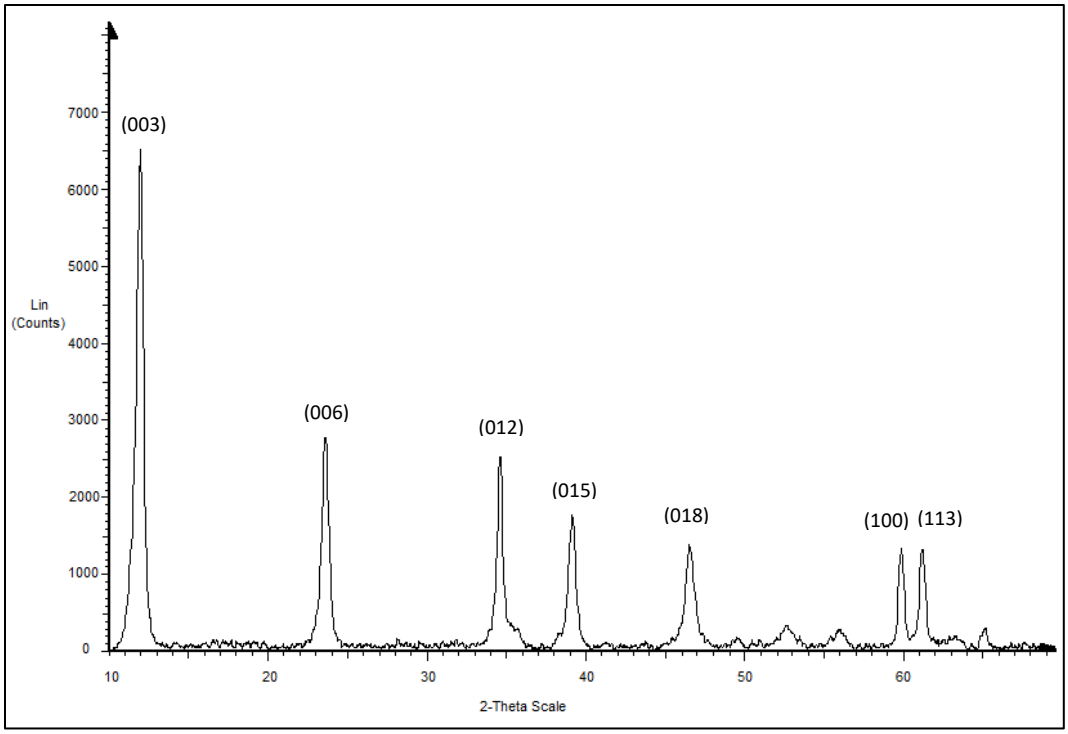

Figure A7 XRD diffractogram of MgFe 0.33.

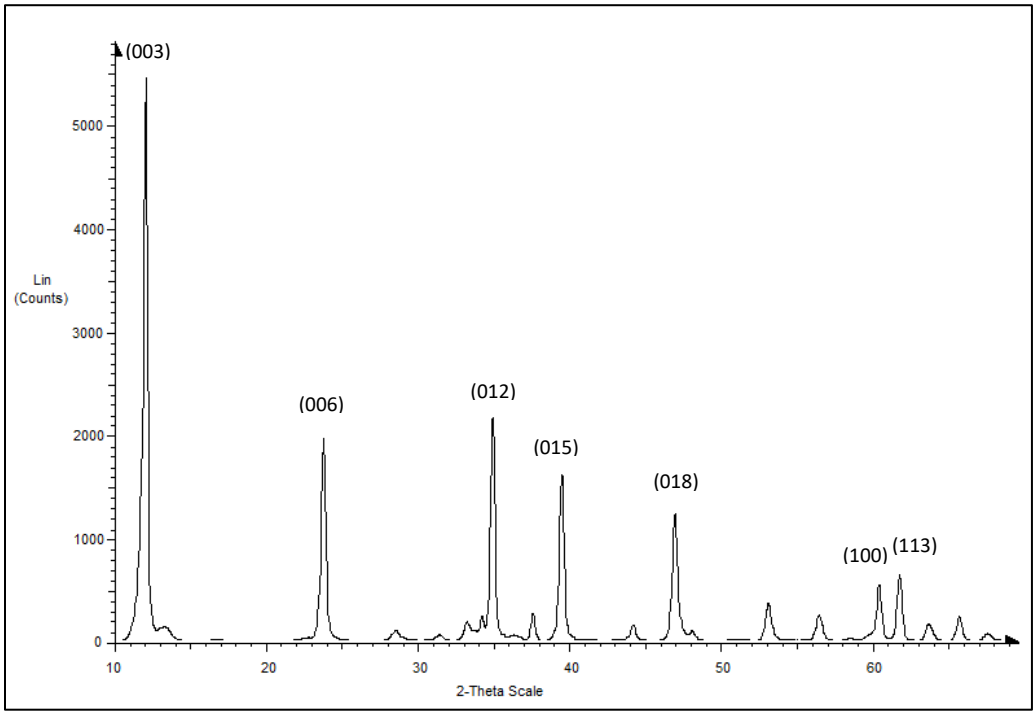

Figure A8 XRD diffractogram of ZnAl 0.25.

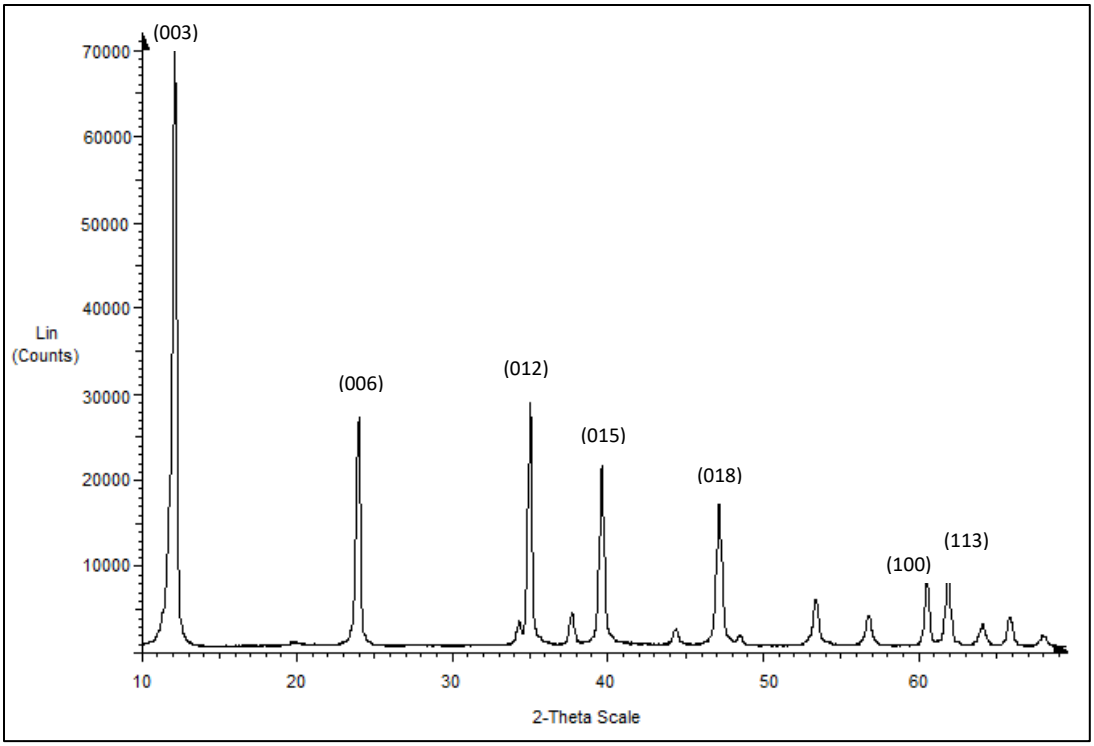

Figure A9 XRD diffractogram of ZnAl 0.33.

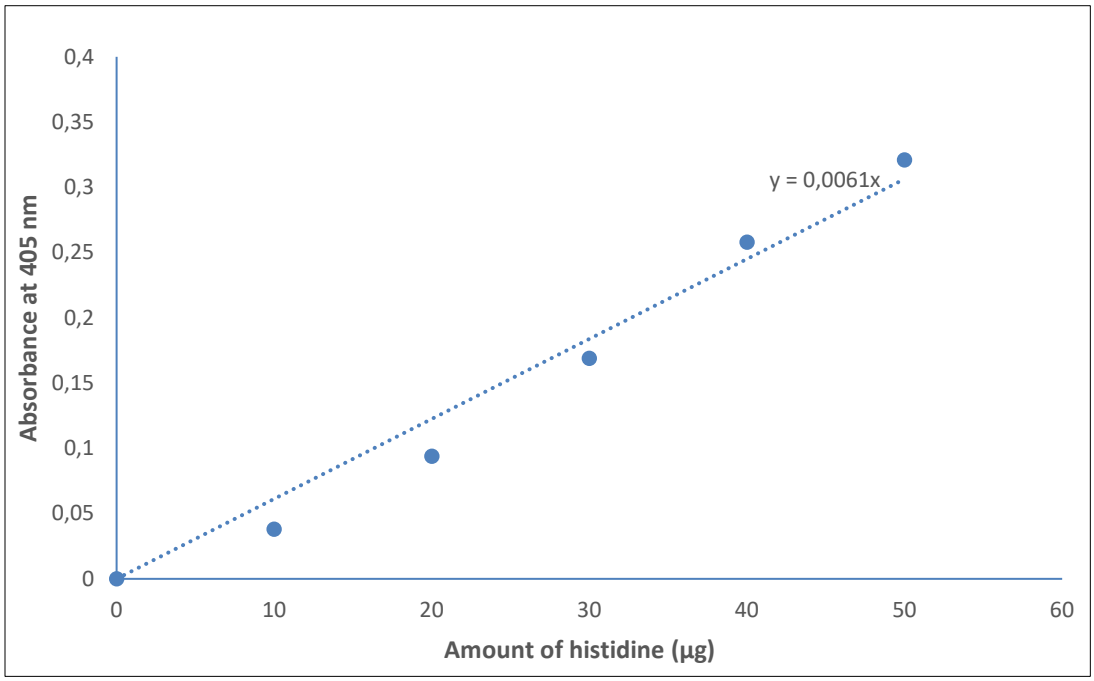

Figure A10 Standard curve for histidine determination.

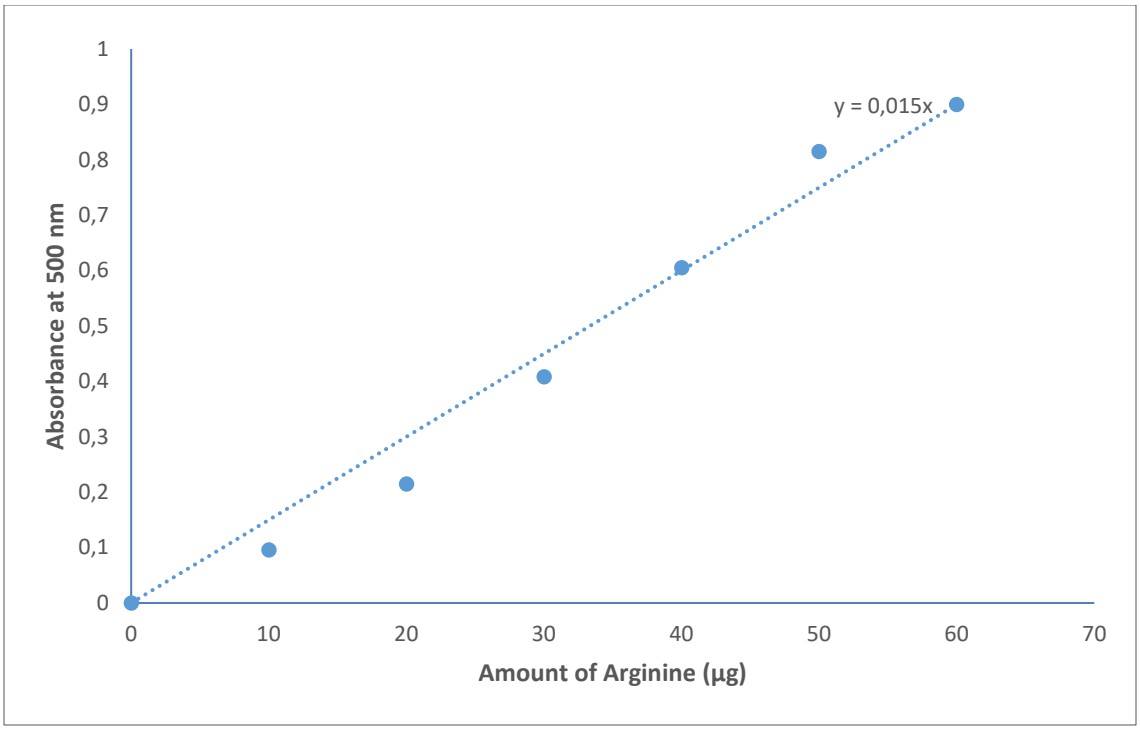

Figure A11 Standard curve for arginine determination.

TURNITIN REPORT

ORIGINALITY REPORT

14%	6%	13%	5%
SIMILARITY INDEX	INTERNET SOURCES	PUBLICATIONS	STUDENT PAPERS

PRIMARY SOURCES

1	www.mindat.org Internet Source	2%
2	Chakraborty, Jui, Manjusha Chakraborty, Swapankumar Ghosh, and Manoj Kumar Mitra. "Drug Delivery Using Nanosized Layered Double Hydroxide, an Anionic Clay", Key Engineering Materials, 2013. Publication	2%
3	edepot.wur.nl Internet Source	1%
4	Goh, K.-H.. "Application of layered double hydroxides for removal of oxyanions: A review", Water Research, 200803 Publication	1%
5	Submitted to Institute of Graduate Studies, UiTM Student Paper	1%
6	Submitted to Bilkent University Student Paper	1%

7	Arne Burzlaff. "Flow cytometry: Interesting tool for studying binding behavior of DNA on inorganic layered double hydroxide (LDH)", Cytometry, 11/2004 Publication	1%
8	Wen-Fu Lee. "Effect of hydrotalcite on the swelling and mechanical behaviors for the hybrid nanocomposite hydrogels based on gelatin and hydrotalcite", Journal of Applied Polymer Science, 04/05/2006 Publication	1%
9	Li, Cang, Lianying Wang, David G. Evans, and Xue Duan. "Thermal Evolution and Luminescence Properties of Zn−Al-Layered Double Hydroxides Containing Europium(III) Complexes of Ethylenediaminetetraacetate and Nitrilotriacetate", Industrial & Engineering Chemistry Research, 2009. Publication	1%
10	Submitted to Universiti Tenaga Nasional Student Paper	<1%
11	etheses.bham.ac.uk Internet Source	<1%
12	Sergey V. Krivovichev. "Natural Double Layered Hydroxides: Structure, Chemistry, and Information Storage Capacity", Minerals as	<1%

	Advanced Materials II, 2011 Publication	
13	Zhitova, E.S., S.V. Krivovichev, I.V. Pekov, V.N. Yakovenchuk, and Ya.A. Pakhomovsky. "Correlation between the d-value and the M2+:M3+ cation ratio in Mg–Al–CO3 layered double hydroxides", Applied Clay Science, 2016. Publication	<1%
	a-c-s.confex.com Internet Source	<1%
14	Nanotechnology and Plant Sciences, 2015. Publication	<1%
15	Khan, Aamir I., and Dermot O???Hare. "Intercalation chemistry of layered double	<1%
16	hydroxides: recent developments and applicationsBasis of a presentation given at Materials Discussion No. 5, 22ï¿½ï¿½ï¿½25 September 2002, Madrid, Spain.", Journal of Materials Chemistry, 2002. Publication	
	Submitted to Durban University of Technology Student Paper	<1%
17	Stoica, Georgiana, IvÃ¡n CastellÃ³ Serrano, Albert Figuerola, Irati Ugarte, Roberto Pacios,	<1%
18	and Emilio Palomares. "Layered double	

	hydroxides as carriers for quantum dots@silica nanospheres", Nanoscale, 2012. Publication	
19	Khalaf Alghamdi. "Base Catalysis with Metal Oxides", Metal Oxide Catalysis, 10/15/2008 Publication	<1%
20	T. Hongo. "Synthesis and adsorption properties of nanosized Mg-Al layered double hydroxides with Cl−, NO 3 − or SO 4 2− as interlayer anion", Materials Science-Poland, 06/2011 Publication	<1%
21	minerva-access.unimelb.edu.au Internet Source	<1%
22	Jing He. "Preparation of Layered Double Hydroxides", Structure and Bonding, 2006 Publication	<1%
23	nvlpubs.nist.gov Internet Source	<1%
24	www.scielo.br Internet Source	<1%
25	repositorio.uam.es Internet Source	<1%

Exclude quotes	On
Exclude bibliography	On